

# **Poster Presentation**

## Poster Presentation

---

### Medical Physics

MP01	Optimum Exposure Parameter with Modified Target/Filter Combination in Digital Mammography.....	3- 1
MP02	Metal Artifact Correction using Model-Based Images.....	3- 5
MP03	Using Monte Carlo digital phantoms to evaluate the feasibility of replacing medical diagnostic LCD monitors with general purpose LCD monitors.....	3- 6
MP04	Quantifying Liver Fat Content Utilize Selective Saturation MRI at 1.5 T Scanner.....	3- 8
MP05	Tumor Delineation using PET in Radiation Therapy .....	3- 9
MP06	Estimate for Osteoporosis of Mice Using Different Low Energy X-ray system.....	3- 10
MP07	Real-Time Dose Measurements of Automatic Tube Current Modulation in Multislice CT.....	3- 11
MP08	Using fMRI to Evaluate the Visual Short-Term Memory.....	3- 13
MP09	Application of Radiation on Nuclear Medicine, Charged Particle Therapy and BNCT in Japan.....	3- 14
MP10	Design of a Novel Imaging Detector with Depth-of-interaction Decoding Capability.....	3- 21
MP11	Study of Maximum-Acceptance-Angle Effects on Image Quantity of Dual-Head PEM System.....	3- 23
MP12	Feasibility Study of Low Energy DEXA Imaging for Bone-density Measurement of Osteoporosis in Mice Using CCD and CMOS.....	3- 24
MP13	Evaluation of Image Restoration Methods for <sup>188</sup> Re micro-SPECT Quantitation.....	3- 25
MP14	Quantitative Imaging of <sup>188</sup> Re-BMEDA-Liposome in a C26 Murine Colon Carcinoma Solid Tumor Animal Model.....	3- 26
MP15	Investigating and Analyzing Reconstructed Images of MDCT Coronary Angiography.....	3- 27
MP16	Dose Evaluation and Analysis for Angiographics.....	3- 28
MP17	Dose Evaluation of Different Tumor Models using Monte Carlo Simulation.....	3- 30
MP18	Estimations of Equivalent Breast Phantom and Breast Dosimetry for Mammography of Taiwanese Women.....	3- 31
MP19	Label-Free Biomolecular Binding Kinetics Detection with Surface Plasma Wave Biosensor .....	3- 35

MP20	The Experience of Using Diagnostic Computed Radiography (CR) System to do Quality Assurance of LINAC.....	3- 38
MP21	Assessment of Image Quality and Radiation Dose Reduction with In-plane Bismuth Shielding for CT Examinations: Phantom tudy.....	3- 43
MP22	Development of Nucleoside Radiotracers Via in Situ Screening of HBTU Amide Forming Libraries for Imaging HSV-1 tk Cancer Gene therapy.....	3- 45
MP23	Using Diffusion Tensor Index Analysis Citrus Water Distribution.....	3- 47
MP24	Comparison of simSET and GATE in Simulation of <sup>124</sup> I PET.....	3- 48
MP25	The profit of Independent component analysis on determining the artery input function in dynamic susceptibility contrast MRI.....	3- 49
MP26	Noise Smoothing using Wiener Filter.....	3- 51
MP27	The uncertainties of diagnostic X-ray machines.....	3- 52
MP28	Evaluation of Iodo, Fluoro, Iodovinyl Arabinosyl Uridines against HSV-1 tk Transfected Murine Sarcoma Cells with MTT Cytotoxic Assay and Their Potential for Imaging Cancer Gene Therapy.....	3- 53
MP29	Aswirl Board Dosimetry Technique for Compensating for the Scalp vVertex and Foot Sole Dosage in Total Skin Electron Therapy.....	3- 61
MP30	The Study of Surface Dose for Golden Coating Thermoluminescence Dosimeter.....	3- 72
MP31	The Optimal Composition of DEMBIG Gel Dosimeter by Taguchi method.....	3- 75
MP32	Optimization of treatment Time by definition of matrix center in Leksell Gamma Knife Radiosurgery.....	3- 76
MP33	Presentation of NORM: problems of their being.....	3- 77

### **Radiation Education**

RE01	A Few Special Educational Schemes for the Course of Radiation Measurement Laboratory in National Tsing Hua University.....	3- 81
RE02	Development of Teaching Materials for Radiation Education using An Imaging Plate.....	3- 85
RE03	Nuclear/ Radiation Education at NuTEC/JAEA and a Distance Learning System JNEN.....	3- 90
RE04	Radiation Education using Sparklers for Entire Beginners.....	3- 92
RE05	Newly established Aomori Branch of Radiation Education Forum: case report on radiation education implementation for the local residents by Aomori Branch.....	3- 96
RE06	Proposal for Active Use of <sup>68</sup> Ge- <sup>68</sup> Ga Milking Generator in Education of Various Categories.....	3- 102

RE07	A New Monitoring System of Natural Radionuclides on Air-Borne Dust Sample Combined with $\beta$ - $\alpha$ Correlated Events as A Teaching Material for Public and Student Radiation-Literacy.....	3- 106
RE08	Revival of "Radiation" in the New Curriculum Guideline for Junior High Schools in Japan.....	3- 108
RE09	A Few Special Educational Schemes for the Course of Radiation Measurement Laboratory in National Tsing Hua University.....	3- 110
RE10	The current basic nuclear education in Taiwan and suggestions.....	3- 112
RE11	The Communication and Personnel Training Programs of Taiwan's Regulatory Authority in the Field of Atomic Energy.....	3- 113

### **Miscellanea**

M1	Effect of Hydrophilic and Hydrophobic Monomers Grafting on Biodegradable Poly (3-hydroxybutyrate) using Irradiation.....	3- 114
M2	Rapid Deployment of Monte Carlo Simulation System by Diskless Remote Boot in Linux.....	3- 120

## Optimum exposure parameter with modified target/filter combination in digital mammography

S.L. Peng<sup>1,\*</sup>, K.S. Chuang<sup>2</sup>, C.F. Chen<sup>1</sup>, C.A. Chen<sup>1</sup>

<sup>1</sup>*Department of Diagnostic Radiology, Chang Gung Memorial Hospital, Kaohsiung 833, Taiwan*

<sup>2</sup>*Department of Biomedical Engineering and Environmental Sciences, National Tsing Hua University, Hsinchu 300, Taiwan*

### Abstract

The dose delivered to patients who were performed the mammography is investigated recently, but the image quality and the exposure dose are conflicting. In clinical mammography, it is employed a molybdenum as the target and the filter because of the optimum energy spectra. The goal of study is tried to use the alternative target/filter assembly, such as molybdenum/ rhodium (Mo/Rh) combination. The figure of merit (FOM) used to evaluate the technique factor is the ratio of SNR to the average glandular dose. The results that the FOM was higher for Mo/Rh assembly because of the fewer glandular dose to patients and the there was no impact on the clinic diagnosis

**Key words:** digital mammography, average glandular dose, breast radiography

### Introduction

For early detection of breast cancer, the mammography is the reliable tool in the clinic with low kVp and high mAs. To achieve the optimal kVp, the combination of a molybdenum target and a molybdenum filter (Mo/Mo) is the most commonly used unit for mammography. In recent work, not only the image quality of mammography should be considered but also the patient dose is very important. However, the image criterion, signal-to-noise ratio (SNR) and the dose delivered to patients are conflicting. Maximization of SNR can be improved by increasing the number of the x-ray photons but leads to increasing the patient dose [1]. Up to now, considering the alternative target/filter combination, such as molybdenum/rhodium (Mo/Rh), rhodium/rhodium (Rh/Rh), and tungsten/rhodium (W/Rh) is investigated. Thilander-Klang *et al* [2] collected 965 women who were examined mammographic screening with screen-film combination and found that both average mean absorbed doses to the glandular tissue and image contrast were lower in the Mo/Rh target-filter combination mammography than the Mo/Mo combination. It is confirmed that the reduction in the patient dose does be a flop in the image quality.

Comparing with screen-film mammography, the full field digital mammography (FFDM) is improved because the displayed contrast could be adjusted. But, the inherent image SNR is fixed as the displayed contrast of the signal is increased, so is the visibility of noise. The goal of this study is to use the alternative target/filter combination, Mo/Rh [3], for the breast, instead of the Mo/Mo combination

which the manufacturer recommended in the digital mammography and try to find the balance between the SNR and the average glandular dose (AGD) using the evaluating factor, figure of merit (FOM).

### Methods and Materials

The commercial full field digital mammography (FFDM) system, Selenia from Hologic using TFT-based detectors overlaid with amorphous selenium was employed in this study. The mammographic unit was equipped with an anode made of Mo and k-edge filters made of Mo or Rh so that the allowable target/filter combinations were Mo/Mo and Mo/Rh as operators selected. The moving grid ratio was 4:1 and the automatic exposure control was used.

79 women with various common clinical conditions were recruited and underwent the mammography exam after the questionnaire survey. The mean age was 52.4 years  $\pm$  7.2 (age range, 39-70 years). For comparison, the right craniocaudal (RCC) view and the left craniocaudal (LCC) view were performed with Mo/Mo and Mo/Rh combinations, respectively. To evaluate the performance of the technique factors, the figure of merit (FOM), was defined as the ratio of the square of the image SNR to the average glandular dose (AGD), both a measurement of the physical image quality. The measured SNR is where the automatic exposure control (AEC) detected. The AGD was determined by using measured entrance skin exposures ( $X_{ESE}$ ) and tabulated values of the normalized average glandular dose ( $D_{gN}$ ) [4], as follows:

$$AGD = D_{gN} \times X_{ESE} \quad (1)$$

By the way, two board-certified radiologists participated in this study to assess the image quality from the two different target/filter assemblies.

### Results

The results showed that, for a given Mo/Rh combination, the average glandular dose (AGD) was reduced and the FOM was increased. The increasing level was dependent on the kVp and the breast thickness as figure 1 illustrated below. For Mo/Rh assembly, the FOM were decreased with the kVp increased because the higher kVp will result in worse image quality. For Mo/Rh combination, the highest FOM was represented in the range from 4.5 cm to 5 cm and that was the most thickness of the Asia women. However, there was no impact on the clinic diagnosis, indicating that the Mo/Rh combination is suitable for breasts in clinic practice.

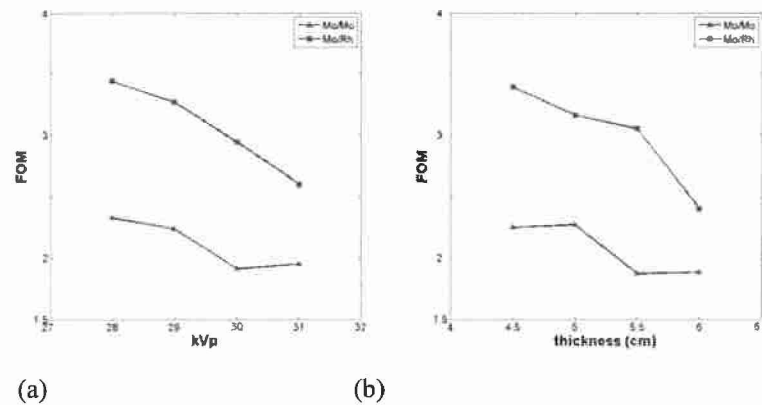


Figure 1

The figure portrayed the relationship between FOM and kVp in (a) and FOM and thickness in (b). For Mo/Rh combination, both have higher FOM.

### Discussion and Conclusions

In early study [5], the tabulated values of the normalized average glandular dose was suitable for 100% glandular breast, 50% glandular-50% adipose breast and 100% adipose breast of phantom images. In clinic, the proportion of glandular tissue in the breast varied among the women examined and it was not easy to find women with 100% glandular or 100% adipose breasts. The objective of this study was to compare the image quality and dose produced with the two target/filter assemblies in clinical mammography, and we implemented  $D_{gn}$  calculations with Matlab code. For arbitrary breast compositions, the interpolating polynomial was utilized. The calculated  $D_{gn}$  of arbitrary breast compositions may not be exactly corrected because of interpolating polynomial. We compared the mean glandular dose to the right breast with that to the left breast in each woman, and the potential error was neglected.

For Mo/Mo combination, it produces energy spectra in bremsstrahlung between 15-20 keV and for Mo/Rh combination, it produces energy spectra in bremsstrahlung between 20-23 keV. When employing Rh/Rh combination, it results in more penetrating beam, but it is not often used in clinical practice. The higher energy spectra results in not only increasing greater radiation penetration, but also decreasing entrance skin exposure and average glandular dose. It is advantageous in mammography. Entrance skin exposure ( $X_{ESE}$ ) is a function of kVp and mAs. For the same kVp and mAs, it will result in the same entrance exposures. For average glandular dose (ADG), it is a function of x-ray tube potential, breast thickness, and breast parenchymal composition. For the same x-ray tube potential and breast thickness, the breast consisted of a higher proportion of adipose tissue will receive more radiation dose than the breast consisted of a higher proportion of glandular tissue. Using the Mo/Rh combination for adipose breasts which compressed thicknesses are thinner than 6 cm is more practical in radiation protection. However, it may associate with the reduction in image quality. The FFDM devices allow for manipulating the display contrast, like window and level functions, so that the effect of display contrast from the higher energy spectra is not taken into account. Employing the alternative

Mo/Rh combination for small breasts in mammography may slightly influence for radiologists, but there is no impact on the clinic diagnosis. Fewer dose to patients is more concerned.

#### References

1. W. Huda, A. M. Sajewicz, K. M. Ogden, and D. R. Dance. Experimental investigation of the dose and image quality characteristics of a digital mammography imaging system. *Med. Phys.* 2003; **30**: 442-448
2. Thilander-Klang A, Ackerholm P, Berlin I, Bjurstam N, Mattsson S, Mansson L-G, et al. Influence of anode-filter combinations on image quality and radiation dose in 965 women undergoing mammography. *Radiology* 1997; **203**: 348-354
3. Mark B. Williams, Priya Raghunathan, and Mitali J. More. Optimization of exposure parameters in full field digital mammography. *Med. Phys.* 2008; **35**: 2414-2423
4. W. T. Sobol and X. Wu. Parametrization of mammography normalized average glandular dose tables. *Med Phys* 1997; **24**: 547-554
5. X. Wu, E. L. Gingold, G. T. Barnes and D. M. Tucker. Normalized average glandular dose in molybdenum target-Rhodium filter and rhodium target-rhodium filter mammography. *Radiology* 1994; **193**: 83-89

## Metal artifact correction using model-based images

Cheng-Ting Shih, Jay Wu

*Institute of Radiological Science, Central Taiwan University of Science and Technology*

Computed tomography (CT) has become one of most favorable choices for diagnosis of trauma. However, high-density metal implants in the CT scans induce metal artifact and compromise image quality. In this study, we proposed a model-based metal artifact correction method.

First, we built a model image using  $k$ -means clustering technique with spatial information and calculated the difference between the original image and model image. The projection data of the original image and model image were then combined together by a weighting factor estimated from an exponential weighting function. At last, the corrected image was reconstructed using the filter back-projection method.

In the cylindrical water phantom image, the metal artifact was removed. The CT number of water was improved from  $-28.95 \pm 97.97$  to  $-4.76 \pm 4.28$ . In the clinical pelvic image, the dark band and metal line were removed and the continuity and uniformity of the CT number of the soft tissue were recovered as well. The CT numbers in the four ROI regions of the corrected image were approached to the theoretical value and standard deviations were below 50% as well.

We conclude that the proposed method is useful for reducing the metal artifact and could improve the diagnostic value.

**Keywords:** Computed tomography, Metal artifact,  $k$ -means clustering

## Using Monte Carlo digital phantoms to evaluate the feasibility of replacing medical diagnostic LCD monitors with general purpose LCD monitors

Chih-Kai Chung<sup>1</sup>, Jay Wu<sup>1</sup>, Shun-Sheng Wang<sup>2</sup>, Cheng-Ting Shih<sup>1</sup>, Yan-Lin Liu<sup>3</sup>

<sup>1</sup>*Institute of Radiological Science, Central Taiwan University of Science and Technology*

<sup>2</sup>*Institute of Biomedical Engineering of Material Science, Central Taiwan University of Science and Technology*

<sup>3</sup>*Department of Radiological Technology, Central Taiwan University of Science and Technology*

### Purpose

Picture Archiving and Communication Systems provide the convenience in medical images transmission. However, development of PACS system needs large cost which has to carefully evaluation. In this study, we evaluate the feasibility of replace the medical diagnostic LCD monitors by general purpose LCD monitors.

### Materials and Methods

We assessment the display characteristics and identification rate of diagnostic high-level BARCO and CHILIN monitors and browse type lower-level EIZO monitors. In display characteristics test, we used the Monte Carlo method to build the digital phantom which with several different size and characteristic spheres and recorded the accuracy and error rate. In identification rate test, we asked five radiologists to observe the Medical CT simulation image display in different monitors and evaluated the result by Receiver Operating Characteristic test.

Before all tests, we also refer the TG-18 report to calibrate the grayscale standard display function curve for standardized the display characteristics of all monitors.

### Results

In display characteristics test, the display performance of diagnostic high-level monitors was better than lower-level monitor. In identification rate test, the area under curve of ROC curve of BARCO, CHILIN and EIZO monitors are 0.74, 0.743 and 0.717, respectively. The P value between

these three monitor are 0.268(EIZO:BARCO), 0.205(EIZO:CHILIN) and 0.897(BARCO:CHILIN), respectively. All P values are bigger than 0.05 that mean there are no significant differences between these monitors.

### **Conclusion**

Diagnostic high-level monitor can be replaced by low-level monitor after calibrate the grayscale standard display function curve and decreases the cost of building of PACS system.

**Key words:** Picture Archiving and Communication Systems, LCD panel

## Quantifying Liver Fat Content Utilize Selective Saturation MRI at 1.5-T Scanner

C.-C. Chuang<sup>1</sup>, D.-M. Ye<sup>1,2</sup>, U.-S. Tyan<sup>1,2</sup>

<sup>1</sup> *School of Medical Imaging and Radiological Sciences, CSMU*

<sup>2</sup> *Department of Medical Imaging, CSMU hospital*

### Purpose

It is not easy to perceive the fatty liver disease which is normally diagnosed by the doctor. The purpose of this study is to validate an MRI technique for measuring liver fat content by calibrating MRI readings with liver phantoms. Then using selective saturation MRI quantities liver fat content acquired from routine exam. These measurement can be used to help fatty liver disease be easily diagnosed. Moreover, it will economize the cost of physical examination so that disease and cure can be found in the early days.

### Method and Material

The MRI protocol consisted of fat and water imaging by selective saturation using a 1.5T scanner. Liver phantoms were made as a calibration standard for quantifying liver fat content. A water phantom and liver phantoms were scanned. Liver fat was also estimated by <sup>1</sup>H-MR Spectroscopy analysis.

### Result

MRI measurements of the liver phantoms were highly reproducible. Measurements of liver fat content in human subjects made by MRI in two areas of the liver were strongly correlated ( $r = 0.97$ ,  $P < 0.001$ ). MRI measurements were highly associated with estimates of liver fat content made by selective saturation MR image analysis ( $r = 0.95$ ,  $P < 0.001$ )

### Conclusion

We validated a technique for quantifying liver fat content based on selective fat imaging. The technique is accurate and reproducible and provides a noninvasive method to obtain serial measurements of liver fat content in human subjects. The technique is accurate and reproducible and provides a noninvasive method to obtain serial measurements of liver fat content in human subjects. However, The method proposed here is sensitive to  $B_0$ -field inhomogeneity and  $B_1$ -field nonuniformity.

**Keywords:** Fat liver ; selective saturation MRI

## Tumor delineation using PET in radiation therapy

Jason WS Sun <sup>1,2</sup>, KY Yen <sup>3</sup>, JA Liang <sup>4</sup>, SS Sun <sup>3</sup>, MS Lee <sup>2</sup>, SK Hung <sup>2</sup>, SM Hsu <sup>1,\*</sup>

<sup>1</sup>*Department of Biomedical Imaging and Radiological Science, China Medical University, Taichung, Taiwan*

<sup>2</sup>*Department of Radiation Therapy and Oncology, Buddhist Dalin Tzu Chi General Hospital, Chia-Yi, Taiwan*

<sup>3</sup>*Department of Nuclear Medicine and PET center, China Medical University Hospital, Taichung, Taiwan*

<sup>4</sup>*Department of Radiation Therapy and Oncology, China Medical University Hospital, Taichung, Taiwan*

Combining the advantages of target treatment of IMRT and IGRT with the molecular imaging technology of PET, radiation oncologists can deliver a better distributed dose to the heart of tumor and to lower the absorbed dose of surrounding critical organs accurately. The limitation to this wonderful marriage of technologies now lies with the effort to precisely determine the target tumor location and size. CT dose provide very anatomically accurate images but presents little biological information about the tumor itself; functional images of PET promises to refine tumor location but the poor spatial resolution of PET images still limit the ability to correctly delineate the target tumor. Our aim in this study is to quantify the tumor size from PET images using homemade cylindrical phantoms of different sizes, and to evaluate the dosimetric impact on radiotherapy plans. PET images were acquired from a 20 cm cubic phantom encompassing five FDG-filled cylinders with volumes of 0.2 to 7.1 cm<sup>3</sup> using a PET Advance NXi scanner. The value of the percent threshold that returned the actual volume was measured. PET emission scans were reconstructed with the OSEM and FBP algorithms with different smoothing levels. The present threshold values were dependent on phantom size, concentration of F-18 FDG used, and level of smoothing, with phantom size less than 0.8 cm<sup>3</sup> presenting marked sensitivity and higher percent threshold values. Careful considerations should be given when using PET to calculate and delineate tumor volume since others factors and variables such as image reconstruction method, smoothing level, geometric shape of phantom/tumor, background level, and lesion concentration must be taken into account when designing a treatment plan for patients.

**Keywords:** IMRT, IGRT, PET threshold

## Estimate for Osteoporosis of Mice Using Different Low Energy X-ray system

H. C. Lu, M. L. Jan\*, H. C. Liang, H. Y. Lai, Y. T. Fang

Dual energy X-ray absorptiometry (DEXA) is one of the popular clinical inspection for osteoporosis. This study will apply DEXA method with our home-made system in low X-ray energy (<50kVp) to discriminate the normal and osteoporosis mice.

But there are two problems in the application of our system. First, DEXA is based on the different mass attenuation coefficients of soft tissue ( $\mu_S$ ) and bone ( $\mu_B$ ) with different energy ( $E_{low}=35kVp$  and  $E_{high}=75kVp$ , for human), but 75kVp of X-ray is not suitable for small animal imaging. Second, the values of mass attenuation coefficients are estimated from ICRU-44 table in single energy, not in continuous energy spectrum. And the wide energy spectrum can't be narrowed by filters, for fewer photons were produced from the small focal spot of the high-resolution X-ray tube.

The corn-beam X-ray tube (in low voltage of 25kV and high voltage of 50kV) with two types of flat panel sensor (CCD and CMOS) were used to get the projection images (512 x 512 and 586 x 560 pixels respecting to CCD and CMOS). The three phantoms in different consistency of Potassium Iodide (KI) solution were 0.25M, 0.4M and 0.5M according to the mean gray value from image of mice bone, and were scanned to simulate the different stage of osteoporosis; these phantoms were also used for evaluation the system linearity. The system linearity results of CCD and CMOS detector were  $R^2=0.9956$  and  $R^2=0.9945$ ; this shows that two systems were positive correlation. The areal density images were constructed from the values of mass attenuation coefficients at mean energy ( $\bar{E}=1/3E_{max}$ ) and DEXA projection images, and the different stage of osteoporosis was discriminated from them. The mice in this experiment were divided into two groups, osteoporosis by ovariectomy (OVX) and normal; then, the bone density of their femur heads was discriminated from areal density images.

This study has developed a method to discriminate the normal and osteoporosis mice through low energy X-ray projection images. In the future, it will be useful for estimation in preclinical treatment experiment.

## Real-time dose measurements of automatic tube current modulation in multislice CT

Hui-Yu Tsai, Ying-Lan Liao<sup>1\*</sup>, Yu-Sheng Tyan<sup>2,3</sup>, Yong-Jie Chang<sup>3</sup>

<sup>1</sup>*Department of Medical Imaging and Radiological Sciences, Chang Gung University, Tao-Yuan, Taiwan*

<sup>2</sup>*Department of Radiology, Chung-Shan Medical University Hospital, Taichung, Taiwan*

<sup>3</sup>*Department of Medical Imaging and Radiological Sciences, Chung Shan Medical University, Taichung, Taiwan*

**Purpose:** To estimate real-time doses which are controlled by automatic tube current modulation (ATCM) in multidetector computed tomography (MDCT), and to verify the dose decrease with the prediction by software.

**Method and Materials:** Brilliance 40 MDCT scanner (Philips) provides five ATCM methods. Those are automatic current selection (ACS), xy-plane dose modulation (D-DOM), z-axial dose modulation (Z-DOM), ACS combined D-DOM, and ACS combined Z-DOM. Real-time doses were measured by two CT pencil-type detectors operating with a Barracuda (RTI-e) electrometer connected to a PC running the software oRTIgo2002 (RTI-e). One detector is DCT10 CTDI ion chamber (RTI-e) with 100 mm sensitive length. The other is CT-SD16 CT slice detector (RTI-e) with 160 mm sensitive length. Several geometric phantoms, which are circular, oval, and elliptic cylinders with 15 cm height, were fabricated to simulate body shapes and to verify the xy-plane dose modulation. An Apollo phantom was also fabricated to verify the z-axial dose modulation.

**Results:** For circular cylindrical phantoms with 16-24 cm diameter, doses decreased 28-69% for ACS, 28-67% for ACS combined D-DOM, and 24-66% for ACS combined Z-DOM. But dose increased 13-20% for 32 cm diameter. For oval and elliptic cylindrical phantoms, doses decreased 17-27% for ACS, 15-40% for D-DOM, 31-39% for ACS combined D-DOM, and 15-28% for ACS combined Z-DOM. D-DOM and Z-DOM real-time dose variation curves were similar for circular cylindrical phantoms. However, real-time dose variation curves got closed along with increasing diameter. For oval and elliptic cylindrical phantoms, ACS and ACS combined Z-DOM real-time dose variations were resembling. But Z-DOM real-time dose variations were remarkable for the Apollo phantom.

**Conclusion:** The methods established by this study could investigate the real-time dose variations. Using ATCM techniques in MDCT scanning could decrease patient doses. However, it needs to pay more attention to use ATCM techniques for obese patients.

## Using fMRI to evaluate the visual short-term memory

Jih-Jie Jiang, Chun-Chao Chuang, Yeu-Sheng Tyan

Department of Medical Image, Chung Shan Medical University Hospital

### 研究目的

研究大腦如何進行記憶運作，是當今科學家們致力研究的部份。短期視覺記憶一般公認為是最快速的記憶方式。當在評估視覺短期記憶時，會因為實驗設計的不同而有所差異，造成無法有效的描述實驗的數據結果。本實驗主要研究如何有效的評估視覺短期記憶，所以本實驗設計一個視覺短期記憶測試，利用fMRI量測腦部反應之活動區域及訊號，進而討論腦部在視覺短期記憶時的運作情形。

### 材料與方法

以十位測試者，接受視覺短期測試。在fMRI的波序設定上，使用BOLD波序，循環問答判斷12次不同記憶問題。以Spm2軟體分析，將實驗數據分成不同分析模組，比較不同模組間的差異及判斷腦部活動區域與相對時間關係，進而分析腦部視覺短期記憶之作用。

### 結果

分析實驗數據可得以下結果

1. 視覺短期記憶腦部激活圖及不同腦部反應區塊之訊號強度與時間之比較圖表。
2. 答題的決策回憶正確性與懷疑不確定性及不同的腦部活動區域相關性。。
3. 預測值與實際實驗數據之比較關係圖。

### 討論

視覺短期記憶在學習上是有相關的;短期記憶容量較大，記的事情也越多，一般也認為與智力有很大的關係。特別是在短期記憶方面受損，無法回想起剛看到的刺激而導致學業失敗、知覺缺陷、符號能力失常和其他學習障礙等。此外，若海馬體（hippocampus）受損將無法將新學習的結果從短期記憶轉換為長期記憶，如果能夠有效的利用短期視覺記憶實驗，對於診斷記憶相關疾病(例如: 失憶症、學習障礙)會有很大的幫助。

## Application of Radiation on Nuclear Medicine, Charged Particle Therapy and BNCT in Japan

Yanagisawa Kazuaki <sup>†1</sup>, Inoue Tomio <sup>†2</sup>, Hayakawa Kazushige <sup>†3</sup>, Shiotari Harutaka <sup>†4</sup>, Nakamura Yoshihide <sup>†5</sup>, Matsuyama Kazuya <sup>†6</sup>, Nagasawa Kiyoshi <sup>†7</sup>

*†1: Japan Atomic Energy Agency (JAEA), 1233 Watanuki, Takasaki, Gunma, 370-1292, Japan,*

*†2: School of Medicine, Yokohama City University, 3-9, Fukuura, Kanazawa-ku, Yokohama 236-0004,*

*†3: Kitasato University School of Medicine, 1-15-1, Kitasato, Sagami-hara-shi, Kanagawa 228-8555,*

*†4: Nihon Medi-Physics Co., Ltd., 3-4-10, Shinsuna, Koto-ku, Tokyo 136-0075,*

*†5: Japan Radioisotope Association, 2-28-45, Honkomagome, Bunkyo-ku, Tokyo 113-8941,*

*†6: Fujifilm Medical Co, Ltd., 2-26-30, Nishiazabu, Minato-ku, Tokyo 106-0031,*

*†7: GE Yokogawa Medical Systems, 4-7-127, Asahigaoka, Hino-shi, Tokyo 191-8503*

### I. Introduction

Our previous study performed in 1997 revealed that the use of radiological technology in medicine was spread. The amount of reimbursement was about 10b\$ (billion dollars) corresponding either to about 4% of the national health expenditures (240b\$) or to about 0.2% of the Gross Domestic Products (GDP; 4,231b\$). An average expenditure was 1,900\$ a year for the Japanese. Since then on behalf of Japanese Cabinet we have an opportunity to study repeatedly an economic scale and the current situation of medicine in Japan.

### II. Method

#### 1. Searching Body

For the present study, a total of seven Japanese specialists, hence medical doctors and researchers working at universities, institutes and private pharmaceutical companies were joined to form the medical working group.

#### 2. Database

Reimbursements or receipts from hospitals to patients issued by the results of medical care are the principal database. As for Japan, a typical database relating to this matter was issued under the title of "Research for socio/medical diagnostic acts in 2005- vol.1, outline and statistics", by the Ministry of Labor, Health and Welfare. The target year was set at 2005, intending to do data comparison with

those from 1997. For radiological application, diagnosis (excluding MRI), radiotherapy and examination by radioisotopes (RI) were taken into consideration and 45 items for medicine and 13 items for dentistry were chosen from the database. A conversion from medical care points to reimbursed money was done by {Medical care points} × 10 yen / points × 12 months × f {adjusting factor; 1 < f < 2}

### III. Results and Discussion

#### III.1 Reimbursed medical care

There occurred two significant changes that affect the aim of present study. At the year of 1999, the Ministry of Labor, Health and Welfare newly added an associated health insurance to the national and the governmental insurances. This caused an expansion of database. Then, at the year of 2003, the Ministry has started to apply DPC (Diagnosis Procedure Combination) to several items of medicine; such as diagnosis and examinations, while DPC was not applied to radiotherapy. No DPC applied to the items of dentistry at all.

It is revealed that the economic scale of radiological technology in medicine is about 14b\$ a year 2005. This is either corresponded to about 4.8% (that is, 4.4% for medicine and 0.4% for dentistry) of the national health expenditure (301b\$) or corresponded to about 0.31% of the nominal GDP (gross domestic products,

4,552b\$). An average expenditure was 2,400\$ a year for the Japanese. It is found that the magnitude of economic scale in 2005 is larger by a factor of 17% than that in 1997. It is worthy of

### III.2 No reimbursed medical care

#### 1. FDG-PET and Lung Cancer

It was revealed in our previous study carried out in 1997 that the economic scale of FDG-PET was 50M\$ (million dollars) for the U. S., and 2M\$ for Japan. Unit cost is about 1,980\$ for the former and about 397\$ for the latter. In 2005, Japan Radioisotope Association (JRIA) studied an economic scale of FDG-PET by questioning the existing 99 facilities. From replied 68, one found that examinations in total were 50,558. A cost of reimbursement in public and private hospitals varied from zero (13%), 816\$ (18%) and 1,020\$ (69%), respectively. By using weighed average of 981\$, one found that a rebated cost for 99 facilities is 72M\$ ( $50,558 \times 981\$ \times (99/68)$ ). It is 36 times larger than in 1997.

CT imaging for lung cancer is not reimbursed and is done as option at ningen (human) dock. This fact masks an accurate scale of economy. The Japanese Society of CT Screening (JSCTS) reported recently (2005) that peoples screened were 85,888 at 50 medical facilities, where an average expenditure was about 101\$ per person. It leads that an economic scale of lung cancer by CT screening is about 9M\$. Peoples aged from 50 to 59 were the majority having a percentage by 35%, where numbers of males are greater than those of females.

In 2005, total sum of no reimbursed economic scale for FDG-PET, CT for lung cancer and breast cancer in Japan was 74M\$, 8M\$ and 181M\$. In 1997, those for FDG-PET, CT for lung cancer and breast cancer were 2M\$, 0M\$ and 0M\$, respectively. Increase of economic scale in those was a significant meaning that people's quality of life (QOL) is under improvement to a high degree.

mentioning that economic scale of radiological items was increased year by year. The diagnostic imaging is the largest in the magnitude of economic scale.

#### 2 Charged Particle Therapy and BNCT

With respect to charged particle therapy, a total number of proton treatments in 1997 were 59 and that of carbon treatment was 159. A total numbers 218 had no economic scale due to poor reimbursement at that time. In 2005, charged particle therapy was carried out in the 4 cancer centers in Japan represented by the National Cancer Center Hospital East, where numbers of treatments were totaled in 927 with economic scale by 24M\$.

For BNCT (Boron Neutron Capture Therapy), treatments were zero in 1997. In 2005, the treatment numbers are increased up to 96 because of medical treatment at KUR research reactor belong to the Kyoto University and JRR-4 belong to JAEA. The numbers, however, had no economic scale due to poor reimbursement.

### IV. Conclusions

With respect to medical reimbursement base, the economic scale of radiological technology in medicine is about 14b\$ a year 2005. An average expenditure is 2,400\$ a year for the Japanese. A total sum of economic scale for FDG-PET, CT for lung cancer, breast cancer and charged particle therapy in Japan is 287M\$ a year 2005. Corresponded value in 1997 is about 3M\$. The needs of these medical treatments are strongly expanded and the contribution of radiological technology is increased markedly for the improvement of Japanese people's quality of life (QOL).

# Application of Radiation in Nuclear Medicine, Charged Particle Therapy and BNCT in Japan

Yanagisawa Kazuaki <sup>†1</sup>, Inoue Tomio <sup>†2</sup>, Hayakawa Kazushige <sup>†3</sup>, Shiotari Harutaka <sup>†4</sup>, Nakamura Yoshihide <sup>†5</sup>, Matsuyama Kazuya <sup>†6</sup>, Nagasawa Kiyoshi <sup>†</sup>

<sup>†1</sup>: Japan Atomic Energy Agency (JAEA), 1233 Watanuki, Takasaki, Gunma, 370-1292, Japan,

<sup>†2</sup>: School of Medicine, Yokohama City University, 3-9, Fukuura, Kanazawa-ku, Yokohama 236-0004,

<sup>†3</sup>: Kitasato University School of Medicine, 1-15-1, Kitasato, Sagami-hara-shi, Kanagawa 228-8555,

<sup>†4</sup>: Nihon Medi-Physics Co., Ltd., 3-4-10, Shinsuna, Koto-ku, Tokyo 136-0075,

<sup>†5</sup>: Japan Radioisotope Association, 2-28-45, Honkomagome, Bunkyo-ku, Tokyo 113-8941,

<sup>†6</sup>: Fujifilm Medical Co, Ltd., 2-26-30, Nishiazabu, Minato-ku, Tokyo 106-0031,

<sup>†7</sup>: GE Yokogawa Medical Systems, 4-7-127, Asahigaoka, Hino-shi, Tokyo 191-8503

---

## Abstract

The economic scale of radiological technologies applied to medical reimbursement is 14b\$ in 2005, which is larger by a factor of 17% than that of 1997. The value 14b\$ corresponds to about 4.8% (4.4% for medicine and 0.4% for dentistry) of the national health expenditure (301b\$). The economic scale of radiation application at FDG-PET and the charged particle therapy is 74M\$ and 24M\$ in 2005. In 1997 it was only 2 M\$ for the former and zero for the latter. The radiation technologies in these fields are rapidly developing. FDG-PET enhanced the survival of 50,558 patients. Charged particle therapy enhanced the survival of 927 patients at 4 specified hospitals and 5,229 patients at the Proton Medical Research Center University of TSUKUBA. Radiological technology is quite beneficial for the improvement of Japanese people's quality of life (QOL).

Keywords: economic scale, medicine, radiological technology, FDG-PET, charged particle therapy

---

## I. Introduction

Application of radiation in the field of nuclear medicine is prominently used for the diagnosis, the radiotherapy and the examination by radioisotopes (RI). Incomes of hospitals are reimbursed by a national health insurance. Advanced radiological technologies represented by FDG-PET, charged particle therapy and BNCT are used in the specified hospitals. In 2005, an economic scale of radiological application at aforementioned fields was studied and obtained results were directly compared with those from 1997.

## II. Method

### 1. Searching Body

A total of seven Japanese specialists, hence medical doctors and researchers working at universities, institutes and private pharmaceutical companies were assembled and established the medical working group (MWG). It was belonged to

the Special Committee for Studying the Economic Effect of the Utilization of Radiation. The Committee was in cooperation with the Japan Atomic Energy Agency (JAEA); the former Japan Atomic Energy Research Institute (JAERI) under the sponsorship by the Cabinet Office, Government of Japan.

### 2. Database

The concept for the economic scale of radiology in the medical field was already discussed in detail and reported elsewhere (JAERI, 2000). Every year the Ministry of Labor, Health and Welfare reports the reimbursed medical cares as "Research for socio/medical diagnostic acts in 2005- vol.1, outline and statistics" (Ministry of Labor, Health and Welfare 2006). Because the socio/medical diagnostic acts covered various types of medical treatments being done in our country, it was necessary for MWG to select the items relating to

radiological application. As a result of selection, a total of 45 items for medicine and 13 items for dentistry were revealed. Since the unit of selected items is composed of “medical care point”, one must convert the point into money. For a conversion, MWG used the following equation;

$$\{\text{Medical care points}\} \times 10 \text{ yen / points} \\ \times 12 \text{ months} \times f \{\text{adjusting factor}; \\ 1 < f < 2\} \dots \dots \dots / 1/$$

Since medical points are only deduced from one month study usually performed on May it should be multiplied by 12. For adjusting factor, an explanation is made later on.

With respect to medical cares at advanced radiological technologies, there exist little references from the Japanese authority. Consequently, MWG collected necessary data by using market reports, website, interviews and hearing by phone.

### III. Results and Discussion

#### III.1 Reimbursed medical care

After the previous study done in 1997, there occurred two systematic changes that affect the result of present study. In 1999, the Ministry of Labor, Health and Welfare added an associated health insurance to the former groups; the national and the governmental insurances. This addition caused an expansion of database, that is, masked the accuracy of economic scales. Subsequently, in 2003, the Ministry introduced DPC (Diagnosis Procedure Combination) system to the fields of diagnosis and examinations in medicine, where radiotherapy was exempted. No DPC was introduced to dentistry. Since a principal aim of DPC is to suppress the whole medical expenses, several different medical cares are put into one basket of reimbursement. When MWG is to evaluate the economic scale of radiation application from the DPC, nobody can understand the percentage of radiation application in the basket. To overcome this difficulty, MWG suggested a correlation that 4% of total DPC

expenditures were composed of radiological technologies. Additionally MWG found that there was a discrepancy between the sum of national health expenditures and the sum of expenditures calculated from the socio/medical diagnostic acts. To bring the latter into line with the former, MWG set an adjusting factor f, which is ranged from 1.46 to 1.77 by a year of study. Consequently, equation /1/ is reformulated as follows;

$$\{\text{Medical care points}\} \times 10 \text{ yen / points} \\ \times 12 \text{ months} \times \{1.46 \sim 1.77\} + 0.04 \text{DPC} \dots / 2/$$

Conversion rate from yen (¥) to US dollar is  
1\$=110.2yen to the present case.

**Figure 1** shows the economic scale of reimbursed medical care obtained in the present study. Because an economic scale of radiological technologies in medicine (circle) is a part of expenditures in the national health care (triangle), the latter is bigger than the former.

The economic scale of radiological technologies in medicine is about 14b\$ a year 2005. It is corresponded either to 4.8% (that is, 4.4% for medicine and 0.4% for dentistry) of the national health expenditure (301b\$) or to 0.31% of the nominal GDP (gross domestic products, 4,552b\$). An average expenditure was 2,400\$ a year for the Japanese. It is worth to mention that in 1997, the economic scale of radiological technologies in medicine is about 10b\$. It was corresponded either to 4% of the national health expenditures (240b\$) or to 0.2% of GDT (4,231b\$). An average expenditure was 1,900\$ a year for the Japanese. The economic scale in 2005 is larger by a factor of 17% than that in 1997.

It is apparent that the magnitude of economic scale in nuclear medicine is increasing from year to year. The diagnostic imaging has the largest magnitude by 12b\$ in 2005, meaning that it is the most useful and convenient tool at the convenient imaging field. Though it is not a radiological technology, the economic scale of MRI (magnetic resonance inspection) is

as high as 4b\$. For examination by RI, the economic scale was 1.7M\$ in 1997 but 0.4M\$ in 2005. The use of RI is tended to decrease. There is no RI usage in dentistry.

A fluctuation of data observed around

1995 was resulted in a currency conversion from yen to dollar, because an original curve plotted by yen was rather smooth.

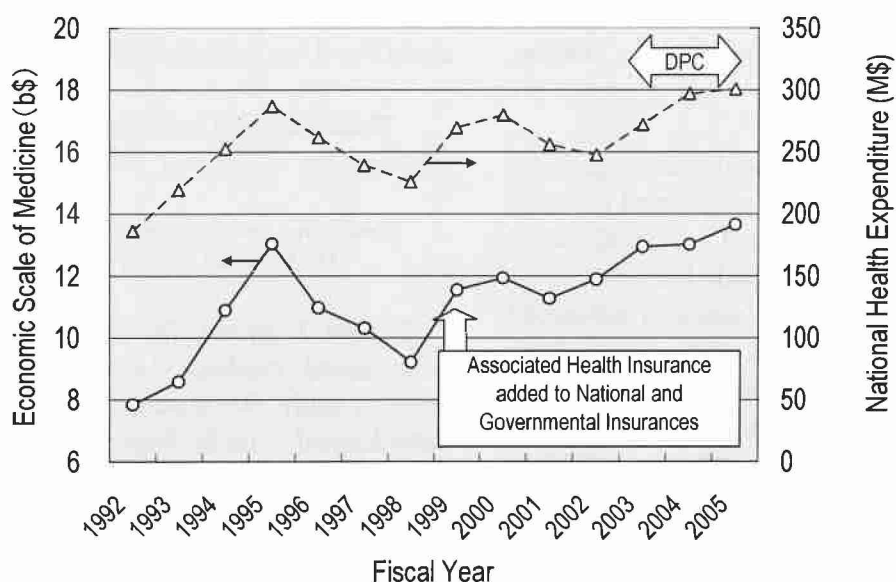


Fig. 1 Economic scale of medicine (left) and national health expenditure (right); Fluctuations of data observed around 1995 is due to the currency conversion from Japanese yen to the U. S. dollar.

### III.2 Advanced radiological technologies

One considered that FDG-PET, lung cancer, breast cancer, prostate cancer, charged particle therapy and BNCT are advanced medical technologies all relating to cancer. Medical treatments by those technologies are carried out at specified hospitals or facilities. In the present study, an economic scale of FDG-PET, charged particle therapy and BNCT is taken into consideration.

#### 1. FDG-PET

In 1997 the economic scale of FDG-PET was 50M\$ for the U. S., and 2M\$ for Japan (Atomic Energy Commission 2008). Unit cost is about 1,980\$ for the former and about 397\$ for the latter.

In 2005, Japan Radioisotope Association (JRIA) studied the economic scale of FDG-PET by questioning the existing 99

facilities. From replied 68, one found that examinations were totally 50,558. A cost of reimbursement in public and private hospitals varied as zero (13%), 816\$ (18%) and 1,020\$ (69%). By using weighed average of 981\$, JRIA concluded that a reimbursed cost for 99 facilities is 74M\$ (50,558 x 981\$ x (99/68)). This value is 36 times larger than in 1997.

#### 2 Charged Particle Therapy

Radiotherapy (RT) is known as the most useful treatments for various types of cancers. In the mid of 1990's American patients rather than Japanese used RT aggressively to cure their disease. Once Americans had any cancers (1.15million patients in 1994), 49% (560,262 patients) of those received RT. For Japanese, of the 440,001 new patients in 1995, only 15%

(71,696 patients) received RT. Japanese patients are willing to have surgical operations than RT. This can be explained in various ways. With respect to cancer treatments, different attitudes exist between Americans and Japanese.

With respect to charged particle therapy, a total number of proton treatments in 1997 were 59 and that of carbon treatment was 159. A total numbers 218 had no economic scale at that time because all hospitals are

not certificated as specified facilities for reimbursement. In 2005, as shown in Fig.2, 4 cancer centers in Japan represented by the National Cancer Center Hospital East got a certification as the specified hospital for charged particle therapy. The numbers of treatments carried out by those hospitals were totaled in 927 with economic scale by 24M\$ in 2005. Note that the Proton Medical Research Center University of TSUKUBA had clinical examination up to 5,229 patients.

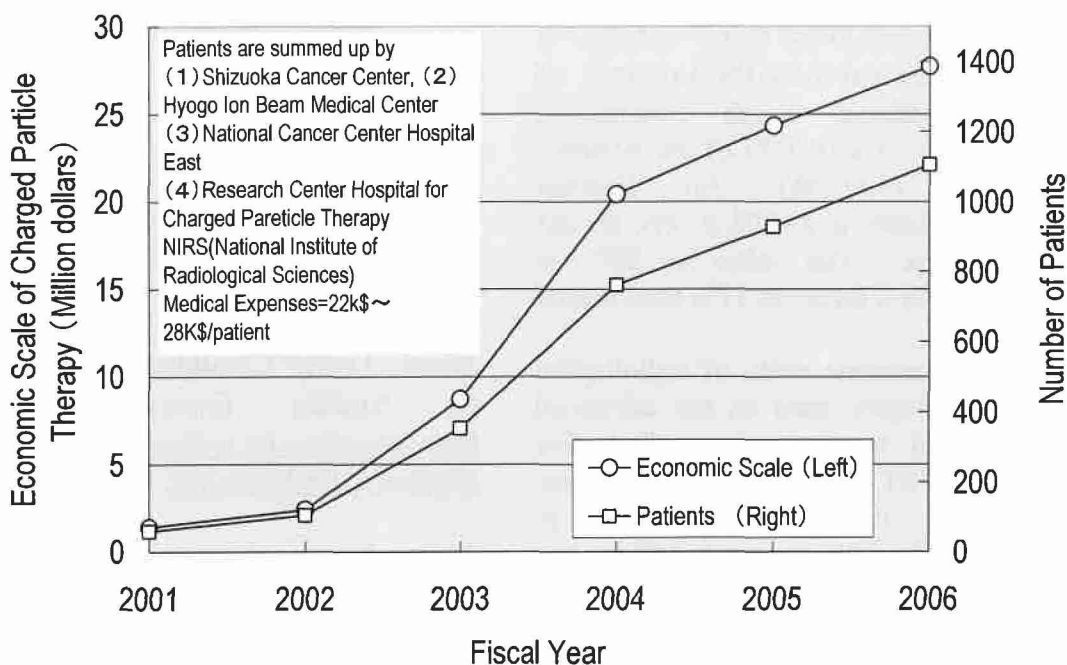


Fig.2 Charged particle therapy. Data are collected from (1) Shizuoka Cancer Center, (2) Hyogo Ion Beam Medical Center,(3) National Cancer Center Hospital East, (4) Research Center Hospital for Charged Particle Therapy NIRS (National Institute of Radiological Sciences). Proton Medical Research Center University of TSUKUBA performed a clinical examination up to 5,229 patients.

### 3. BNCT

By using a nuclear reaction;  $^{10}\text{B}(n,\alpha)^7\text{Li}$  boron neutron capture therapy (BNCT) of brain tumors can enhance survival and cure following blood-brain barrier disruption with injection of sodium borocaptate and boronophenylalanine. BNCT in JAEA for example is mainly used for brain malignant

tumor and melanoma. BNCT operations were 27 at years from 1968 to 1996 by 5 Japanese research reactors. It became zero in 1997 due to shut down of the research reactors. As shown in Table 1, in 2005, BNCT operations were increased up to 48. The figures, however, had no economic scale because of clinical examination.

Table 1 BNCT in Japan (KUR research reactor belong to the Kyoto University and JRR-4 belong to JAEA)

FY	1999	2000	2001	2002	2003	2004	2005	2006	2007
JRR-4	5	4	3	3	5	8	12	24	17
KUR	4	1	3	7	26	15	36	Shut Down	-

#### IV. Conclusions

- (1) The reimbursed economic scale of radiological technologies in medicine is about 14b\$ in 2005. It corresponds either to 4.8% (4.4% for medicine and 0.4% for dentistry) of the national health expenditure (301b\$) or to 0.31% of the nominal GDP (4,552b\$). An average expenditure is 2,400\$ a year for the Japanese. The value in 2005 is larger by a factor of 17% than that of 1997.
- (2) The economic scale of radiological technologies used in the advanced medical treatment is studied. For FDG-PET and charged particle therapy, it is 74M\$ and 24M\$ in 2005. In 1997 it was 2 M\$ for the former and zero for the latter. In 2005, FDG-PET enhanced the survival of 50,558 patients. The charged particle therapy enhanced the survival of 927 patients at 4 specified hospitals and 5,229 patients at the Proton Medical Research Center University of TSUKUBA. The BNCT enhanced

the survival of 48 patients in the two research reactors in Japan.

- (3) Radiological technology is useful for the improvement of Japanese people's quality of life (QOL).

#### Acknowledgment

The authors express our appreciation to the Cabinet Office, Government of Japan for approval of publication of the present study.

#### References

- Atomic Energy Commission ; "White paper on Nuclear Energy 2007 " , <http://www.aec.go.jp/jicst/NC/about/hakusho/hakusho2007/wpe.pdf>, (2008.3).
- Japan Atomic Energy Research Institute (JAERI): *Survey Report for Economic Scale of Utilization of Radiation [I]*, Report to MEXT (2000.3), [in Japanese].
- Ministry of Labor, Health and Welfare; "Research for Socio/Medical Diagnostic Acts in 2005-Vol.1, Outline and Statistics", (2006).

## Design of a Novel Imaging Detector with Depth-of-interaction Decoding Capability

Hsin-Chin Liang\*, Meei-Ling Jan, Wei-Chih Lin, Shih-Fan Yu, Po-Hsiu Kuo,  
Jenn-Lung Su

*Physics Division, Institute of Nuclear Energy Research, Longtan, Taiwan (R.O.C.)*

In the application of a positron breast planar imager, the detector separation distance is suggested to be as close as possible to maximize the acceptance angle and also to improve the sensitivity. However, this causes the parallax error to become more critical and degrades the image quality. A scanner which offers the depth-of-interaction (DOI) information of the incident gamma events can provide corrections for the image quality improvements. In this study a new design of a position-of-interaction (POI) imaging detector, which can reduce the parallax error, is presented.

A  $12 \times 5$  array block composed of  $1.4 \times 1.6 \times 170 \text{mm}^3$  LYSO crystals was assembled. Two 1-inch<sup>2</sup> PSPMTs were optically coupled to both ends of the crystal block. A thin plate detector was placed in the opposite of the long POI detector with its  $0.8 \times 13.2 \text{mm}^2$  edge facing the point source. Via coincidence comparing, the Na-22 point would be collimated to form a positron line source. The collimated line source was positioned at -8, -4, 0, +4 and +8cm relative to the long crystal, and data acquisitions were processed. For all the acquired events, two crystal numbers were obtained from DET 1 and DET 2 according to their crystal LUTs. When they were recognized as the same crystal, the index values  $\ln(E2/E1)$  which comes from the energy ratio of DET 1 and DET 2 and can be used for estimating the position in x-direction were calculated. These values were collected in a histogram to evaluate the accuracy of the position estimation of this DOI detector.

Preliminary results show good crystal identification in the y and z direction, while in the x direction there is an inaccuracy of location estimation of 2.3 cm. To improve the accuracy an energy screen, which trying to estimate two photo-peaks for every incident event, was implemented. In calibration mode, a pair of correlation curves of the photo-peak energies relative to the energy ratios of DET 2 to DET 1, for every crystal "pipe", was built. In real application, for every gamma incident event, two energy values from DET 1 and DET 2 and also their dividing ratio could be obtained. With comparing to the curves mentioned above, two expected photo-peak energies were estimated. If both the two energy values fell within their  $\pm 7.5\%$  windows which are centered at the expected photo-peaks, acquired values of this event were reserved. If not, they would be abandoned. With the position (crystal

number matching) and the energy (photo-peak windowing) filters applying, the inaccuracy is improved to 1.2 cm. Still it needs improvements on the energy resolution of the detector, so that the position estimation in x direction can be more accurate, and thus makes this design practical.

The preliminary results show that this new detector design does provide DOI information. However the poor energy resolution (16~26%), which is caused by the photon attenuation (long light path) and the contamination of the spontaneous radiations, makes it impractical to be used. The analysis shows that it's difficult to make dramatic improvement on the energy resolutions with using LSO/LYSO. Therefore searching for better scintillation materials (higher light yield and no spontaneous radiation, such as LaBr<sub>3</sub>) to gain an energy resolution of about 5% will be required in the future work.

## Study of maximum-acceptance-angle effects on image quantity of dual-head PEM system

Yu-Ching Ni, Meei-Ling Jan\*, Hsuan-Yu Lai, Zhi-Kun Lin, Li-Ting Huang,  
Hong-Chin Lu

*Physics Division, Institute of Nuclear Energy Research, Longtan, Taiwan (R.O.C.)*

Dual-head positron emission mammography (PEM) systems, compare to conventional PET systems, have data with incomplete angles. Closing the distance of two detector heads is expected to increase the angle range, however, it will affect spatial resolution and parallax error of PEM images because of the acceptance angle being enlarged. In this work, the maximum-acceptance-angle effects on image qualities of dual-head PEM system were studied.

A PEM system, which has two opposing detector heads with  $60 \times 120$  crystal arrays and  $1.54 \times 1.54 \times 10.2 \text{ mm}^3$  crystal size was simulated using GATE. 3D images were implemented by the planar tomography reconstruction. Since the maximum acceptance angle is affected by the detector-to-detector distances (DDs), the LORs (lines of response) within acceptance angles at various DDs were calculated. Standard deviations over mean of the LOR-number-acceptance-angle histograms were used to determine the optimum DD. To realize the influences of acceptance angle on spatial resolution and parallax error, a 0.4mm-diameter point source was scanned with various DD setups (100mm, 150mm and 200mm). The percentages of accepted counts with various DDs and acceptance angles were analyzed, and the influenced images will be presented. Moreover, the percentages of parallax-error-count at various DDs were simulated and computed by using two-layer crystal design.

The results show that the smaller DD offers the more angles accepted, but from the shapes of histograms and the Std/M values, the 100 mm DD is considered as the optimal distance. The effects of DD and acceptance angle on images of X-Y plane and Y-Z plane will be presented. The results reveal that increasing the acceptance angle, the degraded spatial resolution at Y-Z plane is improved, however, the parallax error at X-Y plane is increased also. For further study, acceptance-angle effect on scatter factor will be considered.

## **Feasibility Study of Low Energy DEXA Imaging for Bone-density Measurement of Osteoporosis in Mice Using CCD and CMOS**

H. C. Lu, M. L. Jan\*, Y. C. Ni, H. C. Liang, H. Y. Lai, Y. T. Fang

*Physics Division, Institute of Nuclear Energy Research, Longtan, Taiwan (R.O.C.)*

Dual energy X-ray absorptiometry (DEXA) is one of the popular inspections for clinical osteoporosis examination. Two energy peaks of 35 keV/75 keV are usually used in clinical DEXA, however, the high energy is too large for pre-clinical mice imaging. This work is to study the suitable parameters for applying DEXA method for bone-density measurement of mice.

X-ray generated of 50-80 kVp is common for small animal imaging systems. Here an x-ray tube with 50 kV in maximum, and two types of sensor (Dalsa-CCD and Hamamatsu-CMOS) were used to get the projection images (512 x 512 and 586 x 560 pixels respecting to CCD and CMOS) of phantoms and mice. Phantoms with 0.25M-0.5M consistencies of Potassium Iodide (KI) solution were scanned. The x-ray tube was operated ranging from 20 kV to 50 kV for experiments. The areal density was calculated from each low-high energy pair images. The optimum dual energy pair and the linearity of CCD and CMOS were evaluated. The phantom study shows the x-ray voltage pair of 25 kV/50 kV provides the most sensitive result for the KI-consistency measurement.

The C57/BL6 mice with osteoporosis by ovariectomy (OVX) surgery and the control group were scanned with dual energies of 25 kVp/50 kVp. The femur-head region was chosen as the region of interest (ROI), and the bone density of ROI was calculated for analysis. From the results of animal study, it reveals that the low energy DEXA imaging for osteoporosis inspection of mice is promising.

## Evaluation of image restoration methods for $^{188}\text{Re}$ micro-SPECT quantitation

Shiang-Lin Hsu, Meei-Ling Jan\*, Fan-Pin Tseng, Chung-Hsin Yeh, Yu-Ching Ni,  
Zhi-Kun Lin,

*Physics Division, Institute of Nuclear Energy Research, Longtan, Taiwan (R.O.C.)*

The purposes of this study are to evaluate the influence of image restoration methods on  $^{188}\text{Re}$  micro-SPECT images and to improve the accuracy of quantitation. Using proper restoration methods to improve the accuracy of quantitation is expected to help the analysis of pre-clinical animal experiments for  $^{188}\text{Re}$ -(DXR)-liposome drug development.

Three restoration methods, Wiener Filter, CLS Filter and Lucy Richardson, were selected to de-blur the simulated and experimental images. The Shepp-Logan digital phantom with noise (signal-noise ratio: 2dB, 20dB, 200dB) was used to evaluate their ability of noise resistance. The images of digital phantom with noise were convoluted by degraded function of X-SPECT system to simulate the measured images. Then, restoration methods were applied on the simulated images.

Various concentrations of  $^{188}\text{Re}$ -solution (1600, 800, 400, 200, 100 and 50  $\mu\text{Ci/cc.}$ ) in well plates were scanned by X-SPECT/CT (Gamma-Medica-Ideas Inc.) with high-resolution-parallel-hole collimator at time points of 0, 42, 60, and 72 h. Reconstructed images were restored by the methods described above. The restorative results of Wiener Filter, CLS Filter, and Lucy Richardson were evaluated by the linearity of correlation between real activity concentration and average voxel value.

From the correlation between real activity concentrations and ROI mean values, it is concluded that Lucy Richardson method can offer the best recovered results, particularly in the low activity range. It reveals that suitable method may improve the accuracy of micro-SPECT quantitation.

**Keywords:** quantitation, image restoration,  $^{188}\text{Re}$ -SPECT.

## Quantitative imaging of $^{188}\text{Re}$ -BMEDA-Liposome in a C26 murine colon carcinoma solid tumor animal model

Fan-Pin Tseng, Meei-Ling Jan\*, Yu-Ching Ni, Shiang-Lin Hsu, Ya-Jane Chang,  
Zhi-Kun Lin, Chih-Hsien Chang, Te-Wei Lee

*Physics Division, Institute of Nuclear Energy Research, Longtan, Taiwan (R.O.C.)*

The spatial resolution of micro-SPECT with parallel-hole collimation doesn't satisfy the requirement of small animal imaging. In this study, An image restoration method called Lucy Richardson was chosen to recover the quantitative tumor-bearing mice images, and the recovered results were compared with the biodistribution.

A Derenzo phantom (with hot regions of 1.2, 1.6, 2.4, 3.2, 4.0 and 4.8mm diameter inside) was filled with  $^{188}\text{Re}$  ( $\sim 0.1\text{mCi}/0.2\text{cc}$ ). The phantom scanned by X-SPECT (Gamma Medica, USA) was used to evaluate the 3D Lucy Richardson method. A suitable iterative number was determined by analysis of Derenzo phantom. Twenty-seven BALB/c mice were subcutaneously inoculated with  $2 \times 10^5$  tumor cells in the right hind flank. The animals developed tumors of about  $750\text{mm}^3$  in size, and then the  $^{188}\text{Re}$ -BMEDA-labelled pegylated liposomes ( $\sim 0.5\text{mCi}/0.2\text{cc}$ ) was administered to each mouse by intravenous injection. Micro-SPECT images were acquired at 1, 4, 24 and 48 h after injection (n=2).

After comparing full widths of maximum and noise standard deviations of Derenzo phantom image, iterative number was chosen to be three. Standard uptake values (SUVs) of tumor were estimated from recovered and original images. Biodistribution (5 mice for each time point) were studied for comparison.

It is conducted that quantitative results from recovered images can provide better correlation with biodistribution data. After carefully selecting iterative number, image restoration can improve the quantitation of  $^{188}\text{Re}$ -labeled nanoliposomes images and might help to pre-clinical treatment evaluation.

**Keywords:** image quantitation, image restoration, micro-SPECT

## Investigating and analyzing reconstructed images of MDCT coronary angiography

<sup>1,2</sup>Ming-Che Lee, <sup>2</sup> Keh-Shih Chuang, Ph.D., <sup>3</sup>Hsiu-Chu Chen\*, Ph.D.,

<sup>1</sup>*Department of Medical Imaging, Changhua Christian Hospital*

<sup>2</sup>*Biomedical Engineering and Environmental Sciences, National Tsing Hua University*

<sup>3</sup>*Superintendent's Office, Changhua Christian Hospital*

**Objective:** To investigate and analyze reconstructed images of retrospective ECG gating multi-detector row computed tomography (MDCT) for each of the major coronary arteries during the cardiac cycle.

**Materials and Methods:** Multi-detector row coronary artery CT angiographies obtained in 171 patients (103 men, 68 women; mean age, 55 years  $\pm$ 11; age range, 28-83 years) were reconstructed at 35%–85% of the cardiac cycle in increments of 10%. Two independent reviewers who specialize in cardiac radiology assessed the image quality, obtained with three-dimensional post-processing for segments 1–3 (right coronary artery), segments 5–8 (left main and left anterior descending coronary arteries), and segments 11 and 13 (left circumflex artery). Segments were defined according to American Heart Association (AHA) guidelines. The grades were assigned: 1, excellent; 2, good; 3, fair; 4, poor; and 5, very poor.

**Results:** The three-dimensional reconstructed image data were statistically analyzed with SPSS software version 10.0. The authors analyzed 171 patients' data with 2-way ANOVA and found the left anterior descending artery; left circumflex artery and right coronary artery all were best visualized at 75% of the cardiac cycle ( $p < .05$ ).

**Conclusion:** Our results demonstrated that the reconstructed images of coronary arteries usually performed optimally during mid-to-late diastole cardiac cycle. 75% of the cardiac phase was the best visualization phase for all coronary arteries in this study.

**Key words:** MDCT, reconstruction window, cardiac cycle, ECG-gated

## The automatic dose control operation logic in flat-panel detector angiography system

Pei-Ling Lai<sup>1</sup>, Yung-Ying Li<sup>3</sup>, Hui-Yu Tsai<sup>2</sup>, Yeu-Sheng Tyan<sup>3</sup>, Keh-Shih Chuang<sup>1</sup>  
*Institute of Nuclear Engineering and Science National Tsing Hua University<sup>1</sup>,  
Department of Medical Imaging and Radiological Sciences, Chang Gung University<sup>2</sup>,  
Department of Medical Imaging, Chung Shan Medical University Hospital<sup>3</sup>*

**Purpose:** Automatic dose control (ADC) system has a direct impact on the patient's dose.

The purpose of this study is to demonstrate and understand the functionality and operation of ADC for both fluoroscopic and radiographic exposure modes on a modern angiography system.

**Method and material:** In this study we used the Siemens AXIOM Artis dBA Twin angiography system. The experiment consists of two parts: fluoroscopy and exposure modes. A 30cm ×30cm PMMA phantom with thickness varied from 1 to 36 cm was used for dose measurements and the thickness from 1 to 30cm for exposure are used to analyze the operation of automatic dose rate control. Dose was measured with the build-in DAP (dose area product) meter. The impact of the thickness in the relationship between spectral shaping filters with various techniques will be analyzed. Furthermore, try to establish the selection of technique parameter in conjunction with the different field of view (FOV) as well as pulse rate will be studied.

**Result:** In the either fluoroscopy or exposure modes, the operation logic of automatic dose control basically can be divided into four to five stages. In fluoroscopy setup (fig.1), under the same FOV condition, tube potential increases when the thickness of phantom increases, consequently cause the pulse width and tube current to decrease. For exposure mode, similar behavior can be found (fig.2).

**Conclusion:**

The filters and the sophisticated operation logic design of the ADRC for both fluoroscopic and exposure modes are aimed to maintaining the tube potential at optimum levels for a wide range of patient (PMMA thickness).

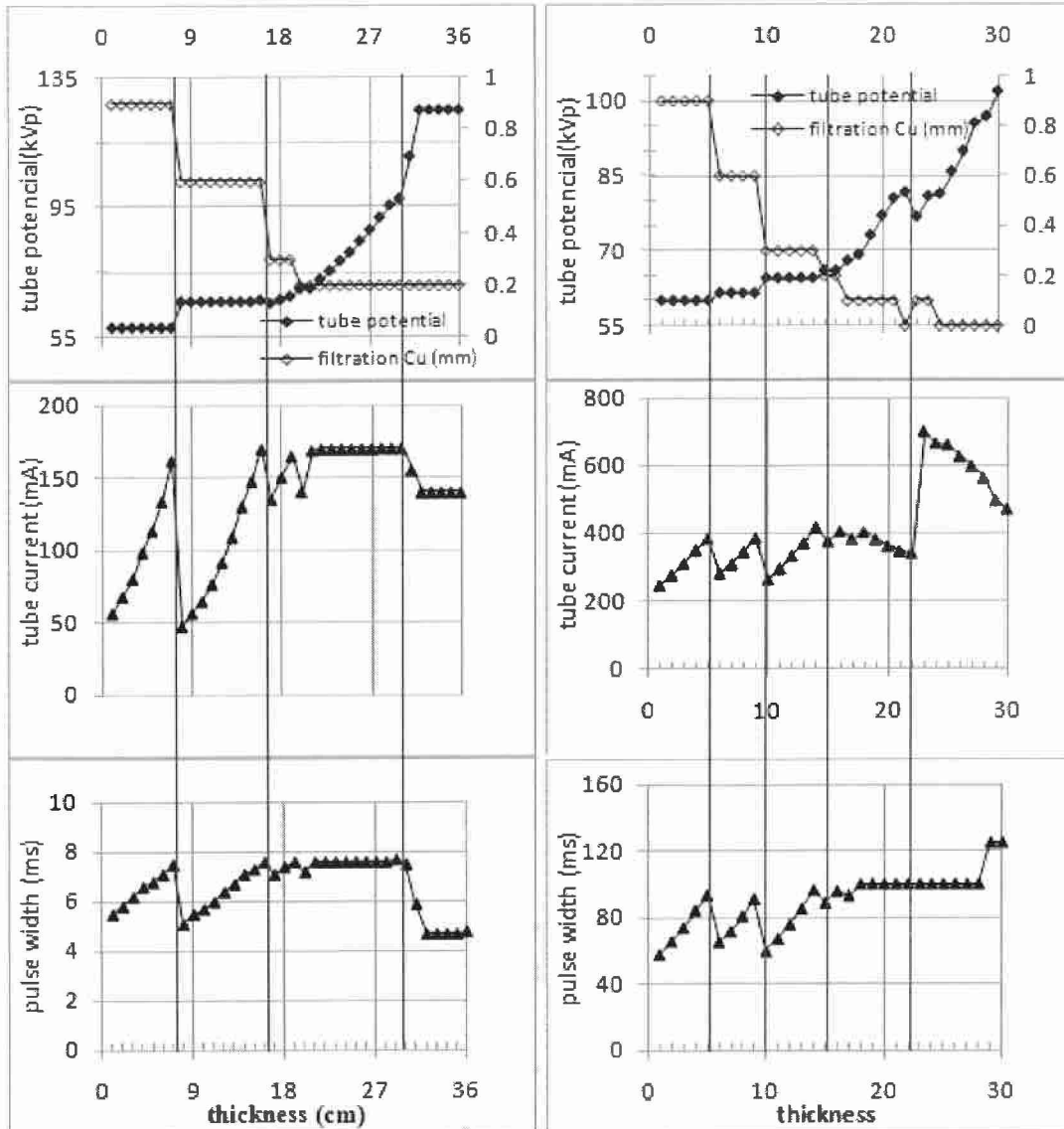


Fig.1

Fig.2

**Fig.1** Various imaging parameters as functions of phantom thickness, for fluoroscopy with FOV=22cm.

**Fig.2** Various imaging parameters as functions of phantom thickness, for exposure with FOV=22cm.

## Dose evaluation of different tumor models using Monte Carlo simulation

Ruo-Lan Chen, Cheng-Ting Shih, Jay Wu

*Institute of Radiological Science, Central Taiwan University of Science and Technology, Taiwan*

### Objectives

The Medical Internal Radiation Dose (MIRD) schema is widely used for internal dose estimation in the nuclear medicine community. As the increase of the radioimmunotherapy, the issue of tumor and normal organ doses caused by administration of specific radioisotopes becomes more important. However, the MIRD reference man cannot take the geometric characteristics of the individual tumor into account. Therefore, the self-absorbed dose of tumors and absorbed dose of normal organs caused by the tumors cannot be estimated accurately. In this study, different tumor models are evaluated to demonstrate the necessity of dose estimation for the individual tumor.

### Methods

The Monte Carlo N-Particle Transport Code (MCNP) version 5 was used. Different shapes of tumor models including ellipsoid, cone, cylinder, and cube with masses of 10 g, 50 g, 100 g, and 300 g were simulated with uniformly distributed  $^{99m}\text{Tc}$ ,  $^{90}\text{Y}$ ,  $^{131}\text{I}$  and  $^{18}\text{F}$ . In addition, we adjusted the dimensions of the 100 g tumor model with different shape described above to evaluate the impact of geometric parameters on the self-absorbed dose. Different shapes of tumor models with a mass of 100 g were inserted into the middle abdomen adjacent to the liver of the ORNL reference man, respectively. Normal organ doses contributed from the tumor model were compared.

### Results

The ratio of the self-absorbed S-values for different shapes and different masses tumor model is above 0.96 for the all radioisotopes. We further changed the dimensions of the 100 g tumor model with long/short axis ratio from 2 to 8. The maximum ratio between different shapes and sphere is 2.4 for 100 g cone distributed with Tc-99m. When we inserted a 100 g cone model instead of a 100 g sphere, the ratio of cross-absorbed dose can up to 121.

### Conclusions

We conclude that although the self-absorbed dose of different tumor models with the same mass has no significant difference, the geometric parameters of the tumor models significantly impact on the normal organ doses. Therefore, real-time Monte Carlo simulation of the individual tumor should be applied to improve the accuracy of dose evaluation of normal organs before radioimmunotherapy.

## Estimations of equivalent breast phantom and breast dosimetry for mammography of Taiwanese women

S L Dong<sup>1</sup>, K S Chuang<sup>1,\*</sup>

<sup>1</sup>Department of Biomedical Engineering and Environmental Sciences, National Tsing-Hua University, Hsinchu, Taiwan

### Abstract

The purpose of this study is to determine the optimal equivalent thickness of a PMMA block used in mammography for Taiwanese women. A screen/film mammographic X-ray unit (SIEMENS, Mammomat 3000) was used. A total of 4147 craniocaudal (CC) projection mammograms were included in this survey. The average CBT of Taiwanese women was  $4.1 \pm 1.0$  cm. The average equivalent thickness of PMMA for Taiwanese women was 4 cm. The average AGD of Taiwanese women in this survey was 1.7 mGy. The results of this study can serve as a basis for further studies to assess image quality and dosimetry of mammography for Asian women.

*Keywords:* Type your keywords here, separated by semicolons;

### 1. Introduction

It is clear that a much higher radiation dose exposes the patient to a higher potential radiation risk, therefore, the average glandular dose (AGD) received must be minimized to achieve the “as low as reasonably achievable” (ALARA) principle in mammography. Since it is not feasible to measure the AGD in the breast of a woman, the AGD must be estimated by using breast phantom. Several breast phantoms, such as standard test block (PMMA material) and standard breast, have been developed for use in mammography. From our previous investigation, we determined that the compressed breast thickness (CBT) and glandularity of the “average breast” of Taiwanese women are distinct from those of the “average breast” of Western women. This indicates that the optimal thickness of the standard test block as derived from assessments of Western women would not be the optimal thickness for Taiwanese women. The purpose of this study is to determine the optimal equivalent thickness of a PMMA block used in mammography for Taiwanese women.

### 2. Materials and Methods

A SF mammographic X-ray unit (SIEMENS, Mammomat 3000) was used, which included three anode/filter combinations that were employed in this work: molybdenum/molybdenum (Mo/Mo), molybdenum/rhodium (Mo/Rh) and tungsten/rhodium (W/Rh). The optical density (OD) setting of the film was 1.6-1.7 under typical clinical conditions. The tube outputs and half-value layers (HVL) were measured for each anode/filter combination associated with a tube potential of 25-28 kV by using a mammographic ionization chamber (Magna; RTI Electronics, Sweden).

A total of 4147 craniocaudal (CC) projection mammograms, of 2180 Taiwanese women, were included in this survey. The imaging parameters of each mammogram were recorded. The imaging parameters of the mammograms included in this study are summarized in **Table I**. The equivalent

**Table I** The imaging and breast parameters of mammograms for each anode/filter combination.

Anode/Filter Combination	Number of Mammograms	Average Age (years)	Average CBT (cm)	Medium kV
Mo/Mo	3063	50.8	3.8	26
Mo/Rh	1001	50.8	5.4	27
W/Rh	83	50.0	6.7	27

thickness and the glandularity of the breast, which was defined as the percentage by mass of glandular tissue in the central region (1990), was determined for each mammogram in an approach similar to that presented by Kruger and Schueler (2001). The AGD of each mammogram was calculated on the basis of the entrance skin air kerma (ESAK), without backscatter, by multiplying a series of appropriate conversion factors, which were published by Dance (1990 and 2000).

### 3. Results and discussion

**Figure 1** shows the distribution of compressed breast thickness (CBT). The range of CBT was 1-8.9 cm in this study. The average CBT of Taiwanese women was  $4.1 \pm 1.0$  cm, which was significant smaller lower than that of American women (5.1 cm) reported by Kruger and Schueler (2001).

**Figure 2** shows distribution of the equivalent thicknesses of PMMA. The range of equivalent thickness of PMMA was 1.7-6.4 cm. The average equivalent thickness of PMMA for Taiwanese women was 4 cm, which was significant smaller lower than that of American women (4.5 cm) reported by Kruger and Schueler (2001).

**Figure 3** shows the relationship between the equivalent thicknesses of PMMA and the CBTs. The results reported by Kruger and Schueler (2001) for American women were also plotted. The relationship between the equivalent thickness of PMMA and the CBT of Taiwanese women in this study is in line with that of American women reported by Kruger and Schueler (2001).

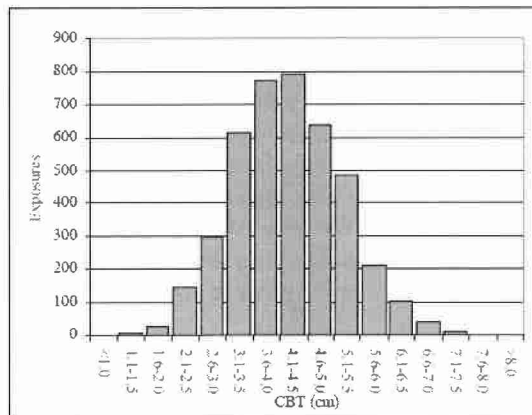


**Figure 1** The distribution of CBTs of Taiwanese women

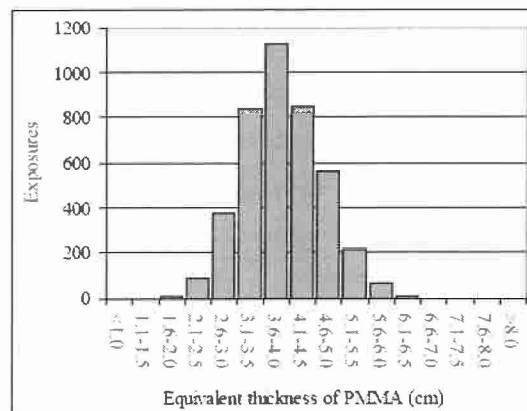


**Figure 2** The distribution of the equivalent thickness of PMMA.

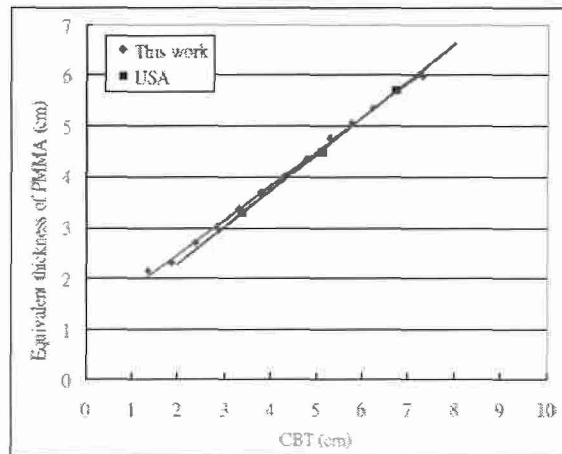


**Figure 3** The variations of the equivalent thickness of PMMA with CBTs.

**Figure 4** shows the AGDs of women in this study. The average AGD of Taiwanese women in this survey was 1.7 mGy. The distribution of the AGDs of women was positively skewed because of the small number of breasts.

**Figure 5** shows the percentage differences between the AGD of each phantom and the average AGD of women in this study. The AGD of each phantom was estimated by using the conversion factors of the 4.5 cm standard breast. The percentage difference of the AGD increases with the thickness of the phantom.

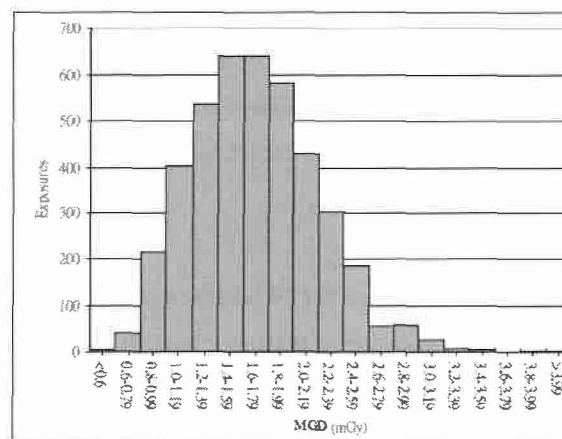


**Figure 4** The distribution of AGDs of Taiwanese women in this survey.

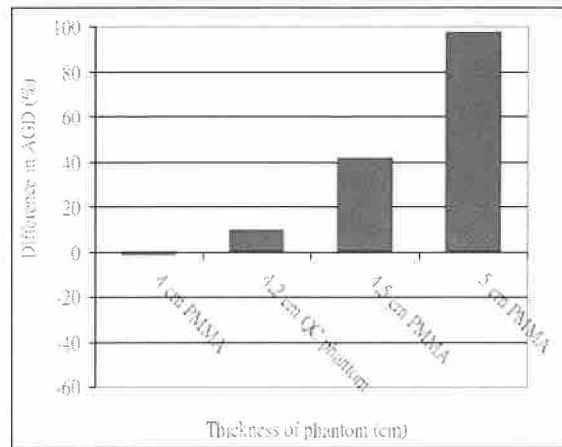


**Figure 5** The percentage differences of AGD for various thicknesses of the phantom.

At present, the use of a 4.5 cm PMMA block to acquire imaging parameters appears to become the most common AGD assessment method for a dose survey. However, the AGD of a 4.5 cm PMMA block was greater than the average AGD of Taiwanese women in this study by 41%. Therefore, it is clear that a substantial overestimation in AGD would be obtained in a national dose survey if the currently used “standard” thickness of the PMMA block applied to AGD assessment in Taiwan. However, the AGD of a 4 cm PMMA block is comparable to the average AGD of women in this study. This indicates that a 4 cm PMMA block appears to be the optimal equivalent breast thickness of Taiwanese women for acquiring imaging parameters in a dose survey.

The AGD of a 4.2 cm QC phantom was greater than the average AGD of women in this study by about 10%. Although the degree of agreement between the AGD of a 4.2 cm QC phantom and the average AGD of women in this study is not perfect, it is informative for definitively establishing the reference values of the AGD by using the 4.2 cm QC phantom combined with a correction factor in a national dose survey.

#### 4. Conclusion

The optimal thickness of a standard test block for Taiwanese women was determined. This information is of great practical importance for the design of mammographical breast phantoms of Taiwanese women. The results of this study can serve as a basis for further studies to assess image quality and dosimetry of mammography for Asian women.

#### Reference

- Dance DR (1990) Monte Carlo calculation of conversion factors for the estimation of mean glandular breast dose. *Phys Med Biol* 35:1211-1219.
- Kruger RL, Schueler BA (2001) A survey of clinical factors and patient dose in mammography. *Med Phys* 28:1449-1454.
- Dance DR, Skinner CL, Young KC, Beckett JR, Kotre CJ (2000) Additional factors for the estimation of mean glandular breast dose using the UK mammography dosimetry protocol. *Phys Med Bi*

## Label-free biomolecular binding kinetics detection with surface plasma wave biosensor

Hsieh-Ting Wu, Hou-Yuan Lo

Department of Medical Imaging and Radiological Sciences, Chung Shan Medical University Taichung 402, Taiwan

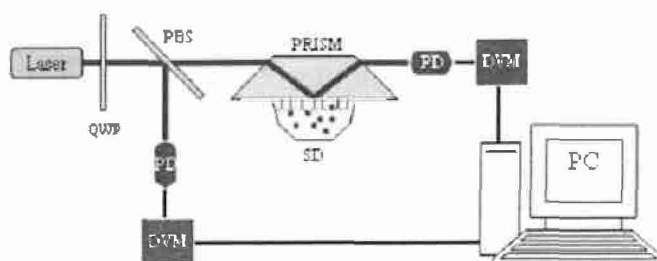
### 1. Introduction

In this study, biomolecular kinetics assay is performed through the use of surface plasma wave (SPW) biosensor, which is based on a label-free and contactless biosensing technique. This biosensing method can detect real-time biomolecular interactions in a localized region near metal/sample surface to get rid of the disturbance of non-specific blending chemical molecules in the reaction solution. Taking advantage of this, the kinetic behavior of target molecules can be truly measured.

C-reactive protein (CRP), an acute phase protein of inflammation is related to the risk factor of cardiovascular diseases and recent medical research reports have demonstrated that CRP is a prognostic indicator of coronary artery disease (CAD) due to its rapid concentration increase within a short period. CRP has at least two distinct forms in conformation, including pentamer (or native) CRP (pCRP) and modified CRP (mCRP). pCRP is a cyclic pentamer composed of five identical, noncovalently bound subunits and mCRP is the dissociated subunit of pCRP with a molecular weight of 23kDa. The expression of different epitopes in a altered conformational form of mCRP is distinct from that of pCRP, which results in the differential binding affinity between antibody and CRP isoforms. Furthermore, mCRP has a higher relativity than pCRP on the development of coronary heart disease. Here, an interferential SPW biosensor is proposed to differentiate the difference in terms of kinetics between pCRP and mCRP quantitatively.

### 2. Materials and Methods

In the experiment, a two-frequency Zeeman laser is adopted to generate a pair of mutually orthogonal with slightly different temporal frequency and linearly polarized laser beam. After



Laser: Zeeman laser; QWP: quarter wave plate; PD: photo detector; SD: sensing device  
PRISM: right angle prism; DVM: digital voltage meter; PC: personal computer

passing through a quarter-wave plate which is placed at a 45° angle to both linearly polarized laser beam, one beam is converted into a state of right-hand circular polarization, and the other one is converted into a state of left-hand circular polarization. These two circular polarized beams then pass through a polarized beam splitter (PBS) to generate two correlated transverse magnetic (TM) waves of different temporal frequency, and two correlated transverse electric (TE) waves are generated for reference beam. The two TM waves are incident into a SPW sensing device in Kretschmann configuration (glass/metal/sample) and the interferential attenuated reflected light is received by a photo detector. Due to molecular adhesion on sample layer, the refractive index and layer thickness are changed; the real-time binding events between molecules on sample layer are recorded through digital voltage meter and personal computer.

In kinetic binding assay, 10 mg/ml sheep anti-human CRP antibody (R&D Systems, Minneapolis, MN) is immobilized onto a CM5 sensing chip (Biacore, Uppsala, Sweden) through amine coupling method. Then, different concentration of human pCRP and mCRP (0.5, 1, 5, 10 µg/ml) are separately added into sensing device to react with the immobilized anti-CRP antibody. Afterwards, the association rate constant  $k_a$  and the dissociation rate constant  $k_d$  are determined by using first-order reaction kinetics given by  $\frac{dR}{dt} = k_a \cdot [Ag] \cdot [Ab] - k_d \cdot R$

where  $R$  is the surface concentration of antigen-antibody complex at time  $t$ .  $[Ag]$  is the concentration of pCRP or mCRP in solution and  $[Ab]$  is the surface concentration of immobilized anti-CRP antibody in this experiment.

### 3. Results and Discussion

The kinetics detection of human pCRP and mCRP interacting with sheep anti-human CRP at various concentrations was measured. Fig. 1 shows a linear response of  $-k_d(-d(dR^*/dt)/dR^*)$  vs. various concentration of human pCRP. The association rate constant  $k_a = 1.30 \times 10^{-6} \text{M}^{-1} \text{s}^{-1}$  and the dissociation rate constant  $k_d = 2.47 \times 10^{-5} \text{s}^{-1}$  were obtained according to the previous formula of first order reaction kinetics. Thus, the equilibrium association constant  $K_A = 2.01 \times 10^{-6} \text{M}^{-1}$  and the equilibrium dissociation constant  $K_D = 4.45 \text{nM}$  were obtained as well. For mCRP, Fig. 2 shows a linear response of  $-ks$  vs. various concentration of mCRP. The association rate constant,  $ka = 9.97 \times 10^4 \text{M}^{-1} \text{s}^{-1}$  and the dissociation rate constant  $kd = 1.67 \times 10^{-3} \text{s}^{-1}$  were obtained. These result the equilibrium association constant  $K_A = 5.97 \times 10^7 \text{M}^{-1}$  and the equilibrium dissociation constant,  $K_D = 16.8 \text{nM}$  in the <mCRP/anti-CRP> interaction. Our experimental results show that the binding affinity between pCRP and anti-CRP is different from that between mCRP and anti-CRP. The equilibrium association constant  $K_A$  between mCRP and anti-CRP is

four orders higher than that between pCRP and anti-CRP. The equilibrium dissociation constant  $K_D$  between mCRP and anti-CRP is four folds higher than that between pCRP and anti-CRP. This means a higher affinity between the epitopes of pCRP and sheep anti-CRP antibody or the number of epitopes of pCRP recognized by sheep anti-CRP is larger than that of mCRP to anti-CRP apparently.

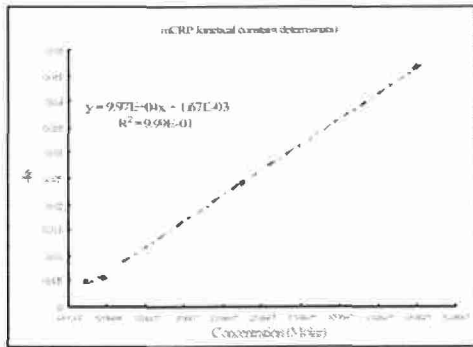


Figure1. pCRP and anti-CRP kinetics determination.

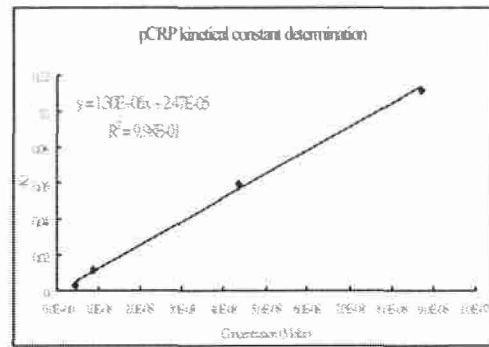


Figure2. mCRP and anti-CRP kinetics determination.

## The Experience of Using Diagnostic Computed Radiography (CR) System to do Quality Assurance of LINAC

Y. T. Cheng , P. Y. Chen , Y. C. Liu

*Department of Radiation Oncology, Chang Gung Memorial Hospital-Linkou Medical Center, Taoyuan ,Taiwan*

**Purpose:** Few years ago, not many new departments of Radiation Oncology had the conventional film processor. During that time, the computed radiography(CR) system used in diagnostic field was very comprehensive. Therefore, we try to use the same system to do the LINAC quality assurance (QA).**Materials and Methods:** First, we use a calibrated accelerator to create a 6MV calibration curve of the imaging plate(IP). The calibration curve of IP is similar to H-D curve of conventional film system. Second, the alignment between radiation field and light field will be completed with appropriate MU and be analyzed accordingly. Third, we will utilize the CR system to check the mechanisms of couch and collimator. **Results:** The absolute dose of the CR system is quite limited, ranging from 0 ~ 20 cGy. Generally, it's not suitable for clinical RT plan verification. However, the alignment between radiation field and light field can be analyzed with CR system. The star shot shows that whether the mechanical error of couch and collimator is within the acceptable range or not. **Discussions:** Although using the CR system need to depend on the direction, but it still can be used for testing the constancy of a LINAC. Therefore, we think that the CR system can be trust for some QA of LINAC.

Keyword: Computed radiography (CR), Quality Assurance (QA), Radiotherapy

### 1 Introduction

In external radiation therapy, it is important to do the quality assurance ( QA ) of a linear accelerator periodically ( LINAC ) ( Kutcher *et al* 1994 ). According to the QA protocol of LINAC, conventional film system is an effectual tool to ensure the alignment of radiation field and light field, field size, radiation center of machine, flatness and symmetry of a field. Few years ago, the computed radiography (CR) system was

introduced in diagnostic field comprehensively. Therefore, many new developed departments of radiation oncology did not have the conventional film processor.

In our department, localization images were routinely taken by diagnostic CR system before starting the treatment. Therefore, we try to use the same system to do the LINAC quality assurance (QA)

## 2 Material and Methods

### 2.1 CR system

The CR system is REGIUS MODEL 190 (Konica Minolta M&G, Inc., Tokyo, Japan). A 1 mm lead is inserted in the cassette to prevent the contamination of low energy photons and to improve the image quality. The geometric size of imaging plate (IP) is 14 by 17 inches (2090 by 2526 pixels). The spatial resolution of the 12 bits image is about 0.17 mm. Therefore, the pixel value distributes from 0 to 4095. To eliminate the potential influence of any post-irradiation fading of the IP (Ang *et al* 2006), the reading was always performed 1.5 minutes after irradiation and erased twice.

### 2.2 Dose Calibration Curve

A Varian iX Linear accelerator, 6MV photon, was used in this study. Every IP has its own character, so we create dose calibration curve for each of them (Fujibuchi *et al* 2006). Three square field sizes, 10 cm, 15 cm, 20cm, and six monitor units (MU), 1MU, 4MU, 8MU, 12MU, 16MU, 20MU, were introduced in this study. The dose will be calculated according to the field sizes factor and the change of MU. The machine was calibrated as following condition: SAD= 100 cm, depth= 5 cm, and field size= 10 x 10 cm. Under above conditions, 1 cGy is equivalent to 1 MU (Fig. 1). In this research, the cassette was always placed at the same position on the couch, and the SSD was kept at 100 cm. The pixel value can be

approximated by:

$$\text{Pixel Value} = a * \ln(D) + b \quad (1)$$

Where D is the absolute dose, pixel value is read from CR system directly, a and b are constant.

### 2.3 Dose Profile and Star Shot

According to our dose calibration curve as below (fig.2), the absolute dose can be figured approximately by pixel value, and the relative dose profile like some reports before (Homma *et al* 2002). After a cassette irradiated by 10 MU with several field sizes, some general QA items, the alignment of radiation field and light field, physical field size, can be analyzed from it. After many times of exposure as our plan, some data, like the alignment, field size, radiation center of machine, flatness and symmetry of a field can be got. These data was useful in QA after carefully analyzing. The dose profile will be compared with the result of "Proflier2" (Sun Nuclear Corporation, Melbourne, FL), step size is 4 mm.

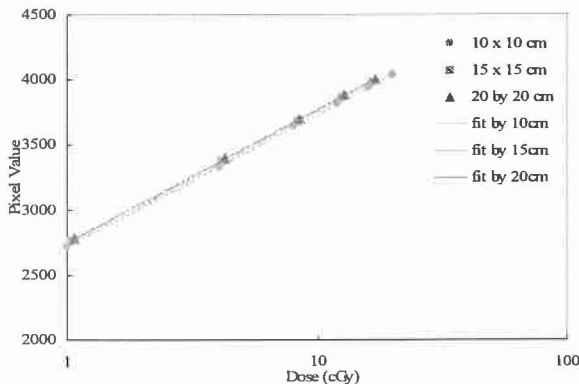
In order to get the start shots of collimator and couch, we placed the cassette perpendicular to the central axis of gantry. However, the cassette must be placed perpendicular to the rotation axis of gantry in order to get the star shot of gantry. At the same time, we kept the same field size for every single exposure was 3 MU. The upper and lower jaws were also kept at 40 cm and 0.2 cm. By analyzing the images, we can understand the radiation center of machine is

tolerable or not.

### 3 Results

#### 3.1 Dose calibration Curve

According to the data we collected, different field size makes different dose calibration curve ( Fig. 2 ). We also take 5MU, 10MU and 15MU images to compare the dose difference between them and the calculated dose by the curve, all absolute dose differences are smaller than 0.76%. However, when dose is over than 20 cGy, the IP is almost saturated. If a calibration curve was created by all data points we got, the smallest dose difference was more than 1.43%, but most of them were over 2%. The parameters, a and b, of equation (1) are calculated by the data



we collected and showed in table 1.

**Fig. 2** Cheng\_Dose Calibration Curve. Each field size has its own calibration curve. However, the  $R^2$  value of all three curves are approximate to 1.

Parameters Field size(cm)	a	b
10 x 10 cm	441.82	2717.5
15 x 15 cm	442	2740.6
20 x 20 cm	442.28	2754.1

**Table 1** Cheng\_Parameters of dose calibration curve. The parameters we get from different dose calibration curve with different field sizes.

#### 3.2 Dose Profile and Star Shot

When the field size is 20 x 20cm, the parameters  $a=442.28$  and  $b=2754.1$ , can be calculated by the dose calibration curve. Furthermore, dose matrix of the field can also be calculated. The dose profile, Y-axis along gantry-couch direction, of field size 20 x 20 cm is illustrated and compared with the results of “PROFILER2” ( Fig. 3 ).

Dose profile can provide some helpful information, like symmetry, flatness, field size of a field, for us to ensure the quality of beam. The results of “PROFILER2”, symmetry is  $-0.6619\%$ , flatness  $1.424\%$ , field size is  $20.06\text{cm}$ . The “normal” curve is trended to right side, but the “reverse” is trended to the left side in figure 3. The field sizes of “normal” and “reverse” curves are  $19.87 \pm 0.01 \text{ cm}$ , and they are in our acceptable range. However, we can’t use the dose profile to analyze the symmetry and flatness of the field size.

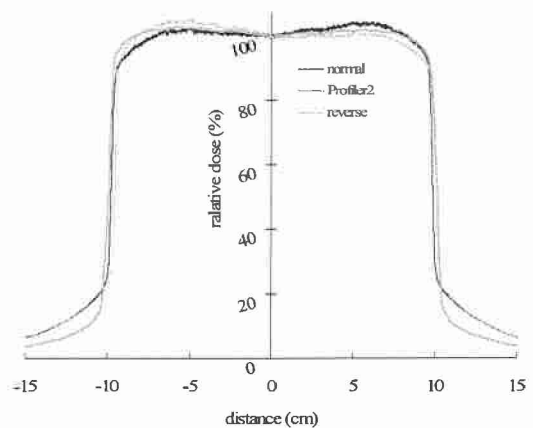


**Fig. 3** Cheng\_Dose Profile of Y-axis. Normal: direction of cassette is the same to clinical use ( $0^\circ$ ). Profiler2: the result from Profiler2. Reverse: rotate cassette  $180^\circ$ .

The star shot shows the radiation center of gantry, collimator and couch are all within the acceptable range, run out smaller than 1mm ( Fig. 4 ).

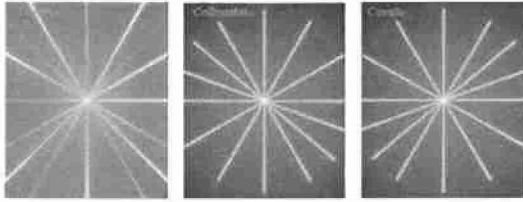


**Fig. 4** Cheng\_Star Shot: The star shot of gantry, collimator and couch are shows that radiation center is not run out than 1mm.

#### 4 Discussion

The dose calibration curve shows that the diagnostic CR system can't detect the exposure dose more than 20cGy. As the results of figure 2, we suggest the appropriate range of dose is between 1 to 16 cGy, and different field size needs its own calibration curve. It is not a good tool for validating the dose in radiation treatment plan, because the IP is so limited. Although the parameters, a and b, of equation (1) are getting larger with the increasing of field size slightly, but we have not found any relationship between them, now.

In common, the dose profile can offer us some useful information of a LINAC, like symmetry and flatness of a field. Nevertheless, from figure 3, we can't get these messages from the dose profile provided by the CR system. The "normal" and "reverse" profiles told us that all the pixels of IP need to be calibrated, because the profiles are almost reverse. In order to calibrate IP, a large and uniform field size is necessary.

However, it is a tough task for a LINAC .

In our experience, the response to radiation of each pixel is so stable, and this character can be used to check the constancy of a LINAC. For above reason, we can use CR system to create dose profile right after the acceptance test for standard. Thus, further dose profile can be used as a power tool for the QA, if it is the same as the initial data, even the IP is not calibrated. Even though the IP need to be calibrated, the modification is about 5~10%, and the drop-off of the penumbra is great. We always keep the setup error of cassette position within 0.5mm. Therefore, the results of alignment between light field and radiation field can still be trusted.

The brightness of radiation lines of gantry are not homogeneous in the star shot of figure 4. They are affected by frame of cassette and the radiation path. Star shot image is so easy to analyze by some free software like "Image J".

#### 5 Conclusion

Some QA of a LINAC can still be performed by the diagnostic CR system. Although, some problems still need to be resolved, but we still consider that it is a convenient QA tool in high-energy photon therapy. We expected that we can use the CR system to create an easier way to calibrate the IP to replace the conventional film system in the future.

**Reference**

- Ang DB, Angelopoulos C, Katz JO 2006 How does signal fade on photo-stimulable phosphor imaging plates when scanned a delay and what is the effect on image quality *Oral Surg Oral Med Oral Pathol Oral Radio Endod.* 102(5) 673-9
- Attaelmanan AG, Borg E, Grondahl HG. 2001 Signal to noise ratios of 6 intraoral digital sensors. *Oral Surg Oral Med Oral Pathol Oral Radio Endod.* 91(5) 611-5.
- Fujita M, Yamaguchi M, Katsuda T, Sakamoto H, Fujioka T, Tada T, and Azuma M 2005 Verification imaging using a computed radiography system for high-energy electron beam therapy *Radiat Med.* Vol. 23(8) 550-6
- Fujibuchi T, Funabashi N, Hashimoto M, Abe Y, Iimori T, Matubayashi F, Sawada K, Kurokawa M, Isobe T Kikawa T, Komuro I 2006 Examination of beam profile measurement using an imaging plate by the light exposure fading method for quality assurance of external radiation therapy *Nippon Hoshasen Gijutsu Gakkai Zasshi.* Vol. 62(12) 1697-706
- Homma M, Tabushi K, Obata Y, Tamiya T, Koyama S, Ishigaki T 2002 A method for measuring the dose distribution of the radiotherapy domain using the computed radiography system. *Jpn J Med. Phs.*, Vol. 22(2)118-24
- Kutcher GJ, Coia L, Gillin M, Hanson WF, Leibel S Morton RJ, Palta JR, Purdy JA, Reinstein LE, Svensson GK, *et al.* 1994 Comprehensive QA for radiation oncology: report of AAPM Radiation Therapy Committee Task Group 40. *Med Phys*, 21(4) 581-618.
- Olch AJ 2005 Evaluation of a computed radiography system for megavoltage photon beam dosimetry *Med Phys.* Vol. 32(9) 2987-99
- Sonoda M, Takano M, Miyahara J, Kato H 1983 Computed radiography utilizing scanning laser stimulated luminescence. *Radiology.* Vol. 48(3) 833-8

## Assessment of Image Quality and Radiation Dose Reduction with In-plane Bismuth Shielding for CT Examinations: Phantom Study

Ying-Lan Liao<sup>1</sup>, Hui-Yu Tsai<sup>2,\*</sup>, Yu-Sheng Tyan<sup>3</sup>, Kai-Yuan Cheng<sup>1</sup>

<sup>1</sup>*Institute of Radiological Science, Central Taiwan University of Science and Technology, Taichung, Taiwan*

<sup>2</sup>*Department of Medical Imaging and Radiological Sciences, Chang Gung University, Tao-Yuan, Taiwan*

<sup>3</sup>*Department of Radiology, Chung-Shan Medical University Hospital, Taichung, Taiwan*

### Purpose

The purpose of this study is to assess the image quality and radiation dose reduction using bismuth shields during in-plane CT scanning.

### Materials and Methods

Bismuth shields were used to filter the low-energy photons to reach an ACR CT accreditation phantom. Foam rubber was placed between bismuth shields and phantom surface to decrease the beam hardening artifact at the interface. Images were acquired by Siemens Sensation 64 CT scanner with four kVps. Image quality affected by bismuth shields, including CT number variation (CTN  $\Delta$ ), contrast-to-noise ratio (CNR), noise ratio, contrast ratio and artifacts, were estimated. Image quality in adjacent zone (A-zone), i.e. close to shield, and in distant zone (D-zone), i.e. far from the shield, was compared. The CT numbers, CNRs, and image noises were compared between shielded image versus unshielded images (paired t test) no matter in A-zone or D-zone. The radiation dose reduction was measured with high sensitive thermoluminescent dosimeters (TLDs).

### Results

Radiation dose reduction factor are 0.93-0.85, 0.68-0.76, 0.58-0.65, 0.58-0.64, 0.48-0.58, 0.40-0.53 for 1 to 6-ply bismuth shields, respectively. After shielding, the CT number differences comparing shielding images with unshielding images for water, polyethylene, acrylic, and air, all increased (0.2 ~ 49.5 HU), whereas that of bone decreased (-2.6 ~ -53.1 HU). The CT number differences were larger in A-zone than that in D-zone. However, the variations of CNR in A-zone were slightly larger than those in D-zone. The noise increased after shielding, and the noise ratio which is comparing shielding with unshielding images are 1.03-1.34 for A-zone and 1.03-1.22

for D-zone at 120 kVp. The contrast ratios diminished from 1.05 to 0.87 when the shielding thickness increased, and they changes significantly in A-zone. A review of all studies revealed that no artifact was caused by the presence of shields. Differences in CT number, CNR, and image noise between with and without shields are statistically significant both in A- and D-zone.

### **Conclusion**

Bismuth shields could filter useless low energy radiation and protect radiosensitive organs. The shields coated with foam rubber which keeps shields away from patient surface to diminish beam hardening artifact and to maintain the diagnostic acceptability. The radiation dose reduction with in-plan shields is remarkable. Covering the bismuth shields on patients potentially changes the CT number accuracy, but it has only slight impact on image contrast. The CT number variation is slightly apparent in A-zone. However, the variations are acceptable. The in-plane bismuth shields are suggested to properly use as a standard procedure during routinely CT examinations.

**Keywords:** Computed tomography, in-plane shield, bismuth, image quality, radiation dose reduction

## Development of nucleoside radiotracers via in situ screening of HBTU amide forming libraries for imaging HSV-1 tk cancer gene therapy

Li-Wu Chiang, <sup>a</sup>Jia-Rong Chen, Hao-Lien Huang<sup>a</sup> Wen K. Yang, <sup>b</sup> Chung-Shi Yang<sup>c</sup>, Li-Chen Wu<sup>d</sup> and Chung-Shan Yu<sup>a\*</sup>

<sup>a</sup>*Department of Biomedical Engineering and Environmental Sciences, National Tsing-Hua University Hsinchu, Taiwan*

<sup>b</sup>*Laboratory of Cell/Gene Therapy, Clinical Medical University Hospital, Taichung, Taiwan*

<sup>c</sup>*The Center for Nanomedicine Research, National Health Research Institutes, Miaoli, Taiwan*

<sup>d</sup>*Department of Applied Chemistry, National Chi-Nan university, Nanto, Taiwan*

---

### Abstract

To monitor cancer gene therapy, PET (positron emission tomography) or SPECT (single photon emission computed tomography) instruments combined with HSV-1 tk (herpes simplex virus type 1 thymidine kinase) or its mutant HSV-1-sr39tk reporter gene have been developed. In addition, [F-18]FHBG, a nucleoside analog, has been approved by the US Food and Drug Administration as an investigational imaging agent recently. For developing nucleoside radiotracers rapidly and efficiently, we introduced HBTU amide forming libraries of nucleoside analogs followed by in situ screening via MTT cytotoxic assay to find out new potential radiotracers for probing HSV-1 tk. During this high throughput screening (HTS), we found that the fragment structure of arabinosyl uridine seems to be more active against HSV-1 tk than ribosyl uridine and ribosyl dihydrouridine. Besides, 4-(4-Chloro-phenyl)-4-oxo-butylamide of arabinosyl uridine analog had 14 times survival ratio between HSV-1 tk transfected cells and native cells. The following purification of this arabinosyl uridine analog to confirm its bioactivity is in progress and the next radioiodo or radiofluoro labeling on 5-uracil are going to be carried out after confirmation.

**Keywords:** HSV-1 tk, reporter gene, PET, SPECT, radiotracers, nucleoside analogs, HBTU amide forming libraries, in situ screening

**Reference**

1. de Vries, E. F. J.; Buursma, A. R.; Hospers, G. A. P.; Mulder, N. H.; Vaalburg, W. *Curr. Pharm. Des.* 2002, 8, 1435.
2. 姜豐武, 羅建苗, 俞鐘山. *中國化學會化學季刊* 2006, 64, 179.
3. Michael E. P. *J. Nucl. Med.* 2000, 41, 661. 4.
4. Kim, E. E.; Yang, D. J. *Targeted Molecular Imaging in Oncology* Springer, 2001
5. Brik, A.; Wu, C.-Y.; Wong, C. H. *Org. Biomol. Chem.* 2006, 4, 1446.
6. Lo, J.-M.; Chiang, L.-W.; Chen, S.-W.; Fu, Z.-W.; Pei, K.; Yu, C.-S. *Chim. Oggi.* 2007, 25, 46.
7. Lei Zhang, L.; Sun, F.; Li, Y.; Sun, X.; Liu, X.; Huang, Y.; Zhang, L.-H.; Ye, X.-S.; Xiao, J. *ChemMedChem* 2007, 1, 1594.
8. Pei, K. *MS Thesis* 2007 (Natl. Tsing Hua Univ.)
9. Deng, W. P.; Wu, C. C.; Lee, C. C.; Yang, W. K.; Wang, H. E.; Liu, R. S.; et al. *J. Nucl. Med.* 2006, 47, 877.

## Using Diffusion Tensor Index Analysis Citrus Water Distribution

Yun-Ya Huang

*School of Medical Imaging and Radiological Sciences, Chung Shan Medical University*

### 研究目的

利用核磁共振造影可以不破壞外表而得到測量物的內部影像的一大特性，本研究希望能用核磁共振造影來檢視有日照充分和日照較少的柑橘類其內的水分的含量變化，以期望本研究可以在生物產業的研究上有更多的幫助。

### 材料與方法

我們選擇國產的桶柑來做為實驗水果，取樣為摘取同一棵果樹上葉子多和葉子少的部份各 10 顆，在水果不同取樣條件下送進 MRI 取得其內部影像。將水果外包覆一層純水的介質並利用 diffusion 的波序，選擇頭部的線圈來進行實驗。將取得的影像利用 MATLAB 的 DTI 程式去計算出水分子擴散係數 ADC 值和等項性指標 FA 值來評估水果內部的水分含量分佈以及纖維素量的多寡。

### 結果

- (1) 分析桶柑在不同的日照充分條件下其內部水分分佈的影響，作成一相對圖表檢視。
- (2) 分析桶柑在不同的日照充分條件下其內纖維含量分佈的影響，作成一相對圖表檢視。

### 討論

對水果而言，人們常常以「汁多味美」來形容其好吃的程度。在詳細紀錄各日照方位和目測觀察水果表面的充分條件下，本研究希望能利用 DTI 來找出柑橘類水果在有無日照中水分的變化。最後由這些數據來評估柑橘類水果的內部結構變化和日照多寡的關係。預期在日照較少的水果其水分分佈也較日曬充分的水果來的多。

## Validation of a PET Monte Carlo Simulator for $^{18}\text{F}$ and $^{124}\text{I}$ PET imaging

Hsin-Hon Lin<sup>a</sup>, Yi-Hsing Lin<sup>a</sup>, Shih-Chi Lu<sup>a</sup>, Han Kuo<sup>a</sup>,  
Chang Shiun Lin<sup>a</sup>, Keh-Shih Chuang<sup>a</sup>

<sup>a</sup> *Department of Biomedical Engineering & Environmental Sciences  
National Tsing-Hua University, Taiwan*

### Purpose

Non-pure positron radionuclides compared with the conventional positron emitters have advantages of longer half life and target-specific. It's suitable for studying prolonged biological process and drug analogues in animals. However, these radionuclides also emit cascade gamma rays (called associated gamma) that may be detected within the energy window and cause additional scatter and random coincidences with the annihilation photons.

In this study, our purpose is to perform Monte Carlo simulations of PET tomograph for F-18 and I-124 isotope with SimSET (Simulation System for Emission Tomography) Monte Carlo software.

### Materials & Methods

The SimSET software (a Simulation System for Emission Tomography ) is widely used in nuclear medicine, but its current model didn't provide the simulation of non-pure positron emitters. In order to perform the characteristics of PET system, we integrated a module for radioactive decay scheme to support the non-pure positron emitter. The modified SimSET software for non-pure positron emitters was validated by comparison to the general purpose Monte Carlo transport code (GATE) that has been extensively validated. A phantom studies was performed to evaluate the effects of these non-true coincidences to the imaging of F-18 and I-124 positron emitter on the PET scanner.

### Results & Conclusion

Preliminary results indicate that the modified SimSET software for F-18 and I-124 positron emitter gets rather good agreement with GATE simulator. Our new model allows fast and accurate modeling of PET acquisition for the non-pure positron emitter. We will explore the possibility of fully Monte Carlo simulation to correct all the non-true coincidences for the non-pure positron emitter in the future.

**Keywords :** PET, Monte Carlo simulation, non-pure isotope

## The profit of Independent component analysis on determining the artery input function in dynamic susceptibility contrast MRI

Sharon Chen<sup>1</sup>, Keh-Shih Chuang<sup>1</sup>, Yuan-Yu Hsu<sup>2</sup>, Ho-Ling Liu<sup>3,4\*</sup>

<sup>1</sup> Faculty of Medical Radiology, Kaohsiung Medical University, Kaohsiung, Taiwan

<sup>2</sup> Department of Biomedical Engineering and Environmental Sciences, National Tsing-Hua University, Hsin-Chu, Taiwan

<sup>3</sup> Radiology Department, Buddhist Tzu-Chi General Hospital – Taipei, Taipei, Taiwan

<sup>4</sup> Department of Medical Imaging and Radiological Sciences, Chang-Gung University, Tao-Yuan, Taiwan,

<sup>5</sup> MRI Center, Chang-Gung Memorial Hospital, Tao-Yuan, Taiwan

**Objective.** Quantitative cerebral blood flow (CBF) measurement using dynamic susceptibility contrast (DSC) MRI requires accurate estimation of the arterial input function (AIF). The present work utilized the independent component analysis (ICA) method to determine the AIF from T2 signal changes in the regions adjacent to the middle cerebral artery (MCA). The determined AIF was employed to calculate absolute CBF because of the alleviated confounding of partial volume effect. Absolute CBF can be calculated by the AIF derived from the ICA and compared with manually determined AIF.

**Subjects and Methods.** A series of spin-echo EPI MR scans (1.5 Tesla, TR = 1.5 s, TE = 60 ms, 7 axial slices, slice thickness = 6 mm, matrix size = 64 × 64, in-plane resolution = 3.4 mm × 3.4 mm, 60 dynamic measurements) were performed in 10 normal subjects. All subjects received 0.2 mmol/kg Gd-DTPA contrast agent. AIFs were calculated by two methods: (1) from the region of interest (ROI) selected manually and (2) weighted average of each component selected by ICA (weighted ICA). The ICA produced 40 spatially independent maps (cover 99% of the eigenvalues). These maps were examined to select two interest maps: map (ICA-aw) of artery and map (ICA-sw) of tissue around middle cerebral artery (MCA). The AIF candidate voxels were selected from the fifty largest voxels of z-value (z-value was defined as  $z_i = \frac{x_i - \text{mean}(\text{map})}{\text{Std}(\text{map})}$ ). Afterward, the AIF was determined after weighting:

$AIF = \sum_{roi} Q \times C_{roi}$ , where Q is the weighting from z-value and C is the concentration of

selected voxels. The CBFs were compared from these two AIF determinations after adaptive singular value decomposition (SVD) calculation<sup>5</sup>.

**Results.** Three selected ROIs for AIF determination with Manu-roi and ICA-weighting methods are presented in Figure 1. ICA alleviates partial volume

effect and results in better boundary discrimination and less inter-subject variance. The corresponding time courses show physiological properties of blood from these three regions, such as a recirculation response for artery and a flatter response for surrounding tissue (see Figure 2). The CBF values calculated by the weighted ICA method were  $41.1 \pm 4.9$  and  $22.1 \pm 2.3$  mL/100g/min for cortical gray matter (GM) and deep white matter (WM) regions, respectively. The CBF values obtained based on the manual ROIs were  $53.6 \pm 12.0$  and  $27.9 \pm 5.9$  mL/100g/min for the same two regions, respectively. The CBF values and GM/WM ratios obtained from both methods were in good agreement with those found in the literatures<sup>6</sup>.

**Discussion.** In this study, two ICA weighting ways are used to determine AIF: average and weighting average. The comparison (see Figure 2) between average-ICA and weighted-ICA showed that there was no significant difference because the selected voxels are highly consistent each other. Therefore the partial volume effect within these voxels had a limited influence. In conclusion, this work provides three benefits to achieve the more precise calculation of CBF: (1) ICA provides a semi-automatic tool to select interest component; (2) ICA decomposes signal without partial volume effect; (3) ICA determines AIF in the tissue around artery for CBF quantification.

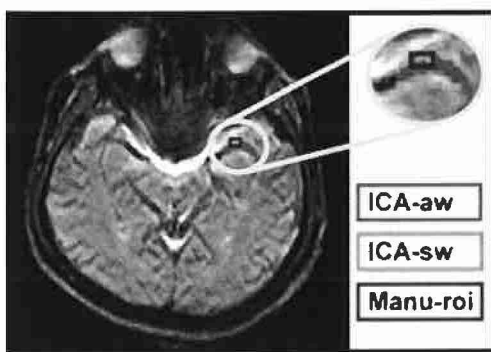


**Figure 1.** Regions selected by manual ROI and ICA method ( blue: manual selection; red and green: artery and its surrounding tissue selected by weighted-ICA). The bigger VOI are shown in the subsection figure.

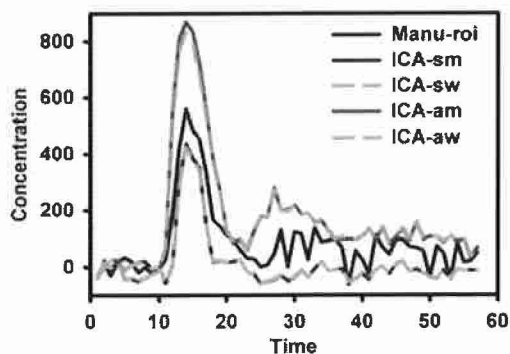


**Figure 2.** Different AIFs were determined by (1) the artery with weighted-ICA (red solid line); (2) average of the artery with manual ROI (blue line); (3) surrounding tissue with weighted-ICA (dark green solid line). This figure also shows the result for the average-ICA in the regions of artery and the surrounding tissue with pink dash line and green dash line, respectively.

**Key Words:** MRI, Cerebral blood flow (CBF), Arterial input function (AIF), weighted Independent component analysis (weighted-ICA).

## Image Restoration By Using Wiener Filter

Yi-Lin Chen<sup>a</sup>, Hui-Jun Yang<sup>a</sup>, Chang-Shiun Lin<sup>a</sup>, Hsin-Hon Lin<sup>a</sup>, Keh-Shih Chuang<sup>a</sup>

<sup>a</sup> *Department of Biomedical Engineering & Environmental Sciences  
National Tsing-Hua University, Taiwan*

### Purpose

Recent technological advances have made digital radiology a practical alternative to the film-based system. The relation between noise and image quality is always an important issue. We propose a hybrid method which combine Moran test and Wiener filter to estimate noise distribution and restore image, hoping the method can improve image qualities of the degraded image and increase correct diagnosis-rate.

### Materials and Methods

We assume that the data bits of a pixel in digital images can be divided into signal and noise bits. The signal bits occupy the most significant part of the pixel and the noise bits occupy the least significant part. The signal parts are correlated of each pixel while the noise parts are uncorrelated. According to the difference of signal and noise bit, using Moran test divided the pixel of image into signal bits and noise bit then redistributes the pixels of the image. Finally noise distribution and power spectrum can be estimated.

Assume the degradation function is uniform and homogeneous. The noise information estimated prior treated as a parameter of Wiener filter, and a degraded image can be restored correctly by the Wiener filter. The compression ratio calculated by Huffman coding used to assess the proposed method.

### Results& Conclusion

The preliminary results show the proposed method could remove noise of the degraded data effectively and correctly. Wiener filter is effective and correct as noise power spectrum, which estimated by Moran test, have known. By this method, we can get correct quantization and increase the image quality. The method can be applied in clinical flexible and fast.

**Keywords:** Moran Test, Wiener Filter, Image Restoration.

## **The uncertainties of diagnostic X-ray machines**

Weng-Song Feng and Tzong-Jer Chen

*Department of Medical Imaging and Radiology, Shu Zen College of Medicine and Management, Lujun Kaohsiung, 82144 Taiwan*

There are several X-ray machines use different type of generator clinically in medical hospitals nowadays, for example, high frequency X ray machine and X ray machine of full wave rectifier and 12 pulse. Will the image quality and radiation dosimetry have consistency when these different type of generator machine operated by radiation therapist to scan patients.

The main purpose of this experiment is based on ISO 13528 to calculate interlaboratory total uncertainty ( $E_n$ ), analyze the variety of output voltage, accumulated exposure time, exposure rate and dose area product (DAP  $\text{kerma}/\text{cm}^2$ ) using different X ray machines. This experiment focuses on two types of generator X ray machines, SEHWA-325 (high frequency generator of 4KHz) and SEHWA-325-GM (full wave rectifier of 60Hz and 12 pulse), which both use the same Toshiba Model-E7239 X ray tube.

This research measure the voltage, timing, exposure rate, and DAP values of these two X ray machines by Fluke Victoreen 4000M+ and calculate the total uncertainty ( $E_n$ ) after measurement. Under different voltage (50~110 kVp),  $E_n$  value of two X ray machines is between 0.03 and 2.1, average 0.68, which is in an acceptable range ( $\leq 1.0$ ). However, the voltage raise causes the  $E_n$  value to increase, which means high voltage increases uncertainties. Exposure time change causes  $E_n$  value between 0.01 and 0.36, average 0.15. Also, the  $E_n$  value decreases, which is acceptable while voltage increases. Nevertheless, voltage change causes high  $E_n$  value of exposure rate between 8.3 and 37.0, average 20.62, and high  $E_n$  value of DAP between 33.56 and 82.06, average 20.62. The higher voltage, the higher uncertainties are.

The result of  $E_n$  value calculation explains high frequency X ray machine and full wave rectifier X ray machine are acceptable in voltage and exposure time change, but diversity of exposure rate and DAP value. Exposure rate and DAP value of X ray machine of full wave rectifier tend to low, while high frequency X ray machine use the same condition to scan, it will cause the DAP shortage and image brighter, increase the percentage of high reject and repeat images, and have an impact on the patient's dosimetry

**Evaluation of iodo, fluoro, iodovinyl arabinosyl uridines against HSV-1 tk transfected murine sarcoma cells with MTT cytotoxic assay and their potential for imaging cancer gene therapy**

Li-Wu Chiang, <sup>a</sup>Jia-Rong Chen, Hao-Lien Huang<sup>a</sup> Wen K. Yang, <sup>b</sup> Chung-Shi Yang<sup>c</sup>, Li-Chen Wu<sup>d</sup> and Chung-Shan Yu<sup>a\*</sup>

<sup>a</sup>*Department of Biomedical Engineering and Environmental Sciences, National Tsing-Hua University Hsinchu, Taiwan*

<sup>b</sup>*Laboratory of Cell/Gene Therapy, Clinical Medical University Hospital, Taichung, Taiwan*

<sup>c</sup>*The Center for Nanomedicine Research, National Health Research Institutes, Miaoli, Taiwan*

<sup>d</sup>*Department of Applied Chemistry, National Chi-Nan university, Nanto, Taiwan*

---

**Abstract**

Up to now, the challenge of cancer gene therapy is how to deliver suicide gene to target tissue or organ. In order to monitor therapeutic gene, PET (positron emission tomography) or SPECT (single photon emission computed tomography) instruments combined with HSV-1 tk (herpes simplex virus type 1 thymidine kinase) or its mutant HSV-1-sr39tk reporter gene have been developed and [F-18]FHBG, a GCV analog, has been approved by the US Food and Drug Administration as an investigational imaging agent recently. In this study, we evaluated the potential of iodo, fluoro, iodovinyl arabinosyl uridines (IaraU, FaraU, IVaraU) for imaging HSV-1 tk with MTT cytotoxic assay using murine sarcoma cell model. We found out that both FaraU and IaraU in 1 nM had significantly different survival ratio between HSV-1 tk transfected cells and native cells. However, the concentration of GCV had to be greater than 10-100 nM to make different survival ratio between transfected cells and non transfected cells. This study indicated that both FaraU and IaraU have more potential than GCV for probing wild-type HSV-1 tk reporter gene.

**Keywords:** HSV-1 tk, reporter gene, PET, SPECT, [F-18]FHBG, FaraU, IaraU, IVaraU, suicide gene, GCV

**Reference**

1. Chiang, C. S.; Yu, C. F.; Chiang, L. W.; Chen, S. W.; Lo, J. M.; Yu, C. S. *Chem. Pharm. Bull.* 2008, 56, 109.
2. de Vries, E. F. J.; Buursma, A. R.; Hospers, G. A. P.; Mulder, N. H.; Vaalburg, W. *Curr. Pharm. Des.* 2002, 8, 1435.
3. 姜豐武, 羅建苗, 俞鐘山. *中國化學會化學季刊* 2006, 64, 179.
4. Michael E. P. *J. Nucl. Med.* 2000, 41, 661.
5. Kim, E. E.; Yang, D. J. *Targeted Molecular Imaging in Oncology* Springer, 2001
6. Yu, C. S.; Chiang, L. W.; Wu, C. H.; Hsu, Z. K.; Lee, M. H.; Pan, S. D.; Pei, K. *Synthesis* 2006, 22, 3835.
7. Yu, C. S.; Chiang, L. W.; Wu, C. H.; Wang, R. T.; Chen, S. W.; Wang, H. Y.; Yeh, C. H. *Nucl. Med. Biol.* 2006, 33, 367.
8. Yu, C. S.; Wu, C. H.; Chiang, L. W.; Wang, R. T.; Wang, H. Y.; Lin, K. I. *Chem. Lett.* 2005, 34, 1390.
9. Deng, W. P.; Wu, C. C.; Lee, C. C.; Yang, W. K.; Wang, H. E.; Liu, R. S.; et al. *J. Nucl. Med.* 2006, 47, 877.

# Development of nucleoside radiotracers via *in situ* screening of amide forming libraries for imaging HSV-1 tk cancer gene therapy

Jia-Rong Chen<sup>a</sup>, Li-Wu Chiang<sup>a</sup>, Wen K. Yang<sup>b</sup>, Chung-Shi Yang<sup>c</sup>,  
Li-Chen Wu<sup>d</sup> and Chung-Shan Yu<sup>a,e</sup>.

<sup>a</sup>*Department of Biomedical Engineering and Environmental Sciences, National Tsing-Hua University Hsinchu, Taiwan*

<sup>b</sup>*Laboratory of Cell/Gene Therapy, China Medical University Hospital, Taichung, Taiwan*

<sup>c</sup>*The Center for Nanomedicine Research, National Health Research Institutes, Miaoli, Taiwan*

<sup>d</sup>*Department of Applied Chemistry, National Chi-Nan university, Nanto, Taiwan*

<sup>e</sup>*Institute of Nuclear Engineering and Science, National Tsing-Hua University Hsinchu, Taiwan*

## Abstract

To monitor cancer gene therapy, PET (positron emission tomography) or SPECT (single photon emission computed tomography) instruments combined with HSV-1 tk (herpes simplex virus type 1 thymidine kinase) or its mutant HSV-1-sr39tk reporter gene emerged as an important tool. For developing nucleoside radiotracers efficiently, a library of nucleoside analogs through rapid amide-forming reaction followed by *in situ* screening via MTT cytotoxic assay to probe HSV-1 TK was developed. From this screening, the core structure with arabinosyl uridine moieties is more active against HSV-1 tk than ribosyl uridine and ribosyl dihydrouridine moieties. Besides, chloro-phenyl-oxo-butamide of arabinosyl uridine analog (AC13) exerted a selective index of 14 between HSV-1 tk transfected cells and native cells. The subsequent preparation and purification of this arabinosyl uridine analog to confirm its bioactivity is in progress and the subsequent radioiodo and radiofluoro labeling on 5-uracil will be performed in due course.

*Keywords:* HSV-1 tk, reporter gene, PET, SPECT, radiotracers, nucleoside analogs, amide-forming libraries, *in situ* screening

---

## 1. Introduction

Cancer gene therapy is a novel approach to cancer treatment. Combination of the expression of a non-host gene followed by the uptake of its substrate, a so-called suicide gene therapy will be committed. The localization of this expression event

could be traced by a tagged probe such as radiolabeled tracers. In order to accelerate the development of suicide gene therapy, the noninvasive monitoring of the *in-vivo* expression through PET or SPECT modalities is of importance (de Vries EFJ *et al* 2002). Up to date, there have been two common reporter genes for monitoring gene therapy namely HSV-1 tk (herpes simplex virus type 1 thymidine kinase) and the mutant HSV-1-sr39tk (de Vries EFJ *et al* 2002). The imaging substrate such as [F-18]FHBG, a nucleoside analog, has been approved by the US Food and Drug Administration as a imaging agent (Yaghoubi and Gambhir 2006). One of the bottom-necks in this approach rests on the development of more potential probes with excellent binding selectivity between the foreign TK genes and the host TK genes such as TK1 or TK2. One of the goals of our laboratory is to discover a potential nucleoside analog to probe wild-type HSV-1 tk gene.

In order to discover drugs efficiently, *in situ* screening of libraries obtained from diversity-oriented synthesis (DOS) is an alternative due to its convenience even though automated parallel HPLC could purify hundreds of compounds per day. The main advantages of *in situ* screening on microtiter plates are no protection in generating library, no isolation and micro scale for bioassay (Brik *et al* 2006). DOS for *in situ* bio-screening has to be high yield and in nontoxic water compatible solvent (Brik *et al* 2006). To date, these reactions used for *in situ* bio-screening after completing DOS have contained at least six kinds of reactions. They were HBTU and NHS based amide bond formation, triazole forming reaction from coupling of alkynes and azides, Pictet-Spengler reaction, tetrabutylammonium fluoride-assisted rapid alkylation, and epoxide opening with amines (Brik *et al* 2006). In this study, we selected HBTU based amide forming reaction to construct libraries of nucleoside analogs of which the number of compounds is 318 before their *in situ* MTT cytotoxic assay for discovering potential structure of nucleoside radiotracers. (Zhang *et al* 2007)

## 2. Materials and Methods

### 2.1. Cell Culture

Both NG4T-TK and NG4T cells supplied from Dr. Wen K. Yang were cultured with MEM medium, supplemented with 10% fetal bovine serum (FBS). Both cells were maintained at 37 °C and 5% CO<sub>2</sub> in a humidified incubator. (Deng *et al* 2006)

### 2.2 Construction of HBTU amide forming libraries

Three kinds of libraries containing 318 crude products were constructed with amide forming reactions which were coupled amino ribosyl uridine (U), arabinosyl uridine (A), dihydrouridine (D) with 106 various carboxylic acids. These reactions were all

catalyzed with HBTU salt for activating all carboxylic acids to create corresponding active esters. (Brik *et al* 2006, Zhang *et al* 2007, Lo *et al* 2007)

### 2.3 MTT cytotoxic assay for *in-situ* screening of HBTU based amide forming libraries

MTT {3-(4,5-dimethyl-2-thiazolyl)-2,5-diphenyl-2H-tetrazolium bromide} (1g) dissolved in PBS saline (5L) was used for evaluating the proliferation of both HSV-1 tk transfected cells (NG4T-TK) and native cells (NG4T). Before *in situ* screening of nucleoside libraries, ~3000 cells were seeded on 96-well microtiter plates for 1 day. After dilution process of each crude product of libraries, each was added to 96-well microtiter plates. Cells and ~100  $\mu$ M crude product of HBTU based amide forming reaction in each well were incubated for 2 days. After incubation of 2 days, each well was added 10  $\mu$ L MTT reagent for incubating 4 h followed by removing medium, adding DMSO to dissolve purple MTT-formazan, and recording the absorbance on 570 nm in an ELISA plate reader. (Pei 2007)

## 3. Results

Before screening of pyrimidine-based nucleoside analogs, we used GCV as positive control and uridine (U) as negative control (figure 1). Figure 2-4 show all results of MTT cytotoxicity assay with *in situ* screening of HBTU amide forming libraries of nucleoside analogs against HSV-1 tk transfected cells and native cells. 106 carboxylic acids were divided into five parts: A1-A23 were mono-aromatic acids, B1-B22 were multi-cyclic or heterocyclic acids, C1-C26 were halogenated cyclic acids, D1-D18 were aliphatic acids or aliphatic acids containing oxygen or nitrogen, E1-E15 were aliphatic acids containing halogen or sulfur or phosphorus. In the first round of screening, we found out three potential compounds (UC3, AC13, DC19) based on the criteria of which ratio of survival ratio between non-TK and TK transfected cells was more than four. In addition, chloro-phenyl-oxo-butylamide of arabinosyl uridine analog (AC13), might have 14 times ratio of survival ratio between NG4T-TK and NG4T cells.

## 4. Discussion

Why could we use MTT cytotoxicity assay to evaluate the potential of radiotracers of nucleoside analogs for imaging HSV-1 tk? The mechanism underlying the principle that we proposed is based on the uptake of the potential compounds before the subsequent suicide. Three potential nucleoside analogs might target some intracellular bio-macromolecules (eg, DNA, RNA, proteins) upon phosphorylation of HSV-1 thymidine kinase and inhibition of thymidylate synthase or incorporation of DNA

(Balzarini *et al* 1994, de Vries EFJ *et al* 2002). However, the confirmation of our proposal using radioiodo or radiofluoro labeling on 5-uracil followed by cell uptake assay and *in vivo* bio-distribution study is needed. Moreover, some HBTU associated by-products might result in false positive (Brik *et al* 2006) in cell survival or proliferation assay. Therefore, preparation and purification of three potential amide forming products to confirm the cytotoxic activity against NG4T-TK is crucial

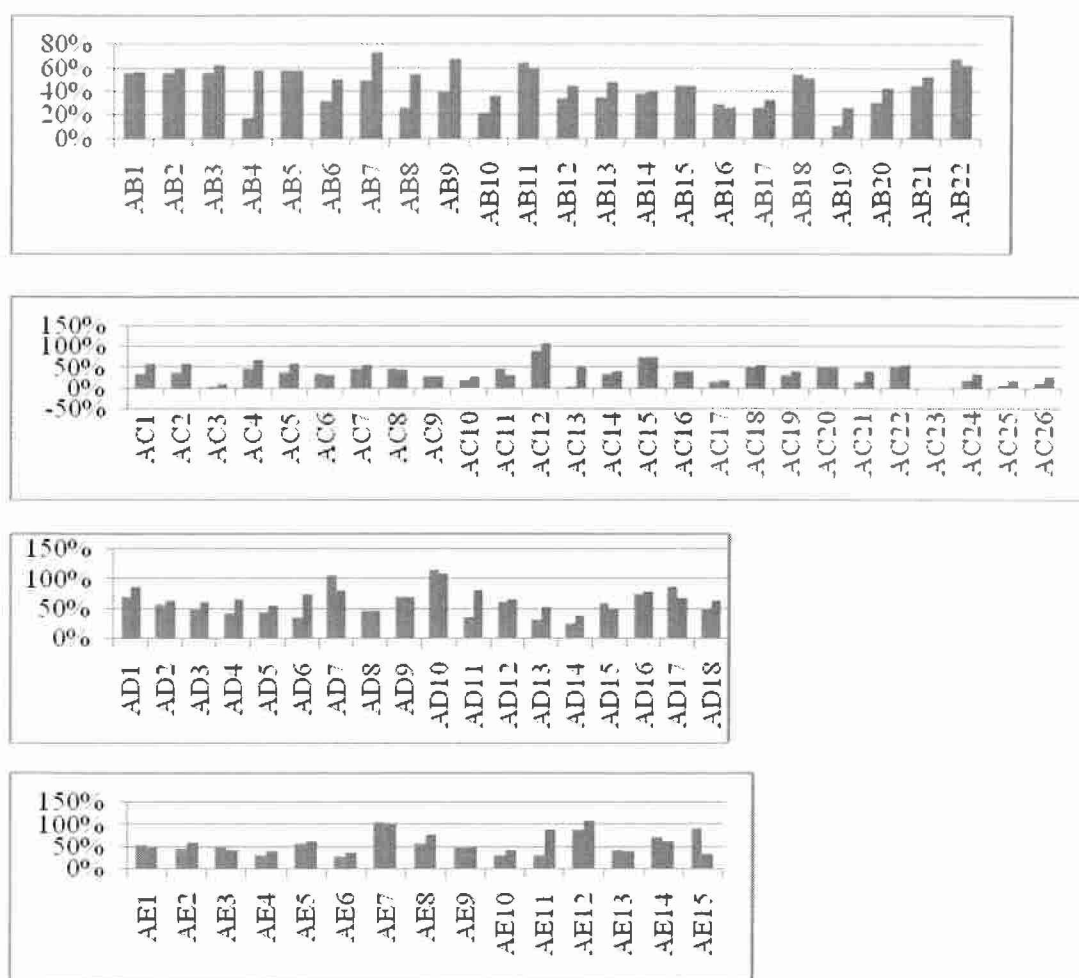


Figure 3 *In situ* screening of arabinosyl uridine-based amide forming library

## 5. Conclusions

For discovering the potential pyrimidine-based nucleoside analogs for imaging HSV-1 tk cancer gene therapy efficiently, the *in situ* screening without isolation after amide forming reactions discovered three potential compounds (UC3, AC13, DC19). The most potential compound, chloro-phenyl-oxo-butamide of arabinosyl uridine

analog (AC13), exerted a selective index of 14 between HSV-1 tk transfected cells and native cells. The confirmation using purification is essential and radio-halogen labeling followed by cell uptake study is going to be carried out after confirmation of cytotoxic activity against NG4T-TK.

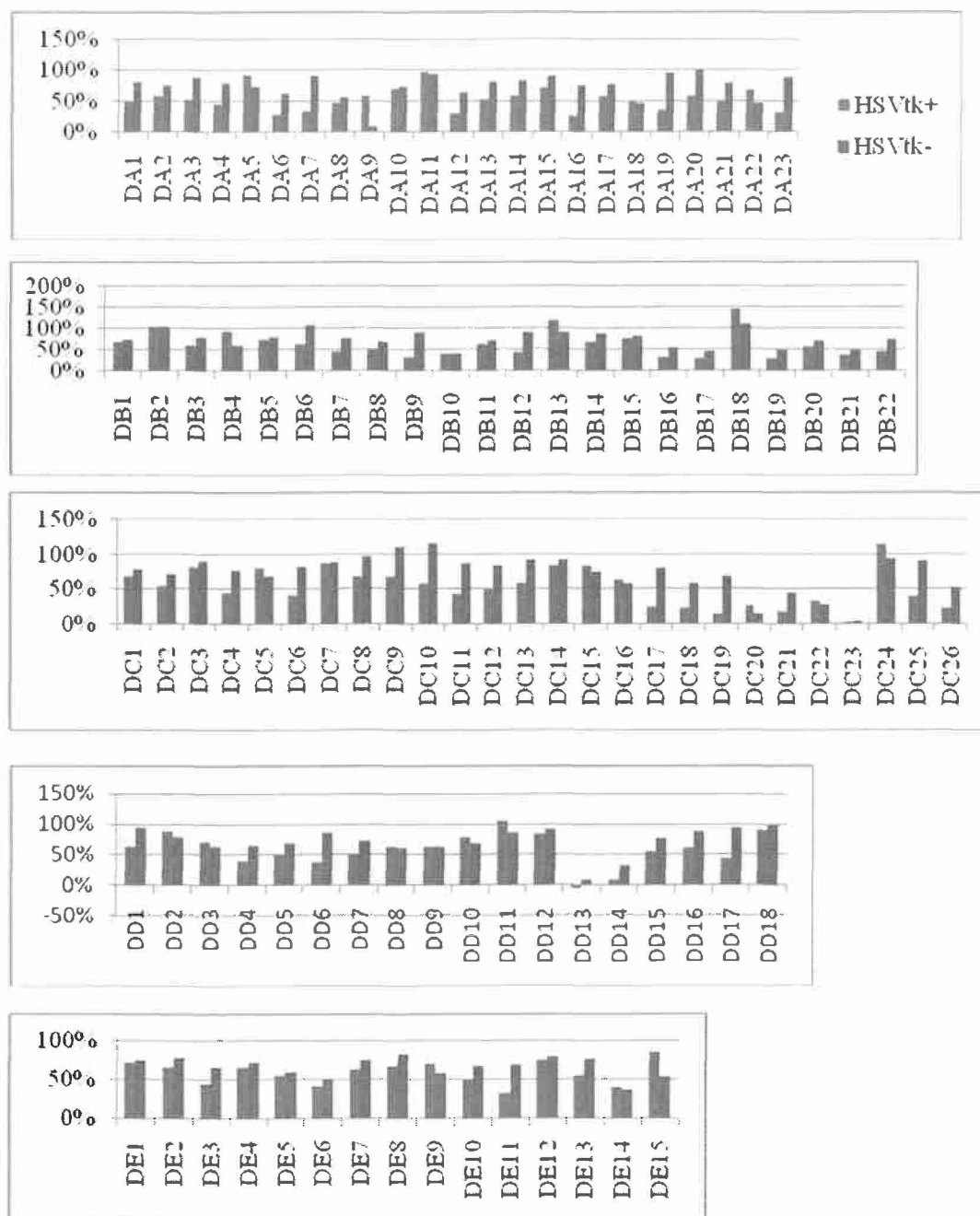


Figure 4. *In situ* screening of dihydrouridine-based amide forming library

## Acknowledgements

We are grateful to the National Science Council of Taiwan and CGMH\_NTHU Joint Research for providing financial support (NSC- 95-2113-M-007-039 and CGTH96N2342E1).

## References

1. Balzarini J, Bohman C, Walker RT, Declercq E 1994 Comparative cytostatic activity of different antiherpetic drugs against herpes-simplex virus thymidine kinase gene-transfected tumor-cells *Mol Pharmacol* 45 1253-8
2. Brik A, Wu CY, Wong CH 2006 Microtiter plate based chemistry and in situ screening: a useful approach for rapid inhibitor discovery *Org Biomol Chem* 4 1446-57
3. Deng WP, Wu CC, Lee CC, Yang WK., Wang HE, Liu RS, et al 2006 Serial in vivo imaging of the lung metastases model and gene therapy using HSV1-tk and ganciclovir *J Nucl Med* 47 877-84
4. Lo JM, Chiang LW, Chen SW, Fu ZW, Pei K, Yu CS 2007 Recent advances in solution-phase derived synthetic libraries and rapid bioassays on microtiter plates *Chim Oggi* 25 46-50
5. Pei K 2007 *MS Thesis* (Natl. Tsing-Hua Univ.)
6. de Vries EFJ, Buursma AR, Hospers GAP, Mulder N H, Vaalburg W 2002 Scintigraphic imaging of HSVtk gene therapy *Curr Pharm Des* 8 1435-50
7. Yaghoubi SS, Gambhir SS 2006 PET imaging of herpes simplex virus type 1 thymidine kinase (HSV1-tk) or mutant HSV1-sr39tk reporter gene expression in mice and humans using [F-18] FHBG *Nat Protoc* 1 3069-75
8. Zhang L, Sun F, Li Y, Sun X, Liu X, Huang Y, Zhang LH, Ye XS, Xiao J 2007 Rapid synthesis of iminosugar derivatives for cell-based in situ screening: Discovery of "Hit" compounds with anticancer activity *ChemMedChem* 1 1594-7

## ASWIRL BOARD DOSIMETRY TECHNIQUE FOR COMPENSATING FOR THE SCALP VERTEX AND FOOT SOLE DOSAGE IN TOTAL SKIN ELECTRON THERAPY

<sup>1,2,3,4</sup>Jia-Ming Wu, <sup>1,2,3</sup>Shyh-An Yeh, <sup>1,2</sup>Kuan-An Chu, <sup>4</sup>Max M. Chao, <sup>4,5</sup>S.W. Leung

<sup>1</sup>*Department of Radiation Oncology, E-Da Hospital, Kaohsiung, Taiwan*

<sup>2</sup>*Department of Medical Images and Radiological Science, I-Shou University, Kaohsiung, Taiwan*

<sup>3</sup>*Department of Medical Imaging and Radiology, Shu-Zen College of Medicine and Management, Kaohsiung, Taiwan*

<sup>4</sup>*Department of Medical Imaging and Radiological Science, Institute of Radiological Science, Central Taiwan University of Science and Technology, TaiChung, Taiwan*

<sup>5</sup>*Department of Radiation Oncology, Yuan's general Hospital, Kaohsiung, Taiwan*

### **Purpose**

The aim of this study is to present a novel technique in which uniform dose to the whole body as well as the soles and vertex of scalp can be achieved in one electron beam treatment fraction. An experiment was undertaken with a home-made aswirl board that enables the patient to lie in supine or prone position for treatment.

### **Material and Methods**

A 6MeV nominal electron beam was delivered using Elekta Precise Sli throughout this experiment. The patient is treated at a source to skin distance of 350 cm. The largest field size available at SSD100cm is 40x40cm<sup>2</sup> and a high dose rate of 3000 MU min<sup>-1</sup> was used. A 0.6cm thick acrylic beam spoiler was placed 90cm away from the surface of the patient to scatter the electron beam for a more homogeneous surface dose. Patients are treated with two groups in prone and supine position by leaning on inner rotational board in prone and supine position, each group can further be separated into two subgroup with tilting and rotation positions for treatment. By incorporating all these four groups of patient positions (Prone Group1, Prone Group2, Supine Group1, and Supine Group2) on the aswirl board with the optimal gantry angle, the patient will final accumulate compensated dosages on whole body surface.

### **Results**

One of the gantry beam was directed 15.5° upward and the other 15.5° downward from the horizontal axis to provide a field size as large as 200cm in height and 140cm in width. An incline angle of 31.5° anteriorly (forward) or posteriorly (backward) of the middle frame and an angle rotated 60° clockwise or counterclockwise of the inner frame is found to be most appropriate. The output dose rate for the AB-TSET was

0.085cGy/mu at SSD 350 cm. The beam characteristics of the AB-TSET depth dose curves were  $R_{50} = 1.25\text{cm}$ ,  $d_{\text{max}}=0.6\text{cm}$   $E_0=2.913\text{MeV}$ ,  $R_p=1.75\text{ cm}$ .

### **Conclusion**

The AB-TSET technique presented in this study is able to deliver a uniform dose to the patient's skin surface as well as to the vertex and the soles all in one time, eliminating the troubles of having to further booth irradiate these two regions when using the Stanford Six Field Technique.

**Keywords:** Total Skin Electron Therapy, vertex and the soles, aswirl board, skin cancer

# ASWIRL BOARD DOSIMETRY TECHNIQUE FOR COMPENSATING FOR THE SCALP VERTEX AND FOOT SOLE DOSAGE IN TOTAL SKIN ELECTRON THERAPY

<sup>1,2,3,4</sup> Jia-Ming Wu , <sup>1,2,3</sup> Shyh-An Yeh , <sup>1,2</sup> Kuan-Yin Hsiao , <sup>4</sup> Max M. Chao  
<sup>4,5</sup> S.W. Leung

<sup>1</sup> Department of Radiation Oncology, E-Da Hospital, Kaohsiung, Taiwan

<sup>2</sup> Department of Medical Images and Radiological Science, I-Shou University, Kaohsiung, Taiwan

<sup>3</sup> Department of Medical Imaging and Radiology, Shu-Zen College of Medicine and Management, Kaohsiung, Taiwan

<sup>4</sup> Department of Medical Imaging and Radiological Science, Institute of Radiological Science, Central Taiwan University of Science and Technology, TaiChung, Taiwan

<sup>5</sup> Department of Radiation Oncology, Yuan's general Hospital, Kaohsiung, Taiwan

---

## Abstract

This study presents a novel technique in which a uniform radiation dose to the whole body, soles and scalp vertex can be achieved in one electron beam treatment fraction. An experiment was undertaken with a home-made aswirl board that enables the patient to lie in a supine or prone position for treatment.

Key words: Total Skin Electron Therapy · vertex and the soles · aswirl board · skin cancer

---

## 1. Introduction

The Stanford total skin electron beam technique is the most commonly accepted treatment for patients with skin cancer or cutaneous T-cell lymphoma (1). In this technique, the patient must stand still in six different subsequent positions. Some skin areas are not uniformly irradiated (2). For standing position total skin electron beam therapy, the contribution of tangential beams is less than the dose from direct vertical beams. Therefore, the dose to the vertex will be inadequate in this approach as it is always treated tangentially. Many papers have

discussed the dose distribution analysis in whole body superficial electron therapy (3-4). Boost treatments are often given to the scalp to ensure an adequate dose (5).

The aim of this study is to present a novel technique in which a uniform dose is delivered to the whole body, the soles and scalp vertex in a single electron beam treatment fraction. An experiment was undertaken using a home-made aswirl board that enabled the patient to lie in the supine or prone position. Measurements were performed experimentally to determine the most appropriate gantry angle, the tilting and rotational angles of the aswirl board to provide a uniformly large electron field implemented in a homogeneous dose to patient's entire body

surface including the scalp vertex and soles of the feet simultaneously in one treatment.

## 2. Materials and Methods

Total skin electron irradiation is used to treat the first few millimeters of the skin. Therefore, a 9 MeV nominal electron beam was delivered using the Elekta Precise Sli throughout this experiment. The patient is treated at a Isocentric point to a Skin Distance of 350 cm (ISD350 cm). The largest field size available at SSD 100cm is 40 x 40 cm<sup>2</sup> and at a high dose rate of 3000 MU min<sup>-1</sup>. A 0.6cm thick acrylic beam spoiler was placed 90 cm away from the surface of the patient to scatter the electron beam for a more homogeneous surface dose. In the standard Stanford TSET technique, the patient is treated in a standing position. Unfortunately, the dosage to the scalp vertex and soles of the feet was found to be relatively low. Further irradiation after treatment must be given to compensate for this dose insufficiency. This process is time consuming. An aswirl board with three wooden frames was designed (Fig. 1) to deliver a uniform radiation dose to the total skin area including the normally under-dosed foot soles and scalp vertex. The procedures in this experiment were as follows:

Determination of the most suitable combination of gantry angles to produce a single irradiation beam providing limited coverage and inhomogeneous dosage.

Determination of the patient's position on the aswirl board for one treatment cycle.

Measurement of the absolute dose output

Measurement of the multiplication factor

All measurements were performed using PTW30013 ion chamber, Unidose electrometer, XV Films and TLDs.

### *Aswirl Board*

The aswirl board is an assembly of three wooden frames (Fig 1). The outermost frame is mainly for fixation, the middle frame is held to the outermost frame with a horizontal axis that enables the board to be tilted forward or

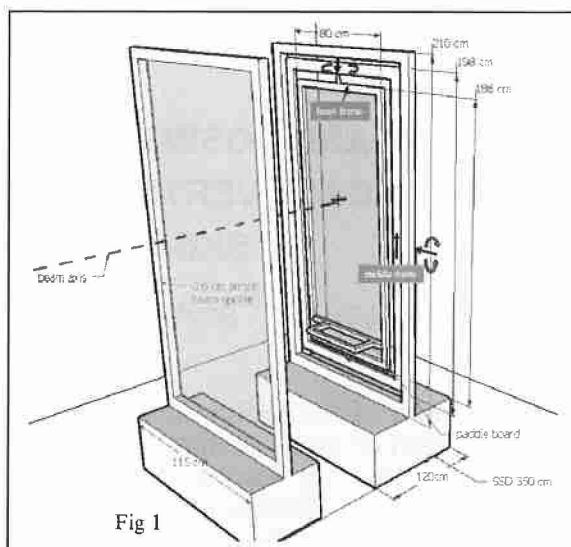


Fig 1

The outermost frame is mainly for fixation. The middle frame has a horizontal rotational axis that enables clockwise or counterclockwise rotation and is locked to the outermost frame. The middle frame is locked to the outermost frame with a vertical axis that enables the board to be tilted forward or backward. All of these movements will enable any possible position for the patient to be irradiated while lying on the middle frame with a tennis-racket support. A tennis-racket step-on board is attached to the middle frame for the patient to tread on. This design provides firm support to the patient, allowing the electron beam to fully penetrate the entire skin surface.

backward. The inner frame has a vertical rotational axis held by the middle frame that enable clockwise or counterclockwise rotation. All of these frames enable any positions necessary for the patient to be irradiated while lying on the inner frame with a tennis-racket support. The trammel material tautened on inner frame is Nylon 6 (polyurethanes), at 1.15 g/cm<sup>3</sup> density. The trammel mesh size is 5 cm X 5 cm. The Nylon wire thickness is 1.5 mm. The electron beam attenuation using these Nylon wires was measured using film. The dose reduction produced by the Nylon wires shown by

film is minute. Patients are fastened to the frame using cloth belts while laying on the inner frame trammels. A tennis-racket step-on board is attached to the inner frame for the patient to step on. This design provides firm support to the patient while allowing the electron beam to fully penetrate.

#### Optimal Beam Angle

Lack of electron scatter from a single horizontal beam to the peripheral of the patient at a distance of 350 cm will cause an inhomogeneous dose along the vertical and horizontal dose profiles. The area coverage at this distance is not large enough. Measurements were made to determine the optimal combination of gantry angles.

#### Patient treatment positions

Once the optimal beam angle is determined, the next procedure is to determine the most suitable patient position to achieve a uniformly delivered electron dose to the entire patient surface. The patient is firmly localized to the tennis-racket support so that the middle frame can be easily tilted and the inner frame easily rotated to achieve the desired treatment positions.

Multiple patient position integration for a complete irradiation course is described as follows.

- (A) Patient prone with the body leaning forward on the inner frame (Fig 2 , left column)
- i. Prone-Forward (P-F) (Fig 2 left upper)
  - ii. Prone-Forward-Counterclockwise (P-F-CCW) The patient is prone on the tennis-racket support; the middle frame inclined forward, with the inner frame rotated counterclockwise. (Fig 2 left middle)
  - iii. Prone-Forward-Clockwise (P-F-CW) The patient is prone on the tennis-racket support; the middle frame inclined forward with the inner frame rotated clockwise (Fig 2 left lower)
- B. Patient prone with the body leaning backward on the inner frame (Fig 2, right column)
- i. Prone-Backward-No rotation (P-B) (Fig 2 right upper)
  - ii. Prone-Backward-Counterclockwise (P-B-CCW) The patient is prone on the inner tennis-racket support, the middle frame inclined backward, with the inner frame rotated counterclockwise (Fig 2 right lower)
  - iii. Prone-Backward-Clockwise (P-B-CW) The patient is prone on the inner tennis-racket support, the middle frame inclined backward, with the inner frame rotated clockwise

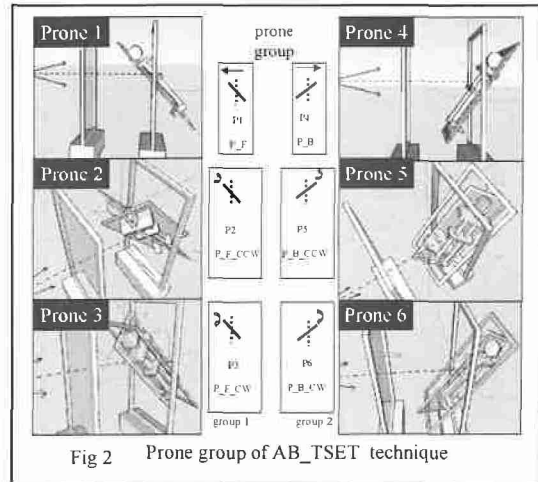


Fig 2 Prone group of AB\_TSET technique

Fig 2.

- A. Patient prone with the body leaning forward on the inner frame (Fig 2, left column)
  - i. Prone-Forward (P-F) (Fig 2 left upper)
  - ii. Prone-Forward-Counterclockwise (P-F-CCW) (Fig 2 left middle)
  - iii. Prone-Forward-Clockwise (P-F-CW) (Fig 2 left bottom)
- B. Patient prone with the body leaning backward on the inner frame (Fig 2, right column)
  - i. Prone-Backward-No rotation (P-B) (Fig 2 right upper)
  - ii. Prone-Backward-Counterclockwise (P-B-CCW) (Fig 2 right lower)
  - iii. Prone-Backward-Clockwise (P-B-CW) (Fig 2 right bottom)

- Patient supine with the body leaning forward on the inner frame (Fig 3 , left column)
- i. Supine-Forward-No rotation (S-F) (Fig 3 left upper)

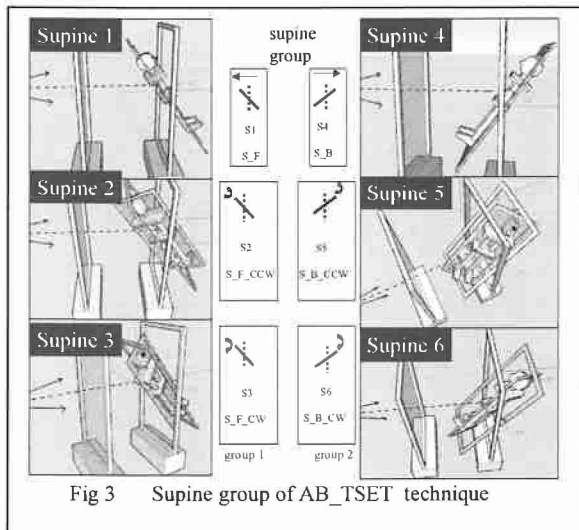


Fig 3 Supine group of AB\_TSET technique

Fig 3.

A. Patient supine with the body leaning forward on the inner frame (Fig 3, left column)

i. Supine-Forward-No rotation (S-F) (Fig 3 left upper)

ii. Supine-Forward-Counterclockwise (S-F-CCW) (Fig 3 left middle)

iii. Supine-Forward-Clockwise (S-F-CW) (Fig 3 left bottom)

B. Patient supine with the body leaning backward on the inner frame (Fig 3, right column)

i. Supine-Backward-No rotation (S-F) (Fig 3 right upper)

ii. Supine-Backward-Counterclockwise (S-F-CCW) (Fig 3 right middle)

iii. Supine-Forward-Clockwise (S-F-CW)(Fig 3 right bottom)

ii. Supine-Forward-Counterclockwise (S-F-CCW)

The patient is supine on the inner tennis-racket support, the middle frame inclined forward, with the inner frame rotated counterclockwise (Fig 3 left middle)

iii. Supine-Forward-Clockwise (S-F-CW)

The patient is supine on the inner tennis-racket support, the middle frame inclined forward, with the inner frame rotated clockwise (Fig 3 left lower)

Patient supine with the body leaning backward on the inner frame (Fig 3, right column)

i. Supine-Backward-No rotation (S-F) (Fig 3 right upper)

ii. Supine-Backward-Counterclockwise (S-F-CCW)

The patient is supine on the inner tennis-racket support, the middle frame inclined forward, with the inner frame rotated counterclockwise (Fig 3 right middle)

iii. Supine-Forward-Clockwise (S-F-CW)

The patient is supine on the inner tennis-racket support, the middle frame inclined forward, with the inner frame rotated clockwise (Fig 3 right lower)

The distance of the patient to the gantry (source) is shorter in the position inclining forward, thus delivering a higher dose to the surface. By incorporating these four groups of patient positions (Prone Group1, Prone Group2, Supine Group1, and Supine Group2) on the aswirl board with the optimal gantry angle, the patient will accumulate the compensated dosages on entire body surface.

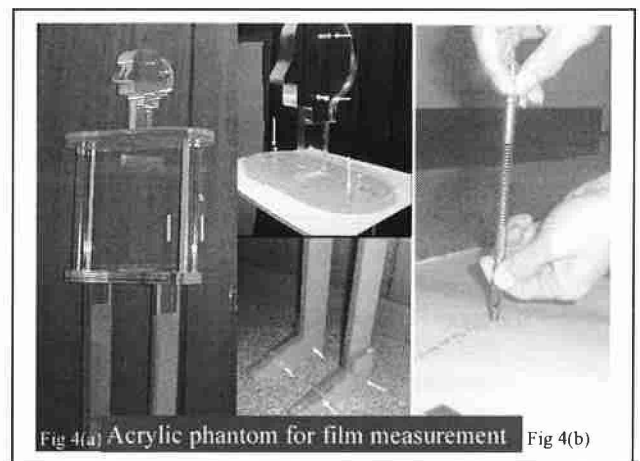


Fig 4.

Two 2 cm acrylic boards were assembled with XV film sandwiched between the boards at the sagittal plane to calculate the dose to the head and soles. Two XV films were placed at the transverse plane representing the dose irradiated to the chest and abdomen (Fig 4a). A special hole-puncher was designed to overcome the inability of the currently available hole-puncher to create holes at any

position needed. The hole-puncher has a circular steel unit attached to a spring. Once the spring is stretched and let go, the steel unit bombards the film creating a circular cut edge on the film (Fig 4b).

#### Acrylic Phantom

A whole body acrylic phantom was designed to inspect if the dose coverage is sufficient. A set of 2cm acrylic boards were assembled and a XV film was sandwiched between the boards at the sagittal plane to be further measured to calculate the dose to the head and soles. Two XV films were placed at the transverse plane representing the dose irradiated to the chest and abdomen (Fig 4a). Whether or not the expected uniform dose to the surface is achieved can be inspected using dose measurements to the films inserted between the acrylic boards. A special hole-puncher tool was designed to overcome the disability of the currently available hole puncher to create holes at any position needed. The designed hole-puncher has a circular steel piece attached to a spring. Once the spring is stretched and let go, the bombardment of the metal to the film will create a circular cut edge on the film (Fig 4b). The films can then be easily held tightly to the phantom with a plastic bolt. The air gap perturbation between the film and phantom can be eliminated (6-7).

#### Percent Depth Dose and Output dose measurement

##### Percent Depth Dose measurement

The distance from the aswirl board geometric center to the radiation source point does not remain consistent with the board movement when tilting or rotation during treatment, therefore, the site of the aswirl board geometric center is positioned with a solid water phantom to determine the percent depth dose measurement. A PTW TM 23343-3765 parallel plate chamber is embedded in the solid acrylic phantom with the chamber window facing the radiation. The gantry irradiation angles set up is denoted in figure 8. The ionization reading depth dose curve was measured step by step using those gantry angles (P3, S6; P1, S4; P3, S5) after each irradiation cycle was completed. Once

the ionization reading depth curve was measured, the readings at each depth were multiplied by the stopping power to derive the absorbed dose at the depth and renormalized to  $d_{max}$  to obtain the percent depth dose.

##### Output Dose measurement

According to AAPM Report # 23, page 38, section 6.5, the output calibration point was positioned at the aswirl board geometric center. A Farmer 0.6cc chamber was embedded at a depth of 0.7cm ( $d_{max}$  of percent depth dose derived from ionization depth curve). The PTW Unidose was connected to the Farmer chamber to take readings and follow the TG-21 protocol to derive the absolute dose.

##### Percent Depth Dose measurement for other areas

To know if the Percent Depth Dose of the other positions differed from the aswirl board geometric center, films were embedded in the acrylic phantom at the head and foot sagittally to compare the Percent Depth Dose difference at the abdomen, head and foot areas.

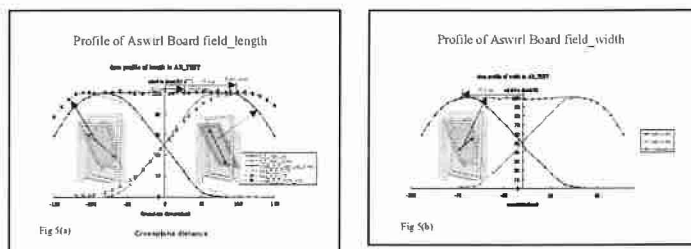


Fig 5.

Combination of a dual-beam technique was used to compensate for the field size limitation projected from a single horizontal beam to a distance of 350 cm away from the isocenter. One beam was directed 15.5° upward and the other 15.5° downward from the horizontal axis. These two beams were combined to provide a field size as large as 200 cm high (Fig 5a) and 140 cm wide (Fig 5b).

### 3. Results

#### The Optimal Gantry, Middle and Inner Frame Angles

#### Gantry Angle Determination

In our experiment to determine the most suitable angle, the estimated beam angle was used first to deliver the dose at three points. The upper, middle and lower points were then measured. If the measured dose to the middle point was smaller than the other two points, the beam angle was then directed closer to the center and vice versa to obtain a homogeneous dose distribution. A combination dual-beam technique was used to compensate for the field size limitation projected from a single horizontal beam to a distance 350 cm away from the isocenter. One beam was directed 15.5° upward and the other 15.5° downward from the horizontal axis. These two beams were combined to provide a field size as large as 200 cm high (Fig 5a) and 140 cm wide (Fig 5 b).

The optimal angled beams were obtained based on the experimental measurement results. The dose profile from a horizontal beam with a field size of 40x40 cm, ISD 350 cm was measured to investigate the dose efficiency. Dose profiles from two angled beams with one directed above the horizontal while the other directed below were then obtained. The individual dose profiles were then summed into a composite dose profile to estimate the angle needed to tilt for a uniform dose. The estimated tilt angle was then carried out on the linac and measurements were made to confirm a uniform dose. Our experiment found that the most suitable angle beam would be  $\pm 15.5^\circ$ .

#### Inner and Middle Frame

The frame incline angle toward or away from the source is an important factor for dose homogeneity to the scalp vertex and soles of the feet. From our experiment, the best tilt angle for the middle frame is 31.5° and the best rotational angle for the inner frame is 60° (because 6 beams are directed to the whole body, 360 divided by 6 equals 60). Treatment can be delivered to the patient in either the prone position from P1 to P6 (Fig 2) or supine position from S1 to S6 (Fig 3).

## 4. Discussion

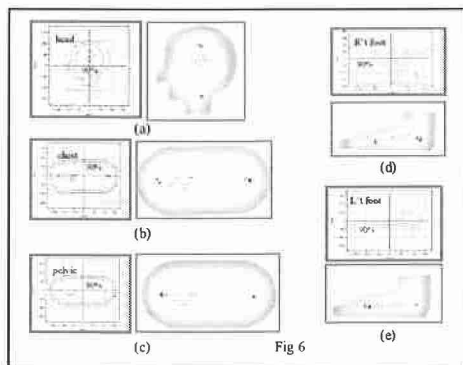
#### Dose Profile

Figure 5 a represents the composite dose profile from ion chamber readings obtained from the complete irradiation of paired angle beams directed 15.5° upward and downward. The middle frame was tilted 31.5° and the inner frame rotated 60°. The schematic diagram on the left shows the actual aswirl board position with ion chamber readings measured diagonally at the inner frame. The schematic diagram on the right shows the actual aswirl board position to measure the dose profile along the vertical axis of the inner frame. This vertical dose profile is shorter than that obtained diagonally. The beam was directed  $\pm 15.5^\circ$  upward and downward, the lower field edge of the 40 x 40 cm field size projected at ISD 350cm would be 25.7 cm away from the horizontal plane and the field central axis would intersect at a distance 97.1 cm away from the horizontal plane. Because there is a symmetry area beyond this length, the total vertical length required will be 200 cm. Figure 5 b represents the composite horizontal dose profile obtained with the middle frame tilted and inner frame rotated. Similar to the configuration analyzed above, the central axis of the original 40 x 40 cm field size at SSD100 cm will intersect at a distance 70.9 cm away from the vertical plane when projected at ISD350cm. Thus, a width of 140 cm would provide enough coverage. Based on the measurements shown in Figures 5a and 5b, we conclude that a uniform dose can be delivered to an area of 200 x 140 cm at ISD 350 cm

#### Dose Distribution

Figure 6 shows the film dosimetry obtained from the entire body acrylic phantom irradiated using a whole treatment course. We can see the homogeneous dose accumulations on the exposed films, and the relative dose converted from the optical density also revealed that the 90% isodose is uniformly delivered at a depth of 0.8 cm. According to our Stanford Six Fields experience (8-9), the phantom was also used to irradiate standard Stanford TSET (Fig 9) film for

comparison. It is clear that the AB\_TSET dominates the Stanford Six Fields technique for better dose homogeneity in the foot soles and scalp vertex. In order to know the PDD of other areas, dose from a film irradiated with a conventional 9 MeV at SSD 100cm was compared to the dose obtained from the films placed on the head, abdomen and foot sole regions of the phantom using the aswirl board with whole cycle irradiation. There were only slight differences for the various PDD areas shown in the film results.



**Figure 6**  
Figure 6 shows the films dosimetry obtained from the whole body acrylic phantom with a whole irradiation treatment course. We can see the homogeneous dose accumulations on the exposed films, and the relative dose converted from the optical density also revealed that a 90% isodose is uniformly delivered at a depth of 1.4 cm.

**Percent Depth Dose and Output**

The AB-TSET described here achieved a uniform dose distribution to the skin using a combination of the tangential beams. The PDD obtained from the AB-TSET tangential beams moved closer to the surface when compared to those obtained from vertical beams (Fig 7). In the AB-TSET, the beam characteristics of  $R_{50} = 2.48\text{cm}$ ,  $E_0$  can be derived from  $2.33 \times 2.48 = 5.78\text{ MeV}$ . The output dose for the AB-TSET was  $0.046\text{ cGy}/\mu\text{u}$  at ISD  $350\text{ cm}(10)$ .

**Multiplication Factor and MU Calculations**

A film was placed directly at the geometrical isocenter of the phantom for the optical density measurement. The same number of MUs were

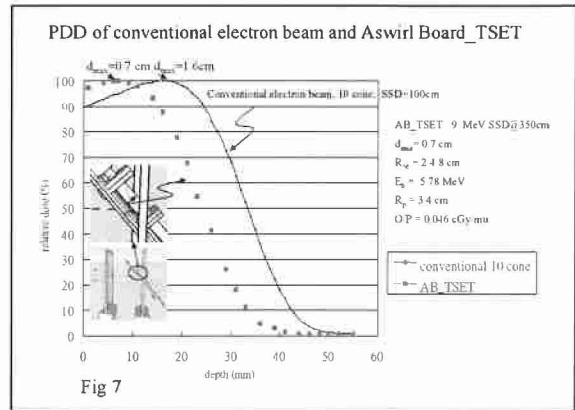


**Figure 7**  
The PDD obtained from the tangential beams move closer to the surface when compared to the one obtained from vertical beams in this Fig. In AB-TSET, the beam characteristics of  $R_{50} = 2.48\text{ cm}$ ,  $E_0$  can be obtained with  $2.48 \times 2.33 = 5.78\text{ MeV}$ .

**Determination of beam multiplication**

$$\text{Multiplication Factor (MF)} = \frac{D_{p1} + D_{S4} + D_{p3} + D_{S6} + D_{p2} + D_{S5}}{\text{dose from vertical fields}}$$

$$\text{MF} = 5.42 \text{ ( range } 5.0 - 6.0 \text{ )}$$

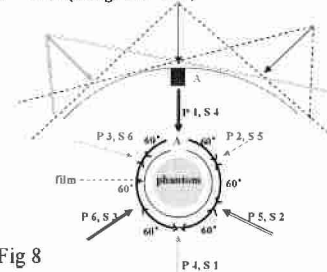


**Figure 8**  
The Points P1, P2, P3, P4, P5 and P6 in Figure 8 represent Prone Forward (P1), Prone Forward CCW (P2), Prone Forward CW (P3), Prone Backward (P4), Prone Backward CCW (P5) and Prone Backward CW (P6). Points S1, S2, S3, S4, S5 and S6 represent Supine Forward (S1), Supine Forward CCW (S2), Supine Forward CW (S3), Supine Backward (S4), Supine Backward CCW (S5) and Supine Backward CW (S6). In one complete irradiation of all the beams, the film placed directly on the geometrical isocenter (Point A) will be irradiated 12 times with the angled beams.

Multiplication factor was then derived by the ratio of the dose converted from optical density of the Points P3, S6 and P2, S5 and P1 and S4 to the dose from the vertical fields. In our experiment, the multiplication factor was calculated as 5.42.

given to the fields directed vertically. The dose ratios converted by measuring the optical density from these two sets of irradiated films was calculated as the multiplication factor. Points P1, P2, P3, P4, P5 and P6 in Figure 8 represent Prone Forward (P1), Prone Forward CCW (P2), Prone Forward CW (P3), Prone Backward (P4), Prone Backward CCW (P5) and Prone Backward CW (P6). Points S1, S2, S3, S4, S5 and S6 represent Supine Forward (S1), Supine Forward CCW (S2), Supine Forward CW (S3), Supine Backward (S4), Supine Backward CCW (S5) and Supine Backward CW (S6). In one complete irradiation from all beams, the film placed directly on the geometrical isocenter (Point A) will be irradiated 12 times with the angled beams. The multiplication factor was then derived by the dose ratio converted from the optical density of Points P3, S6 and P2, S5 and P1 and S4 to the dose from the vertical fields. In our experiment, the multiplication factor was calculated as 5.42.

$$MF = \frac{\text{dose of p1 and S4} + \text{dose of p3 and S6} + \text{dose of p2 and dS5}}{\text{dose from vertical fields}}$$

This value is used mainly to calculate the required MU for each beam to achieve a uniform dose distribution.

The equation is

$$MU = \frac{\text{prescribe dose}}{M.F. \times \text{output of aswirl board} \times 6}$$

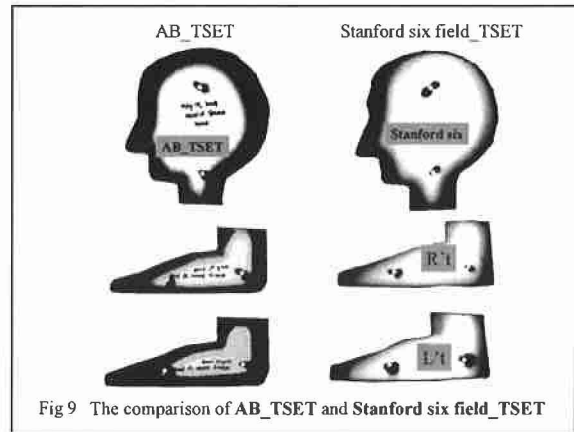


Fig 9 The comparison of AB\_TSET and Stanford six field\_TSET

Figure 9

This figure show the phantom was also used to be irradiated with the films of standard Stanford TSET for comparison. The AB-TSET dominate over Stanford Six Fields technique on a better dose homogeneity in soles and vertex is clearly seen.

## 5. Conclusions

The AB-TSET technique presented in this study is able to deliver a uniform dose to the patient's entire skin surface including the scalp vertex and the soles of the feet at one time, eliminating the trouble of having to further irradiate these two regions when using the Stanford Six Field Technique. Based on these measurements, we found that the dose homogeneity of the skin surface was within  $\pm 10\%$ . The supine and prone position on the Aswirl Board provides full comfort to patients, preventing soreness. We conclude that the AB-TSET is a more convenient and time effective approach for future clinical skin cancer treatments.

**Acknowledgement:** The author would like to thank Professor Chen Shou-Chui for his contributions on this study..

## Acknowledgements

The author would like to thank Prof Chen Shou-Chui for his contribution on this study.

## References

1. American Association of Physicists in Medicine. Total skin electron therapy technique and dosimetry. Report No. 23. New York (NY): American Institute of Physics;1988
2. Peters V G, FCCPM. Use of an electron reflector to electron therapy. *Int. J. Radiation Oncology Biol. Phys.* 2000, 46(4):1065–1069.
3. Weaver RD, Gerbi BJ, Dusenbery KE. Evaluation of dose variation during total skin electron irradiation using thermo-luminescent dosimeters. *Int J Radiat Oncol Biol Phys* 1995;33: 475–478.
4. Antolak JA, Cundiff JH, Ha CS. Utilization of thermo-luminescent dosimetry in total skin electron beam radiotherapy of mycosis fungoides. *Int J Radiat Oncol Biol Phys* 1998;40: 101–108.
5. TAREK SHOUMAN, M.D. and ZEINAB EL-TAHER, Ph.D. Total Skin Electron Therapy: A Modified Technique for Small Room Linear Accelerator. *Journal of the Egyptian Nat. Cancer Inst.* 2004; 16( 4): 202-209.
6. Ellen El-Khatib. Evaluation of film and thermo-luminescent dosimetry of high-energy electron beams in heterogeneous phantoms. *Medical Physics* 1992;19(2):317-323.
7. Tatsuya Fujisaki. Contribution of Cerenkov radiation in high-energy x-ray and electron beam film dosimetry using water-substitute phantoms. *Phys Med Biol.* 2003; 48:105-109.
8. JM Wu, SW Leung, et al. Lying-on position of Total Skin Electron Therapy. *Int J Radiat Oncol Biol Phys.* 1997 Sep 1;39(2):521-8.
9. Leung SW, Hsu HC, Huang PH. Total Skin electron beam irradiation in scleromyxoedema. *British Journal of Radiology* 1998;71:84-86.
10. Ester Carrasco Pavón, Francisco Sánchez-Doblado et al, Total skin electron therapy treatment verification: Monte Carlo simulation and beam characteristics of large non-standard electron fields. *Phys. Med. Biol.* 2003; 48:2783–2796.

## The Study of Surface Dose for Golden Coating Thermoluminescence Dosimeter

Yi Chi Liu<sup>1</sup>, Jao Perng Lin<sup>1</sup>, \* ChiChang Liu<sup>2</sup>

<sup>1</sup>*Department of Radiological Technology, Yuanpei University, Taiwan*

<sup>2</sup>*Radiation Monitoring Center, AEC*

### **Purpose**

Dose enhancement was found in an environment of tissue-equivalent material close to the surface of a metallic gold thin film. Validity of estimation of dose perturbations is critical in the evaluation of radiation effect associated with high-Z interface. The magnitude of dose enhancement has been debated due to limitation of measurement device and the thickness of high-z materials. In this research, we tried to study the interface effect of sub-micro scale metallic gold thin film that is thinner than other reported works.

### **Materials and Methods**

Monet Carlo simulation has been proposed for interface effect but been questioned about the results due to poor statistics in small spatial bins. Penelope 2006 was shown to be a Monte Carlo code suitable for micro-dosimetric study that might be also acceptable for this work. GR-200S thin film thermoluminescence dosimeters covered with different thickness of gold foil were used as interface dose measurement device. The irradiation source used in this work is photons generated by a 6MV LINAC.

### **Results**

The results simulated by PENELOPE show dose reduction for the thickness of gold foil within sub-micrometer region. The dose enhancement can only be found when gold foil thicker than several micrometers. The measured data were not exactly the same as simulation ones however the trend seemed quite consistent. This phenomenon might be due to the range of secondary electrons induced from gold by photon with energy above several hundred keV. If gold foil is thick enough, the flux of secondary electron increases and enhances the interface dose.

### **Conclusion**

In this work, we found that the interface dose enhancement is related to the thickness of gold film. The ultra-thin film with high-Z material could reduce interface dose is confirmed by Monte Carlo simulation and measurement. With proper design this ultra-thin film might be applied for skin dose reduction.

**Keywords:** Interface dosimetry, gold, Monte Carlo

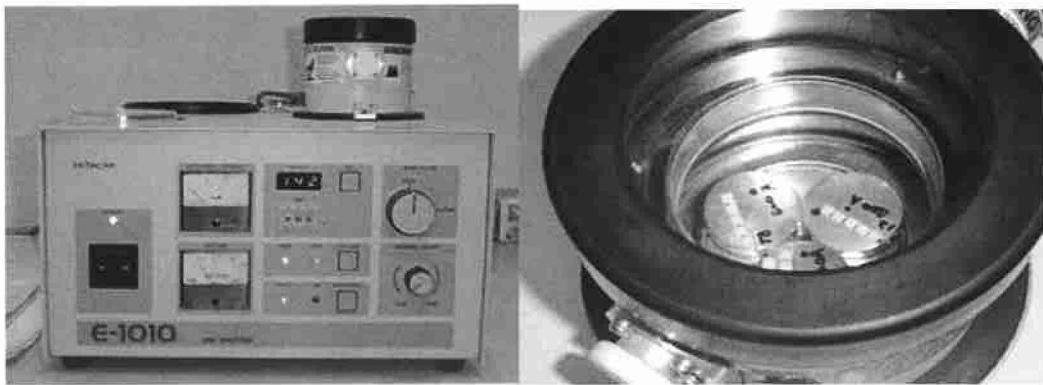


Fig.1 Hitachi ion sputter coater E-1010

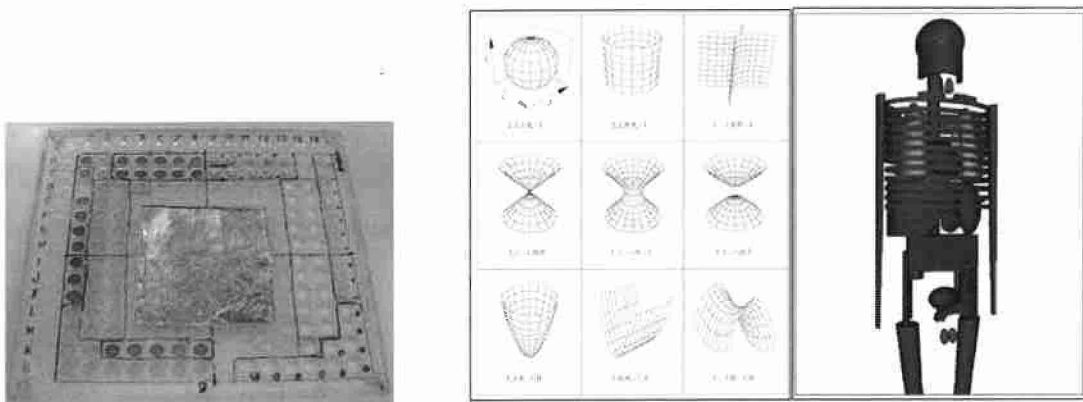


Fig.2 The gold foil area is 4.5 x 5cm, overlaps 100 pieces, thickness is 10 microns

Fig.3 Simulated by Penelope 2006

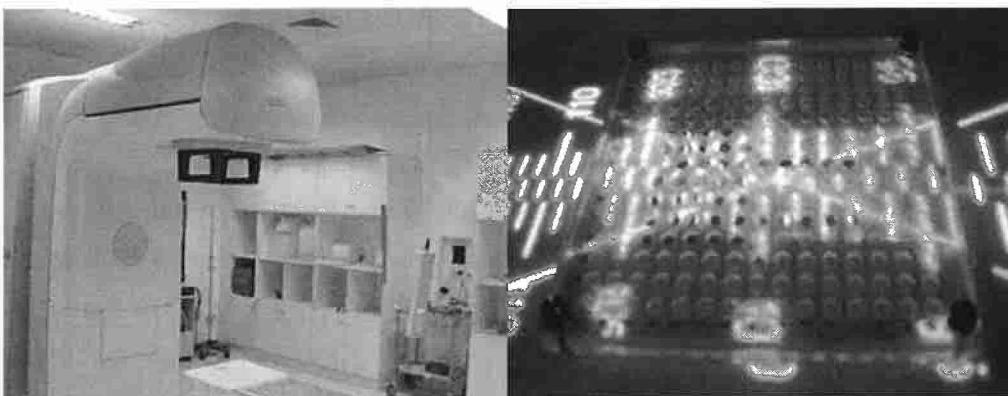


Fig.4 The irradiation source used 6MV LINAC

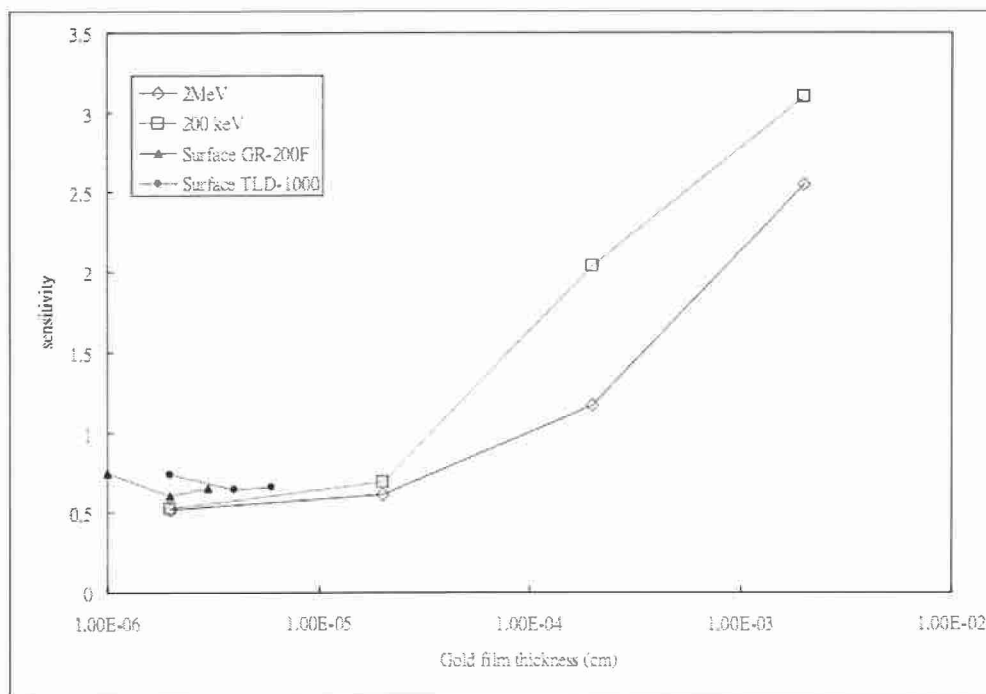


Fig.5 Dose reduction for the thickness of gold foil within sub-micrometer region. The dose enhancement can only be found when gold foil thicker than several micrometers.

## References

1. McCaffrey J. P., Shen, B. Downton, E. Mainegra-Hing. Radiation Attenuation by Radiation Shielding Garments, *Medical Physics*, 2007;34:530-537
2. Hedi K., Amel A. , Mohamed-Karim K. Monte Carlo simulation X-ray buildup factors of lead for shielding calculations, *Medical Physics*, 2007; 34:505-515
3. Helmut S., Maria Z, Heinrich E., Christoph H., Shielding properties of lead-free protective clothing, *Medical Physics*, 2007; 34:4270-4280
4. Regulla D. F., Hiebert L. B., Seidenbusch M., Physical and Biological Interface Dose Effects in Tissue due to X-Ray- Induced Release of Secondary Radiation from Metallic Gold Surfaces. *Radiation Research*, 1998; 150: 92-100
5. Byongim J. Min, Sookil Kim, John J. K. Loh, Young Kap Cho. Photon energy dependence of the sensitivity of LiF TLDs loaded with thin material. *J. Korean Soc Ther Radiol Oncol* 1999; 17: 256-260.

## The optimal composition of DEMBIG gel dosimeter by Taguchi method

Chi-Tsung Chiang, Yuan- Jen Chang<sup>2</sup>, Ji-An Liang<sup>3</sup>, Bor-Tsung Hsieh<sup>1</sup> \*

<sup>1</sup> Institute of Radiological Science, Central Taiwan University of Science and Technology, Taichung, Taiwan

<sup>2</sup> Department of Management Information Systems, Central Taiwan University of Science and Technology, Taichung, Taiwan

<sup>3</sup> Department of Radiation Oncology, China Medical University Hospital, Taichung, Taiwan

### Object

The malignant disease has been a main death reason for threatening Taiwanese life all the time in Taiwan. The way to management the malignant disease was invasion such as surgery and non-invasion such as chemical therapy, radiotherapy. This study was used Taguchi method to determine optimal composition of DEMBIG gel dosimeter and observe the dose response, sensitivity, dose response range.

### Method

The base composition of gel dosimeter from reference was Gelatin: 5%, monomer: 3%, BIS: 3%. Using zero-point proportional of Taguchi method, when based on reference's composition, found the optimal gel compositions that have best sensitivity and linearity of dose response curve by difference gel composition.

### Results

The optimal composition of DEMBIG gel was Gelatin : 7%, DEMA: 5%, BIS: 4%. The recipe was varied three times to find good reproducible of DEMBIG gel. The slope was  $0.99\% \text{ mm}^{-1} \text{ Gy}^{-1}$  and linearity was 0.99.

### Conclusion

Three major results were obtained in this study.

1. The optimal gel composition: Gelatin : 7% , DEMA : 5%, BIS : 4% , called DEMBIG gel.
2. The dose response sensitivity of DEMBIG gel: Slope:  $0.09\% \text{ mm}^{-1} \text{ Gy}^{-1}$ ;  $R^2$ : 0.997.
3. The linear dose range of DEMBIG gel : 0-30 Gy.

## Optimization of treatment time by definition of matrix center in Leksell Gamma Knife Radiosurgery

Cyong-Lian Guo, M. Sc., Cheng-Loong, Liang, M.D., M. Sc.

*Department of Neurosurgery, E-Da Hospital, I-Shou University, Kaohsiung, Taiwan<sup>2</sup>*

### Introduction

The Leksell Gamma Knife Radiosurgery (GKRS) is widely used for the intracranial lesions. The property of high dose and single fraction makes the accuracy of treatment time should be calculated carefully. If the uncertainty of the treatment time reached 3%, there will be some risky effect on radiation output. The purpose of the study is to optimize the treatment time by comparison of three different methods for the matrix center definition.

### Materials and Methods

The dose distribution in a GKRS treatment planning is calculated by  $31 \times 31 \times 31$  matrix calculation points (CP) in the region of interest (ROI). The ROI can be verified by altering the grid size and changing the center of matrix. There are three different methods of the matrix center definition for comparison in this study. The first method is the random method that the center of matrix is defined randomly with a minimal grid size. The second method is the geographic center method that the center of matrix is defined as the center of all the isocenters with a minimal grid size. The third method is the maximal dose point (MDP) method that the center of matrix is defined accordance with that the MDP is located on one of the CP.

### Results and Discussion

Among the 30 treatment plans, 15 have a small tumor size (range: 2.8-4.9 ml) and the remainder have the large tumor size (range: 9.3-15.2 ml). The treatment time of the same treatment planning calculated by the random method, geographic center method and the MDP method were compared. The treatment time of the MDP method is the shortest compared with the other methods. There is a 2-3% difference between MDP method and the other methods. The results of the study suggest that matrix center defined by the MDP method could optimize the treatment time.

### Conclusions

After GKRS planning is completed, using the MDP method to defined the matrix center could obtain an optimal treatment time

**Keywords:** Gamma Knife Radiosurgery, exposure time, maximum point, calculated point

## Presentation of NORM: problems of their being

Etsuko FURUTA

*Ochanomizu University*

### 1. Introduction

Radioisotope of  $^{226}\text{Ra}$  was added to consumer products in Europe in the early 20<sup>th</sup> century<sup>1)</sup>. These consumer products are called Radioactive Consumer Products (RCP). Fluorescent paint for writing figures on clockfaces and gas lantern mantles are famous RCP. In that era, some cream and powder cosmetics added uranium. However, production of almost all these RCP in Europe stopped in the late 1970s. These RCP are not sold in the European markets today. However, there might be still small numbers of RCP sold on the antique markets<sup>1)</sup>.

There are lots of RCP, which contain radioactive materials, in our living space now. When the radioactive sources in RCP are natural materials, they are called NORM (naturally occurring radioactive materials). Recently many NORM are sold all over the world through the Internet. These NORM claim hormesis effects<sup>2)</sup>, minus-ion effects, infrared-ray effects and so on. Makers claim these products are healthful for users. I found that some of their home pages (HP) are linked to one HP which presents the effects of irradiation by low energy  $\gamma$ (X)-ray on cells and/or small-size animals<sup>3)</sup>. However, the effects that people consider healthful have not been

examined with the products themselves; the idea that these effects are indeed healthful is generally accepted by the public, though no actual evidence for each product exists. Almost all these products have no problems legally. However, some of them, for example, cosmetics prohibited in the EU<sup>4)</sup> because they contain radioactive materials, are accepted as NORM in Japan. There are no prohibitions to add radioactive materials to products in Japan. There are only density and quantity limits when adding radioactive materials to consumer products. How is in your country? Do these products need the addition of radioactive materials? Is there any risk to people from radiation exposure by normal use or misuse? My purpose of the poster is the presentation of some NORM and the consideration of the risk and their justification.

### 2. Experimental

Twelve kinds of radioactive consumer products were chosen as samples with a random-selection, which are commonly sold in Japan.

Radioactivities contained in the samples were determined by gamma-ray spectrometry using a high purity Ge detector (HPGe). The measurement

condition of the HPGe detector and the MCA (CANBERRA) are 4 MeV-8192 ch and relative efficiency is 35%. Each sample was measured for 1-96 hours depending on their activities. The efficiency was calculated by using analysis software of LabSOCS (CANBERRA)<sup>5)</sup>.

### 3. Evaluation of exposure

**External exposure:** The skin equivalent dose rate constants intended for only gamma rays of  $2\pi$  directions. The calculation used irradiation geometry from the front to the back (AP) which was one of the skin absorption dose (DT /KA) mentioned in the Table A 14 of ICRP 74<sup>6)</sup>. The calculation of the contribution by the beta rays used an effectiveness dose to the skin by electrons mentioned in the Table A 43 of ICRP 74.

**Internal exposure:** The concentrations of radon (Rn) were measured by the monitor of "pico-rad" and/or "Lucas scintillation cell". The calculation of internal exposure from the hormesis cosmetics were used the soft ware of IDEC Ver.1.0<sup>7)</sup>.

### 3. Results and discussion

All samples contained thorium (Th) and uranium (U) series except sample numbers 9 and 12. The radioactivity densities of samples were from 0.3 Bq·g<sup>-1</sup> of <sup>138</sup>La to 690 Bq·g<sup>-1</sup> of <sup>238</sup>U as shown in Table 1. All exposure doses by normal use were lower than the limits set by law

**Table 1 Radioactivity densities (Bq/g)**

Sample	Th series	U series	Other nuclides
1	44	15	
2	68	13	
3	1	1	
4	220	4	
5	460	88	
6	17	2	
7	160	33	( <sup>40</sup> K)
8	33	4	
9	0.3	—	<sup>138</sup> La : 0.3
10	330	—	
11	170	—	
12	—	690	

as shown in Table 2. However, Rn densities were higher in some cases. Though we cannot confirm that the claimed effects of all NORM are correct or not, we can detect higher densities of Rn when we use them. Moreover, when we use hormesis cosmetics, inhalation of them increases the risk of lung damage and so on.

EURATOM (96/29) is a publication of that chartered organization of the European Union. Items to which radioactive material may not be added mentioned in this publication. At the same time, import of these radioactive items is prohibited, too. The items are foods, drinking water, feed, toys, accessories and cosmetics. Six countries, Germany and so on, in the EU

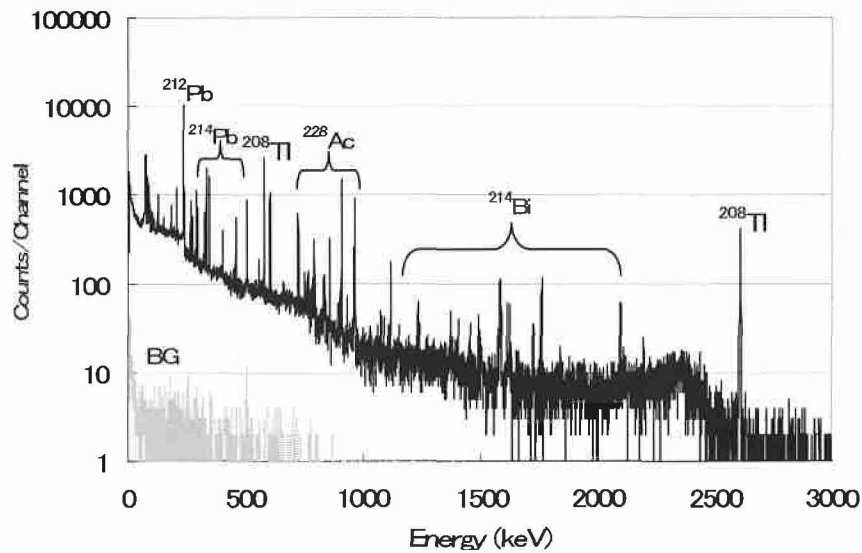


Figure 1  $\gamma$ -Ray spectrum of hormesis jell measured for 1 h by HPGe detector.

Table 2 Exposure dose

Sample	External exposure ( $\mu\text{Sv/h}$ )	Annual dose (mSv / 2000h)	Internal exposure
1	0.2	0.4	Born : 60 $\mu\text{Sv/y}$
2	$6 \times 10^{-2}$	0.1	Lung : 5.5mSv / y
3	$1 \times 10^{-2}$	$2.0 \times 10^{-2}$	Rn : 34 Bq / m <sup>3</sup>
4	0.1	0.2	—
5	2	4	—
6	$8 \times 10^{-6}$	$1.6 \times 10^{-5}$	—
7	$2.3 \times 10^{-3}$	$4.6 \times 10^{-3}$	—
8	0.26	0.5	Rn : 79 Bq / m <sup>3</sup>
9	1	0.2	—
10	0.7/ 1 pack	1.4	( <sup>228</sup> Ac, <sup>212</sup> Pb, <sup>212</sup> Bi, <sup>208</sup> Tl)
11	9	18	—
12	40 ( $\beta$ ray)	80 ( $\beta$ ray)	—

established a prohibition of similar items by law. The EU has decided that there is no justification to add any radioactive materials to the items on the lists and so

they do not check each NORM's radioactivity densities. The idea of "alara" (as low as reasonably achievable) by the ICRP is very important for our

safety from the radioactive materials. The idea is suitable for consumer products containing NORM. If we cannot prove the benefit of each NORM is greater than the risk, then there is no place for the NORM in our living space.

#### 4. Conclusion

Many kinds of consumer products which contain radioactive materials (NORM) exist in our living space. Almost all kinds of NORM contain minerals of Th and U series. Some of NORM raises the risk of exposure in our every day lives.

#### References

- 1) J. Shaw, J. Dunderdale and R. A. Paynter: *Radiation Protection*, 146, p14, 2007.
- 2) T. D. Lucky: *Health Phys.*, 43, p771, 1982.
- 3) Hoshi Y, Nomura T, Oda T, Iwasaki T, Fujita K, Ishikawa Y, Kato A, Ikegami T, Sakai K, Tanooka H and Yamada T.: *J. Radiat. Res.* 41, p129-137, 2000.
- 4) EURATOM; Council Directive 96/29, OJ L159, p7, 1996.
- 5) F.L. Bronson: *J. Radioanal. Nucl. Chem.*, 255, p137-141, 2003.
- 6) ICRP 74E: Conversion coefficients for use in radiological protection against external radiation, ICRP, 194, 223, 1997. (In Japanese)
- 7) JAEA, Internal dose easy calculation code: IDEC Ver.1.0, 2000. (In Japanese)

# A few special educational schemes for the course of radiation measurement laboratory in National Tsing Hua University

Chih-Hao Lee, H.P.Chou and S.H.Jiang

*Department of Engineering and System Science, National Tsing Hua University, Hsinchu, Taiwan.*

*Institute of Nuclear Engineering and Science, National Tsing Hua University, Hsinchu, Taiwan.*

## Abstract

With 30 years of teaching experience in National Tsing Hua University, the schemes for the laboratory course of radiation measurement experimental were modified many times to inspire the creativity of the students and to learn the correct concepts by making errors. A few special designed schemes for this course were introduced and elucidated in this manuscript.

Keywords: radiation measurement laboratory; radiation measurement teaching; nuclear instruments

## 1. Introduction

The laboratory teaching course on nuclear radiation detection and measurement is a very unique curriculum in College of Nuclear Science, National Tsing Hua University. The goal of this course is to offer the student a clear hand on experiments on the nuclear instruments, such as Geiger Mueller (G-M) counter, gas proportional counter, scintillation counter, surface barrier detector and Si and high pure germanium (HPGE) detectors to measure the charged particles, X-and Gamma rays and neutrons. In addition, this course also teaches students to understand the electronics of nuclear instrument modules and the counting statistics on the applications of nuclear industries and radiation applications on all the scientific aspects. This course is offered for more than 30 years at National Tsing Hua University. More than 1000 students have attended this course. The major content of this course is based on the technical notes of ORTEC and CANBERRA companies. This is a supplemental course to a classroom course of "radiation detection and measurement" using the textbook written by G.F.Knoll (1989). With 30 years of teaching experiences, the radiation measurement experimental schemes were modified many times to inspire the creativity of the students and to learn the correct concepts by making errors. A few special designed schemes for the course were prepared to educate the students major in nuclear engineering in setting up a wholesome concept

on radiation measurement. Among them, a few good examples were elucidated in the following:

## 2. Special design of experimental schemes

In the following, thirteen special features in experimental schemes were designed and given :

### 2.1 To understand the impedance match

To understand the impedance match is very important for the student to realize whether the real signal is observed by an oscilloscope. In the experiment of setup of basic nuclear electronic modules, to monitor the pulse height output from a module using a T-connector connected to an oscilloscope is found to be different from the voltage measured with open loop measurement. Students learn that the output voltage will be dropped due to the loading effect or impedance mismatch. By calculating the input resistance of next nuclear module and the output impedance of the output of nuclear module to be measured, the voltage drop and calculated.

### 2.2 Error propagation resulting negative detector dead time

Two methods were used in the laboratory to measure the dead time of the G-M counter, namely, the direct oscilloscope observation and two-source method. The oscilloscope observation is very straightforward to see the time depending pulse height output to measure

the dead time and recovery time. Usually, a strong source was used in these experiments to enhance the dead time contribution. However, in the dead time measurement of a two-source method, a weak radiation source was deliberately used resulting in a very bad statistical error in determining the dead time. Many groups of students found a negative dead time after the error propagation in data analysis. Those negative dead time measured were automatically deleted by students and never reported, resulting in a biased statistical distribution in the error determination after averaging the results from the whole class of students. The instructor, then give a warning to the students that a human judgment resulting in a bias distribution is not a right way to do the experiment. The students learn the academic discipline and the right meaning of a scientist should acted as a nature observer only.

### 2.3 Noise of the discriminator

To test the function of low level discriminator using the output of a pulser as an input source, the instructor asked students to adjust the gain of pulser to obtain half of the count. A difficulty was faced to adjust the gain to an exact half of the counting rate due to the high precision of electronics. Only the noisy electronics can easily achieve half count by adjusting the gain. By counting the data many times, the standard deviation reveals the noisy situation of the electronics system. The student go through the difficulty to adjust the gain own a better nuclear module actually.

### 2.4 Concept of Gaussian distribution and P-value test

For the student to learn about the P-value test in the counting statistics, a ensemble of counting data was collected. Chi-square test was performed to see if the data distribution follows the Gaussian distribution. A mixture of output signal from pulser and the detector preamplifier was feed in the amplifier. A counting statistics on the output of pulses was performed to show a large P value. The pulser provides a 60 Hz pulse, with the weak radiation source, the counting result is distributed in a very narrow distribution which away from the Gaussian distribution with the radiation source alone. On the hand, for a mixture signal of white noise and the radiation source signals, the result will be wider distribution compared to a Gaussian distribution and small P-value can be observed. Students learn the P-value to judge whether the nuclear

electronic system is under normal conditions or not.

### 2.5 To set the right trigger slope and level of a oscilloscope

To really measure the correct pulse shape on the oscilloscope, the trigger level and slope should be set at right position. A pulse with shape of undershot was prepared on purpose by detuning the P/Z cancellation for student to try. Many students can not get the right pulse shape shown on the oscilloscope. Figure 1 shows the result of pulse measurement from the output of an amplifier. An undershot pulse can be seen with the the trigger point at A of Figure 1. The observed pulse is positive. However, when the oscilloscope set at trigger point B with the negative trigger slope of oscilloscope, and larger time base, the pulse height is negative (see inset in Fig. 1) and the measured pulse height is no longer correct. The students usually set a wrong trigger slope and level and wrong time base resulting in a measurement of only incomplete pulse shape. In order to perform this experiment, only analogy oscilloscope was used instead of using the very popular digital oscilloscope.

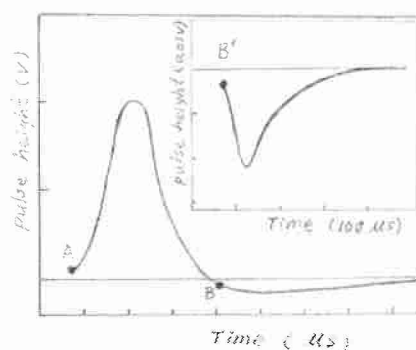


Fig. 1 The measurement of an pulse output from an amplifier with oscilloscope trigger point set at A. The inset shows the trigger point set at B with negative trigger slope.

### 2.6 Error reduction after cumulating the counts

To teach students in understanding the right concept of counting statistics, a group of 30 counts experiments with each measurement 10 s was conducted. The standard deviation obtained from the counting of 30 times is to compare with the one measurement of 300 s. Students might not know which counting scheme can get a better counting statistics error. The comparison of standard deviation obtained by 30 counts each 10 s and one measurement with 300 s should

be similar, which many students get confused.

### 2.7 Gamma ray response to the neutron proportional counter

To test the gamma ray sensitivity of a neutron proportional counter, an intensive  $^{60}\text{Co}$  gamma source was put very close to the  $\text{BF}_3$  detector after calibrating by neutron nuclear reaction peaks. The measured spectra show no peak of  $^{60}\text{Co}$  at the position of 1.172 and 1.332 MeV on MCA. Can students really understand why these peaks are missed? Usually, the gamma ray interaction with the  $\text{BF}_3$  gas proportional counter is small. No signal can be detected. With a strong gamma ray source, the interaction probability can be increased, but still no signal can be detected. Why? The interaction of gamma ray with gas molecules inside the detector creates a long track of ion-pairs compared to the neutron signal. The limited diameter of the proportional counter collects only small part of track of ion pairs generated by the gamma-ray. The pulse height due to the gamma-ray usually is so low to discriminate from the electronic noise.

### 2.8 The low level discrimination for the slope of counting curve

To measure the difference of the slopes of counting rate vs. applied bias on  $\text{BF}_3$  counter and boron lining neutron detector to understand the importance of the response function of a detector under applied bias related to the discrimination levels. In the boron-lining neutron counter, the response function is usually flat at every energy until the maximum energy. The low level discriminator will cut substantially counts resulting a steep slope in the counting curve as functions of bias voltage.

### 2.9 Alpha spectroscopy correction due to the self-absorption of the source

In the alpha spectroscopy measurement, two kinds of  $^{241}\text{Am}$  alpha sources were used. One of them is a standard thin source prepared by electroplating technique. The other one is a thick  $^{241}\text{Am}$  source by depositing for a longer time. The result shows a peak shift to the lower energy and poor energy resolution in measuring the thick sample. Students spend a lot of time to learn that the problem of different results is not due to the detector system at all. It might be due to the source itself also. Actually, only the alpha spectroscopy gives a serious problem of energy shift due to the self-absorption. The gamma-ray

spectroscopy gives no energy shift for the gamma ray or X-ray because no stopping power for photons.

### 2.10 Gamma ray spectroscopy under the insufficient bias

For the gamma ray spectroscopy, usually 3000 V is needed for an HPGe detector. The instructor asked students to compare the response function of detector run at only 300 V to see the peak broaden, peak shift and decrease of peak to Compton ratio for them to really understand the function of HPGe detector. The peak shift with poor resolution is mainly due to incomplete charge collection. The small peak to Compton ratio is due to the small depletion region in the germanium under low bias voltage. The peak efficiency was found to be decreased also. From the peak efficiency decrease an estimation of active depletion region can be estimated.

### 2.11 Understand the offset of energy calibration of an MCA.

During the energy calibration of MCA of the gamma ray spectroscopy measurement, using the HPGe measurement, the instructor asked the students to measure the keV/channel using calibration sources  $^{60}\text{Co}$  and  $^{137}\text{Cs}$ . Then, using the calibrated keV/channel value to predict the peak position of  $^{241}\text{Am}$  source. Usually, the measured channel number is different from the prediction one due to the non-zero offset of MCA which was deliberately detuned by the instructor. The student usually suspects that the keV/ch they calibrated is not accurate enough instead of aware of the MCA consists of an offset in the zero channel.

### 2.12 Understand of the major background of natural radiation

In the HPGe background measurement for 30 min, usually several background gamma ray peaks can be found. The most pronounced peak is  $^{40}\text{K}$  and the intensity can be increased if many students get together to share one detector. This is to illustrate that the major radiation background comes from a human being. A very important understanding on the nature background can be set quantitatively. Another peak,  $^{41}\text{Ar}$ , was frequently found when the Tsing Hua open pool reactor (THOR) was on. The intensity of  $^{41}\text{Ar}$  usually is smaller than  $^{40}\text{K}$  to show the radiation safety of the operation of THOR. In the experiment, usually, two peaks are

always observable with energy of 1.173 and 1.332 MeV. This result is due to the poor experiment condition of the student who never put the standard  $^{60}\text{Co}$  source far away from the detector. Students also learn how far the  $^{60}\text{Co}$  should be put away and how thick the lead shielding is needed to remove this gamma signal.

2.13 XRF (X-ray fluorescence) spectroscopy using Si-pin diode and using digital processor instead of amplifier and MCA

An XRF measurement was carried out using an Amptek Si pin diode and digital processor system. The students learn that the traditional analogy amplifiers and ADC might be obsoleted in the future. The USB connection to a PC might be the best data acquisition system for a great convenience. The XRF experiment is to identify the composition of a material. Usually, a currency coin was used as a standard sample together with a token coin (a fake coin) measurement for students to learn the forensic science. After this experiment, students are eagerly to put their golden rings or platinum necklaces to check their genuineness. It is an experiment of great interest for the students.

## 1. Discussion and Conclusion

In this laboratory course, students work more than 5 h each week in the lab. Most of their time

spending on understanding the experimental result. The instructor will not sign off the experimental course if the student cannot answer the questions listed in the experimental note. A group discussion always took place with a hot debate under the guidance of the instructor.

In summary, we present thirteen points which to be learned in the teaching laboratory course. Each scheme demonstrates an important concept of using the detector with a deep understanding. The students do not only learn how to operation detectors and also to understand the principle thoroughly.

## Acknowledgements

The constant support of Department of Nuclear Engineering, Department of Engineering and System, Department of Nuclear Science for maintenance of equipment and operation cost of the radiation measurement laboratory is acknowledged.

## References

Knoll G.F. Radiation detection and measurement, John Wiley and Sons, New York 1989.

## Development of teaching materials for radiation education using an imaging plate

Eisaku Hamada

*Department of Liberal Arts and Engineering Sciences, Hachinohe National College of  
Technology, Hachinohe, Aomori 039-1192, Japan*

Imaging plates have been used as two-dimensional position detectors for radiation imaging. As the imaging plate with the high detection sensitivity can also record the distribution of the  $^{40}\text{K}$  in the plant, it is useful as a teaching material which can visually confirm the existence of natural radiation. However, the imaging plates cannot be used in the school, because the expensive equipment with a photomultiplier tube (PMT) to read the image.

In order to use the imaging plate for the teaching materials of radiation educations, a new imaging plate reader has been developed. The photostimulated luminescences (PSLs) released from the imaging plate are detected instead of the PMT by a cooled charge-coupled device (CCD) camera (BITRAN, BS-44UV) through an optical filter and an objective lens. Optical filter (SURUGA SEIKI, S76-BG25) is placed front of the CCD camera to block scattered laser light, and to let the stimulated luminescence light pass through.

For confirming the validity of this equipment, a Pb-sheet with five holes was held between the  $^{241}\text{Am}$  alpha-ray source and an imaging plate (FUJI PHOTO FILM, BAS-MS). Figure shows the PSL image measured by the new imaging plate reader.

By the preliminary experiments, it is confirmed that the image of PSL emitted from the imaging plate can be measured by this new method using a cooled CCD camera.

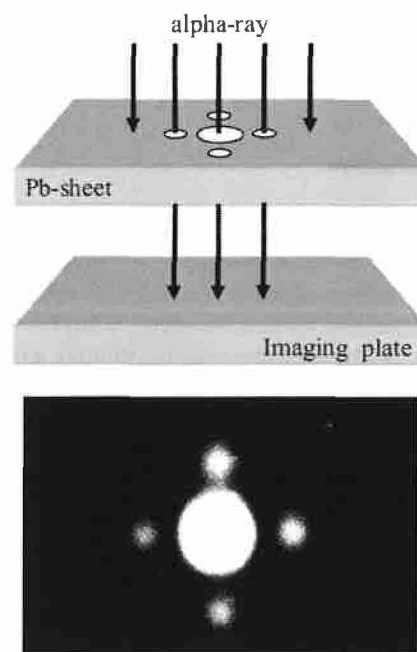


Figure The image of imaging plate measured by the new imaging plate reader.

# Development of Teaching Materials for Radiation Education Using an Imaging Plate

Eisaku Hamada\*

*Department of Liberal Arts and Engineering Sciences, Hachinohe National College of Technology, Hachinohe, Aomori 039-1192, Japan*

---

## Abstract

In order to use an imaging plate for the teaching materials of radiation educations, a new imaging plate reader has been developed. The photostimulated luminescences released from the imaging plate are detected instead of a photomultiplier tube by a cooled charge-coupled device (CCD) camera through an optical filter and an objective lens. The imaging plate which partially irradiated the alpha-ray was read in order to confirm the performance of this system. By the preliminary experiments, it is confirmed that the image of the photostimulated luminescences emitted from the imaging plate can be measured by the new image reader using the cooled CCD camera.

*Keywords:* imaging plate ; photostimulated luminescence ; teaching materials

---

## 1. Introduction

The imaging plates have been used as two-dimensional position detectors for radiation imaging. It has a wide dynamic range and high spatial resolution. Because of these advantages, it has been utilized in many fields, such as medicine, biology and physics (Miyahara *et al* 1986, Amemiya *et al* 1988).

By using the imaging plates with high sensitivity, distribution images of natural radioactivity contained in various natural materials can be observed (Mori *et al* 1996). These images are very exciting for the student. Therefore imaging plates are extremely useful as a teaching material which can visually confirm the existence of natural radiation and radioactivity. In addition, the imaging plates can be used repeatedly by exposing it to visible light.

However, it is difficult to use the imaging plates in a school, because the expensive equipment with a photomultiplier tube needs to read the radiation image.

In this study, a new imaging plate reader has been developed in order to utilize the imaging plates as the teaching material of radiation educations.

## 2. Experimental and results

### *2.1. The mechanism on the storage and readout processes of imaging plates*

The mechanism of an imaging plate has been known as follows (Takahashi *et al* 1984, Miyahara and Kato 1984, Takahashi *et al* 1985) : In the sensitive layer of the imaging plate made of BaFX:Eu<sup>2+</sup>

---

\* Corresponding author. Tel.: +81-298-27-7249; fax: +81-298-27-7249; e-mail: hamada-g@hachinohe-ct.ac.jp

(X=Cl, Br, I) phosphor, ionizing radiation creates a large amount of trapped centers, which record information about the deposited energy and its position.

When the exposed imaging plate is irradiated by He-Ne laser light (633 nm), a photostimulated luminescence is released from the position of the trapped centers.

## 2.2. Outline of the new readout system

The photostimulated luminescences emitted from the storage phosphor are low intensity ultraviolet light (central wavelength is about 390 nm). Generally, the luminescences are detected by a photomultiplier tube in the image reader.

A charge-coupled device (CCD) slightly has the sensitivity for the ultraviolet light. If the photostimulated luminescences can be detected by the CCD camera, it is possible to utilize the imaging plate as the teaching material.

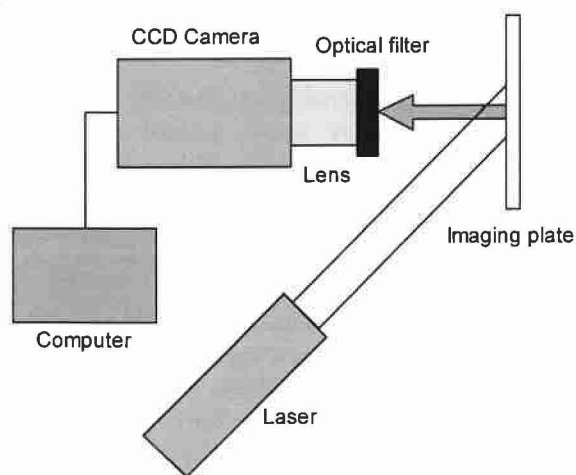


Figure 1: Outline of the new readout system.

Figure 1 shows the outline of the new readout system. The exposed imaging plate is irradiated by the He-Ne laser light (KIKOH GIKEN, MLXI-A13-660). The wavelength of laser is 660 nm (40 mW), and the intensity distribution of laser beam has a non-gaussian profile. The photostimulated luminescences released from the imaging plate are detected by a cooled CCD camera (BITRAN, BS-44UV) through

an optical filter and an objective lens (KOWA, LM8HC). The absolute quantum efficiency of this CCD camera is about 40% for 390nm. The CCD camera is controlled by the computer, and the laser is controlled manually.

Optical filter (SURUGA SEIKI, S76-BG25) is placed front of the CCD camera to block the scattered laser light and to let the photostimulated luminescences pass through.

## 2.3. Experiment procedures

For confirming the validity of this equipment, a Pb-sheet (1.5 mm thickness) with five holes was inserted between the  $^{241}\text{Am}$  alpha-ray source (3 kBq) and an imaging plate (Figure 2). Diameters of each hole were as follows: The central hole was 3.0 mm, and the holes in the outside were 1.2 mm.

The imaging plate used was BAS-MS manufactured by Fuji Photo Film Co. The size was  $70 \times 80$  mm. The exposure time was 8 days in the shielding box of the simplicity made by lead blocks of the 5cm thickness.

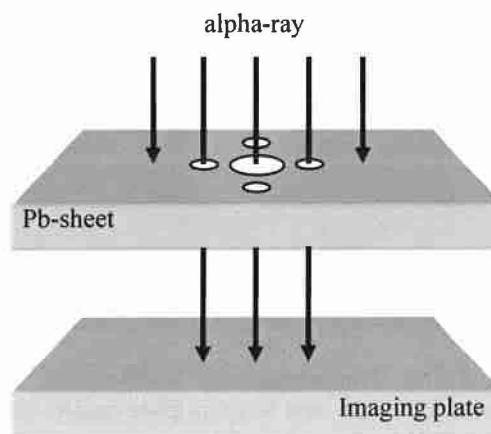


Figure 2: The exposure condition for confirming the performance of the new system.

## 2.4. Results

Figure 3 shows the photostimulated luminescence image obtained by the new imaging plate reader.

The exposed imaging plate was measured in the darkroom in order to cut off the ultraviolet light of the outside as a noise. The cooling temperature of CCD was  $-8^{\circ}\text{C}$ . The measurement time was only five seconds. The laser was on while the shutter of the CCD camera was open.

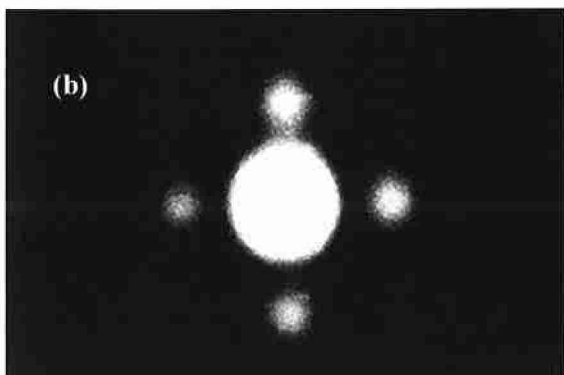
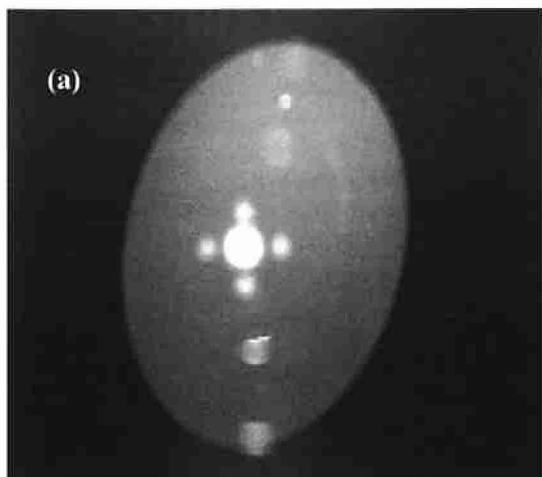


Figure 3: Photostimulated luminescence image measured by the new imaging plate reader. (a): raw image, (b): processed image.

This measurement time was very shorter than that of the conventional reading method. In case of the conventional reader using the photomultiplier tube, a few minutes was necessary in order to read the image, because the photostimulated luminescence was detected by scanning point-by-point by laser beam.

The profile of the laser light was observed in the raw image (Figure 3 (a)), because the optical filter

could not perfectly cut off scattered laser light. Then, the contrast and brightness of the image were adjusted (Figure 3 (b)).

We can observe the five circular images. Those positions are corresponding to the arrangement of the holes of the Pb-sheet.

### 3. Conclusions

By this preliminary experiment, it is confirmed that the image of the photostimulated luminescences emitted from the imaging plate can be measured sufficiently by the new readout system.

The cost of this new equipment is 1/5 of the reader which the company sells. However, this equipment uses the expensive cooled CCD camera to reduce the noise in the measurement. If the luminescences can be detected by a general digital camera, it is possible to utilize the imaging plate in various scenes as teaching materials of the radiation education.

### Acknowledgements

This study was partially supported by the Ministry of Education, Culture, Sports, Science and Technology (MEXT), Grant-in-Aid for Young Scientists (B) (19700622).

### References

- Miyahara J, Takahashi K, Amemiya Y, Kamiya N and Sato Y 1986 A new type of X-ray area detector utilizing laser stimulated luminescence *Nucl. Instr. Meth. in Phys. Res. A* 246 572-578
- Amemiya Y, Matsushita T, Nakagawa A, Sato Y, Miyahara J and Chikawa J 1988 Design and performance of an imaging plate system for X-ray diffraction study *Nucl. Instr. Meth. in Phys. Res. A* 266 645-653
- Mori C, Suzuki T, Koido S, Uritani A, Miyahara H, Yanagida K, Miyahara J and Takahashi K 1996 Effect of background radiation shielding on natural radioactivity distribution measurement with imaging plate *Nucl. Instr. Meth. in Phys. Res. A* 369 544-546
- Takahashi K, Kohda K, Miyahara J, Kanemitsu Y, Amitani K and Shinoya S 1984 Mechanism of

- photostimulated luminescence in BaFX:Eu<sup>2+</sup>  
(X=Cl, Br) phosphors *J. Lumin.* 31-32 266-268
- Miyahara J and Kato H 1984 *OUYO BUTURI* 53  
884-890 [in Japanese]
- Takahashi K, Miyahara J and Shibahara Y 1985 Pho-  
tostimulated Luminescence (PSL) and Color Cen-  
ters in BaFX:Eu<sup>2+</sup> (X=Cl, Br, I) Phosphors *J.*  
*Electrochem. Soc.* 132 1492-1494.

## **Nuclear/Radiation Education at NuTEC/JAEA and a Distance Learning System JNEN**

Kouhei N. KUSHITA, Hiroshi KATO, Hisao OJIMA\* and Jun SUGIMOTO

*Japan Atomic Energy Agency  
Nuclear Technology and Education Center*

While the energy crisis has become of great concern, and the global warming has got more apparent, which could seemingly be ascribed to the increasing consumption of the oil-originated fuels in the world, nuclear energy receives special attention to be one of the promising answer to these issues. Then the constructions of new nuclear plants are scheduled in US, Europe and Asian countries in the coming years. A problem is that we lack nuclear human resources because of the long slackening years in the nuclear world after several serious nuclear accidents. For the coming possible nuclear age, we need sufficient number of nuclear human resources to conduct those plans and operate the plants safe and sound.

There are number of activities of nuclear and radiation education in Japan as well as in the world. Japan Atomic Energy Agency (JAEA), as the largest nuclear institute in Japan, tries to contribute to the nuclear/radiation education through original training courses and cooperative education activities, in addition to research activities.

At Nuclear Technology and Education Center (NuTEC) of JAEA, we have organized various kinds of training courses to meet the domestic and international needs.

We have conducted international nuclear/radiation training through JTC (Joint Training Courses) with some Asian countries, and cooperated with FNCA, ANSN, or IAEA activities. We also cooperate with domestic universities for nuclear/radiation education, in addition to research activities. JAEA, through NuTEC, has made cooperation agreements with 14 graduate universities and 1 university for the nuclear/radiation education, as of 2008. We dispatch 55 JAEA staff as the visiting professors to these universities, and accept 23 graduate students under the agreements.

We also cooperate for the Nuclear Human Resources Development Program conducted by MEXT (Ministry of Education, Culture, Science and Technology) and METI (Ministry of Economy, Trade and Industry) of Japan by dispatching our staff as the lecturers, accepting facility visitors, or by

providing the students with experimental training using our laboratories. Special cooperation has been carried out between JAEA and the Nuclear Professional School, University of Tokyo (NPS/UT). More than 100 JAEA staff, researchers and engineers cooperate with NPS/UT in the lectures and training experiments.

A new multi-directional distance learning system for the nuclear/radiation education has been formally launched in 2007 connecting several sites of JAEA and three universities based on the agreement. This system is called the Japan Nuclear Education Network (JNEN), which expanded in 2008 to include five universities.

Through JNEN, students of distant universities can take lectures of the professors of another university on the real time. The professors and the students of various universities can

make Q&A or to discuss on the topic of interest through wide monitors multi-directionally on the real time. The students can review the lessons by the e-learning system after the lectures. In 2007, about 70 students of participant universities took the lectures through this system.

In addition to the lectures, some experimental courses are organized in the summer vacation season to experience the handling of nuclear materials, radioisotopes, or glove boxes, using the facilities of Nuclear Fuel Cycle Engineering Laboratories of JAEA.

We plan to expand this network to some more universities of Japan, and preferably to some foreign universities in the future.

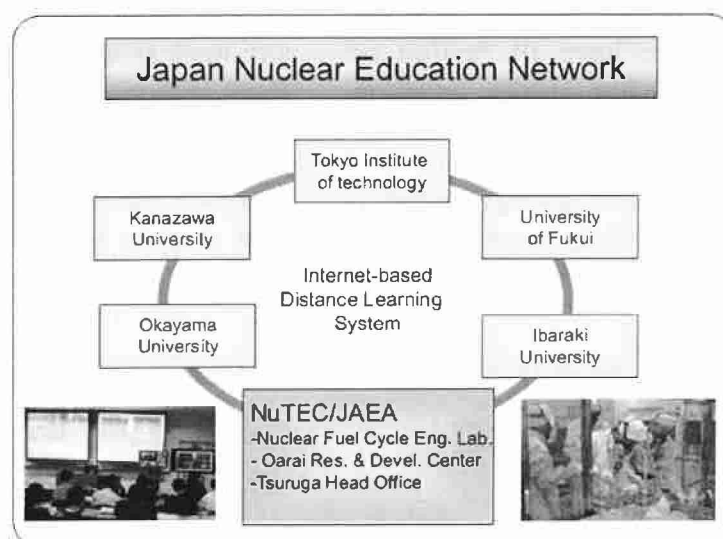


Fig.1 Japan Nuclear Education Network

---

## Radiation Education using Sparklers for Entire Beginners

Michi Aratani

Rokkasho Culture Societ, Rokkasho Cultural Exchange Plaza, Swany

1-8, Nozuki, Obuchi, Rokkasho, Aomori, 039-3212, Japan

---

### Abstract

Local residents at the nuclear site as Rokkasho are said to be entire beginners of radiations, because they have not been given any kind of fundamental knowledge on nuclei and radiations at their school times. Lectures by Public Acceptance (PA) activities are sometimes performed for them, but these kinds of official efforts are not so fruitful that they may be left as ignorant as before. After many try-and-errors during several years, a hint is come from an essay of Terada Torahiko on a Japanese sparkler (toy firework, 線香花火). The toy firework is made of 0.1g of black gunpowder, which is packaged by thin cellulose paper, and twisted into a thin string as incense. After firing, the powder is molten to be a fireball. Soon it begins emitting sparks during about 40 sec. This fireball of molten salt may be regarded as a visual model of excited state of a nucleus, from which radiations (sparks) are emitted on their inherent lifetimes. Neither nuclei nor radiations are seen by our eyes. Both a fireball and sparks, however, are seen well by our eyes. It has been concluded that Japanese sparkler is a powerful tool for radiation education for entire beginners of radiations above-mentioned.

*Keywords: Japanese sparkler; Toy firework; Visual model of nuclei and radiations*

---

### 1. Introduction

About 35% of electric power depends on 54 atomic power stations in Japan. People, however, have ill feeling on atomic power, nuclear energy, radiation, and so on. Even after 63 years of the nuclear events at Hiroshima and Nagasaki, a nuclear allergy, what is so-called, is seen widely among Japanese society. To make bad things worse, the

nuclear allergy is always being reproduced by various kinds of anti-nuclear expressions or people. So, those who work in public acceptance for national policy of nuclear energy, especially with recycling facility of spent fuel as at Rokkasho site, must powerfully give a great sense of security to local residents as entire beginners, before they

---

\*Corresponding author Tel.:+8-117-572-3400; fax: +8-117-572-3404; e-mail: suwany97@jomon.ne.jp

have encountered to the anti-nuclear people or expressions. Several methods for radiation education are tried and are observed to be effective or not. One of the most effective methods has been shown to be utilization of a periodic table, which serves as a very powerful tool, especially those who have studied chemistry (Aratani M. and Osanai Y. 2000). This method, however, seems to be limited to rather highly educated people. So, an almighty method even to entire beginners has been explored for several years. One of hints is come from the Essay of Terada Torahiko (1878 - 1935), a famous earth scientist and, at the same time, a notable man of letters. His essay on a sparkler has been adopted and appeared in a national language textbook of junior high school authorized by the Ministry of Education.

## 2. Materials and Methods

The sparkler is made of 0.1g of black gunpowder, components of which are potassium nitrate, sulfur, and very fine carbon powder from special pine tree resin (the last material is said to be same with high class ink stick for art of calligraphy). The powder is packed with thin cellulose paper, which is twisted into a thin string as incense. After firing at the bottom of the string, combustion of packing paper is seen to start. Terada described sparkler combustion processes from start to end as four stages (Terada 1927): The first stage is great flickering flames of a packing paper combustion as **peony petals**; the second one is melting of gunpowder due to heat of the paper combustion, formation of a quietly bubbling fireball of molten powder followed by emitting of sparks as **pine needles**; the third one is weakened hanging sparks with a partially parabolic orbit as **a weeping willow**; the fourth one is very weak, short, and thin sparks from the fireball diminishing smaller as

**scattering chrysanthemum petals.**

## 3. Results

List of performances using sparklers is as follows:

- 01: Osanai Y, Aratani M, and Tsushima K 2003 Aoimori Science BBL Seminar Let's do Koshiha ! Science Class for Father and Children, Sanbohgakuen Asunaro Kindergarten Aomori September
- 02: Aratani M, Hamada E, and Saji H 2004 Joyful Science: Stars and us *Institute of Environmental Sciences Delivery Lecture Meeting* Aburakawa Kindergarten, Aomori February
- 03: Osani Y, Aratani M, and Tsushima K 2005 Miraculous Science Experiment Class, Lifelong Learning Fair Social Education Center Aomori October,
- 04: Aratani M, Osanai Y, Maki S 2006 Science World seen through Sparklers Science Fair Towada August
- 05: Osanai Y, Aratani M, and Tsushima K 2006 Miraculous Science Experiment Class Radiation Measurements using Rat Sparklers Lifelong Learning Fair Social Education Center Aomori September
- 06: Osanai Y, Aratani M 2007 Energy Experiment using Sparklers Aoimori Science BBL Seminar, Cycle Information Center Aomori March
- 07: Aratani M, Inomata Y and Sasaki M 2007 Learning of High-level Natural Radiations through Experience *The Ministry's Summer School for Eggs of Scientists and Engineers* National Women's Education Center Musashi Ranzan August
- 08: Osanai Y, Aratani M, Tsushima K, Hosokawa S, Miyakawa M, 2007 Joyful Experiment Lifelong Learning Fair Social Education Center Aomori October
- 09: Aratani M, Osanai Y, and Hosokawa

S 2007 Let's Learn the Universe and Radiation using Sparklers Science Fair Aomori Arena October

- 10: Atatani M and Inomata Y 2008 Learning of Natural Radiation through Nuclear Phenomena in the universe *The Ministry's Summer School for Eggs of Scientists and Engineers* National Women's Education Center Musashi Ranzan August

The fireball above described seems to give us intuitively an image (P03-06) of energetic condensed mass emanating energies, and plays an important role as a visual model of excited nucleus emitting radiations. Although neither nuclei nor radiations are to be seen by our eyes, both the fireball and the sparks due to sparklers are seen well by our eyes, even in case of children in Kindergartens (P01-02). Both children and adult (their parents) have in mind a clear image of nucleus as like as the fireball. In case of rather the highly educated, this model is to be able to lead them far from the earth or Japan and to bring them to limit of the universe. In other words, the present model is able to elevate us to height of universality in recognition, and even make us go farther across the right (energy for daily life) and the wrong (bombs). In some big events of science some house wives have confessed that her image on nuclei and radiations had drastically changed (P05-10) after observation of sparklers and following radiation measurements. They feel that nuclei and radiations in the universe may be so beautiful as the fireball and the sparks from the sparkler. This result means that they have recognized nuclei and radiations free from ill feeling they have had held before without reason.

#### 4. Discussion

The description of the four stages of

sparklers by Terada is so beautiful that we may go back to a juvenile mind, because we all have experiences and reminiscences on the sparkler playing in summer evening or night with family or friends. Terada himself wrote that whenever his mother and he played sparklers, she had enjoyed expressing at the stage of the weak short sparks as "scattering chrysanthemum petals!"

Recently Prof. Dr. Yamana (Yamana 2008) talked about big ball skyrocket of fireworks, sparklers, and firefly blinking or flickering as what correspond to kinds of radiations and counting rates of radiation sources. In Japan men of fireworks express their works as stars (Yoshida et al 2007). This fact has symbolical meaning in history of sciences. Gamov has told that his big bang theory had been stimulated by the first explosion with mushroom-shaped cloud in the first plutonium bomb experiment in Nevada. A fireball, irrelative to be small or big, seems to leads us an essential recognition. So, this model is easily expanded to the sun (also star, which is fireball of nuclear fusion of hydrogen into helium, and the supernova, which seems to us as like as cosmic firework (Aratani 2003, Agawa 2007) in practice.

#### 5. Conclusion

Neither nuclei nor radiations are seen by our eyes. But, the fireball and the sparks of sparklers are well seen by our eyes. So, the fireball and the sparks offer visual model of nucleus at excited states and radiations being emitted there. It is concluded that sparklers are powerful tool for radiation education of entire beginners who have not been given any kind of fundamental knowledge on nuclei and radiations in their school times. They may have an intuitive image on nuclei and radiation through the beautiful processes of sparkler co

### Acknowledgements

The author expresses her thanks to Late Dr Y Osanai for her sincere interest in sparklers, and for her winning of Inspiration Laboratory Agilent 2007 Prize. The author expresses her thanks to Mr Konishi, Director of Agilent Technology Co Ltd for his appreciation of our idea and activities for science Education using sparklers. The author also her thanks to Ms K Tsushima for her suggestion of utilizing a tea storage box as a safety chamber for sparkler demonstration because of its inner surface made of a zinc sheet.

### References

- Aratani M, Osanai Y, Tsushima K 2004 Periodic Table as a powerful tool for Radiation Education Proceedings of the Third International Symposium on Radiation Education Nagasaki
- Aratani M 2003 Caught Neutrinos at the Kamioka Mine Institute of Environmental Sciences Mini Encyclopedia 83 Photograph of the Supernova 1987A
- Aratani M and Osanai y Tsushima K 2003 Science Education in Lifelong Education Annual Report of Society of Japanese Women Scientists 4
- Aratani M 2006 the Society of Japanese Women Scientists NEWS No 100 5
- Aratani M, Osanai Y, Tsushima K 2006 Science Education in Lifelong Education 2 ibid 29-45
- Aratani M, Osanai Y 2006 Miraculous Science Experiment Class, Lifelong Learning Fair Social Education Center Aomori
- Aratani M, Osanai Y, Tsushima K 2007 Radiation Education using sparklers Proceedings of the 51st Annual meeting of Radiochemistry, the Society of Japanese Radiochemical Sciences, Shizuoka
- Agawa H 2007 Lives of Stars Bungei Shuju 7
- Terada T 1927 Essay Collections 2 Sparkler Iwanami Edited by Komiya T
- Yamana H 2008 Environmental and Energy in Future and Recycling Factory of Spent Nuclear Fuel The 16th Pacific Basin Nuclear Conference Cultural Exchange Program, Open Lecture for Citizens Aomori
- Yoshida T et al 2007 Introduction to Fire works Research Pleiades Press

## **Newly established Aomori Branch of Radiation Education Forum: case report on radiation education implementation for the local residents by Aomori Branch**

Sumiko Sasagawa

*NPO Radiation Education Forum*

*Shimokubo 1-3-6-C, Misawa, Aomori Prefecture 033-0023, Japan*

### **Background and introduction**

Many kinds of nuclear industry facilities are located in the districts, e.g. Rokkasho-mura, Higashidori-mura, Mutsu-shi, Ooma-machi, etc. throughout the Shimokita Peninsula in Aomori Prefecture, Japan. In Rokkasho-mura nuclear fuel cycle facilities have been constructed on the commercial basis and a large scale processing facility is now on the final stage of test run before the commencement of operation in due time. In Higashidori-mura a nuclear power plant of Tohoku Electric Power Co. Ltd. is in operation and generating electricity of 1.1 GWh. In Mutsu-shi the project to construct an interim storage facility storing spent fuel is in progress by Recyclable-Fuel Storage Co. Ltd. In Ooma-machi, construction of an advanced boiling water reactor (ABWR) which uses mixed oxide nuclear fuel is now under way. These situations around the Shimokita Peninsula area, thus, have enhanced the need to provide precise and up-to-date knowledge and information relating to nuclear and radiation safety to all people including local residents, local administrative bodies, operators of the plants as well as consultative specialists.

Radiation Education Forum (REF) has recognized a new role to meet such a situation and decided to establish its branch in Aomori (Aomori Branch, REF-AB) in FY 2007 in order to effectively assign its manpower and experiences to social and lifelong education as well as school education in which REF has been entirely concerned so far. The mission of REF-AB is, therefore, to communicate with the local residents, and to help them feel at ease where nuclear and radiation safety becomes of concern, taking fully into account the interests and anxiety occurring in their minds. REF-AB has been organizing seminars (REF-AB seminar) near the sites as an effective means to facilitate information exchange with the local residents.

In this paper, we are introducing the experience of REF-AB in the first year when we started our activities.

### **Results and discussions**

The first REF-AB seminar was held at 14 July in Rokkasho as Commemorative

seminar with a theme “Harmony of Nuclear Energy, Radiation and Music”. The seminar was opened by a musical performance of a trio of piano, koto which is a Japanese traditional music instrument, and cello, followed by a keynote lecture by Dr. Tatsuo Matsuura, Secretary-general of REF and a special lecture by Dr. Akito Arima, President of REF. The reason why the musical performance was set up in the opening of the seminar was to create an atmosphere which all the participants could feel at ease and spend pleasant time, as if they were in a café.

The second REF-AB seminar was held at 10 November, in Rokkasho, with a theme “Radon spa, its components and health effects”, to which Dr. Kimiko Horiuchi, a board member of REF, was invited to present a special lecture. The seminar also included an experimental section in which all the participants could handle usual radiation measuring instruments and carry out measurements of radiation surrounding them.

At each seminar, REF-AB carried out an inquiry to the participants by asking to fill a questionnaire on what issues to be focused in the discussion at the seminar and on how to be organized the seminar. From analysis of answers, REF-AB recognized the necessity to organize an occasion where any stakeholder can easily meet and exchange each other information on what the problem is. REF-AB also recognized the necessity to organize small meetings like so-called “science café” where everyone can participate in the discussion not only on the scientific issues concerning nuclear energy and radiation effects but also on the cultural and social sciences, including art, music and literature as he or she participates in a chatting on his or her ordinary life.

# Newly established Aomori Branch of Radiation Education Forum: case report on implementation of radiation education for the local residents by Aomori Branch

Sumiko Sasagawa

*NPO Radiation Education Forum, Shimokubo 1-3-6-C, Misawa, Aomori Prefecture 033-0023, Japan*

---

## Abstract

Radiation Education Forum Aomori Branch (REF-AB) was established with a mission to communicate with the local residents, and to help them feel at ease taking fully into account interests and anxiety occurring in their minds where issues on nuclear and radiation safety become of concern. In the first year of FY2007, REF-AB organized two seminars near the sites as an effective means to facilitate information exchange with the local residents and carried out an inquiry to the participants by asking to fill a questionnaire on what issues to be focused in the discussion at the seminar and on how to organize the seminar. Analysis of the answers suggested that it was necessary to organize an occasion where any stakeholder could easily meet and exchange each other information on what the problem is. REF-AB also recognized the necessity to organize small meetings like so-called “science café” where everyone could participate in the discussion not only on the scientific issues concerning nuclear energy and radiation effects but also on the cultural and social sciences, including art, music and literature as he or she participates in a chatting on his or her ordinary life.

*keywords:* radiation education, lifelong education, local residents, nuclear safety, Rokkasho

---

## 1. Introduction

Many kinds of nuclear industry facilities are located in the districts, e.g. Rokkasho-mura, Higashidori-mura, Mutsu-shi, Ooma-machi, throughout the Shimokita Peninsula in Aomori Prefecture, Japan (Sasagawa 2007). In Rokkasho-mura nuclear fuel cycle facilities have been constructed on the commercial basis and a large scale spent fuel reprocessing facility is now on the final stage of test run before the commencement of operation in due time. In Higashidori-mura a nuclear power plant of Tohoku Electric Power Co. Ltd. is in operation and generating electricity of 1.1 GWh. In Mutsu-shi the project to construct an interim storage facility storing spent fuel is in progress by Recyclable-Fuel Storage

Co. Ltd. In Ooma-machi construction of a nuclear power plant with an advanced boiling water reactor (ABWR) which uses mixed oxide nuclear fuel is now under way. These situations around the Shimokita Peninsula area, thus, have enhanced the need to provide precise and up-to-date knowledge and information relating to nuclear and radiation safety to all people including local residents, local administrative bodies, operators of the plants as well as consultative specialists (Sasagawa 2007).

Radiation Education Forum (REF) has recognized a new role to meet such a situation and decided to establish its branch in Aomori (Aomori Branch, REF-AB) in FY 2007 in order to effectively assign its manpower and experiences to social and lifelong education as well as school education in which REF has been entirely concerned so far (Sasagawa 2006). The mission of REF-AB is, therefore, to

communicate with the local residents, and to help them feel at ease where nuclear and radiation safety becomes of concern, taking fully into account interests and anxiety occurring in their minds. REF-AB started its activity by organizing seminars (REF-AB seminar) near the sites as an effective means to facilitate information exchange with the local residents.

In this paper, the author is introducing the experience of REF-AB in the first year.

## **2. Outline and Activities of REF-AB in the First Year**

### *2.1. Organization of Aomori Branch*

REF-AB is composed of a chief, a secretariat-general, and several staff. REF-AB is also composed of voluntary members and local supporters who join the seminars and share partly monetary funds for the activities of REF-AB.

### *2.2. First REF-AB seminar*

The first REF-AB seminar (Radiation Education Forum Aomori Branch 2007-1) was held at 14 July in Rokkasho-mura as a commemorative seminar with a theme "Harmony of Nuclear Energy, Radiation and Music". The seminar was opened by a musical performance of a trio of piano, koto which is a Japanese traditional music instrument, and cello, followed by a keynote lecture by Dr. Tatsuo Matsuura, Secretary-general of REF and a special lecture by Dr. Akito Arima, President of REF. The reason why the musical performance was set up in the opening of the seminar was to create an atmosphere which all the participants could feel at ease and spend pleasant time as if they were in a café.

### *2.3. Second REF-AB seminar*

The second REF-AB seminar (Radiation Education Forum Aomori Branch 2007-2) was held at 10 November, in Rokkasho-mura, with a theme "Radon Spa, its Components and Health Effects", to which Dr. Kimiko Horiuchi, a board member of REF, was invited to present a special lecture. The seminar also included an study class in which all the participants could handle usual radiation measuring instruments

and carry out measurements of radiation surrounding them.

### *2.4. Analysis of questionnaire*

At each seminar, REF-AB carried out an inquiry to the participants by asking to fill a questionnaire on what issues to be focused in the discussion at the seminar and on how to organize the seminar. The response rate through two seminars was around 60%, i.e., 22 out of 45 participants replied at the first seminar, whereas 20 out of 25 participants replied at the second seminar. There were a lot of informative findings which would help us to pursue our activities more effectively, especially on the measures for notifying our planning and program and groups of residents to be notified. It is not so easy in general to attract interests of the local residents to the issues on nuclear and radiation safety, which is rather complicated to understand and far from their ordinary lives. It would be important, therefore, to know how the participants got information on the REF-AB seminars and who intended to attend them.

According to the result of questionnaire, source of information about the seminar for the participants was mainly handbill which REF-AB printed and distributed and word-of-mouth (Fig. 1). The seminars were notified through three commercial newspapers and one village paper "Koho Rokkasho" printed and distributed by Rokkasho Village Office, but these papers seem not to have been much effective. This means that face-to-face communication is a key measure to inform the activities of the private-sector organization like REF to the local residents. As a matter of course, widely distributed papers may be usefull, judging from the fact that participants came not only from Rokkasho-mura but also from neighboring cities including Misawa, Towada, Oirase, and districts all-over Aomori Prefecture.

The age of participants in two seminars ranged from 30s to 70s and over. However, the elderly older than 50s had the majority than younger generations (Fig. 2), and the number of women was almost twice as many as that of men. This meant that participants of the seminars were occupied by elderly women rather than younger men. In future REF-AB seminar, it will be anticipated that younger men and women as well as the elderly are encouraged to join and develop the scientific literacy.

The speakers were outstanding in the field of concern and well known to the general public in Japan, therefore, the participants were pleased with such an occasion and discussion set up after each lecture.

Furthermore, from analysis of answers, REF-AB recognized the necessity to organize an occasion where any stakeholder could easily meet and exchange each other information on what the problem was. In this context, the REF-AB felt the efficiency and efficacy of small meetings like so-called "science café" (Watanabe 2005) where everyone could participate in the discussion not only on the scientific issues concerning nuclear energy and radiation effects for instance but also on the cultural and social sciences, including art, music and literature as he or she participated in a chatting on his or her ordinary life (Sasagawa 2002, Sasagawa 2004, Sasagawa and Matsuura 2007). And the analysis of questionnaire showed that a musical performance of a trio of piano, koto, and cello at the opening of the first seminar was willingly accepted by all the participants.

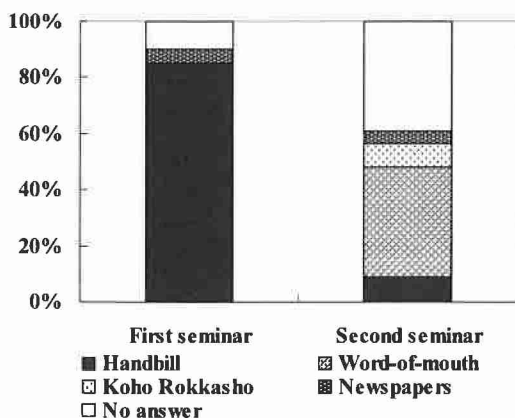


Fig. 1. Source of information of seminar

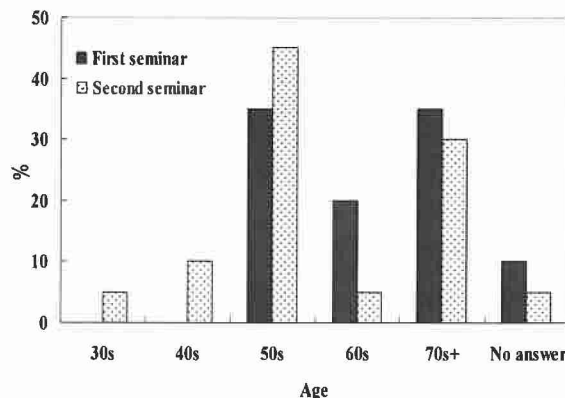


Fig. 2. Distribution of ages of the participants

### Acknowledgements

The author would like to appreciate all the staff and all the participants to seminars of REF-AB.

### References

- Sasagawa S 2002 A story of the Nobel Prize: a trial of science literacy for citizens *Ann Soc Jap Women Sci* 3 56-60 (in Japanese)
- Sasagawa S 2004 How public relations can bind nuclear safety and peoples' anxiety *Radiation Education* 8 31-8 (in Japanese)
- Watanabe M 2005 How can we plan science and technology communication: from one-way communication to two-way communication *Science & Technology Journal* No.4 20-1 (in Japanese)
- Sasagawa S 2007 Report of FY2007 activities of Aomori Branch of Radiation Education Forum *Radiation Education* 11 41-52 (in Japanese)
- Sasagawa S 2006 Toward establishing Aomori Branch *Radiation Education Forum Newsletter* No. 34 p.6 (in Japanese)
- Sasagawa S, Matsuura T 2007 FY2007 report of Aomori Branch of Radiation Education Forum *Proceedings of 44th Annual Meeting on Radioisotope and Radiation Research* Tokyo 4-6 July 2007 p.127 (in Japanese)

- Radiation Education Forum Aomori Branch (ed)  
2007-1 "Harmony of Nuclear Energy, Radiation  
and Music" *Proceedings of first seminar of  
Radiation Education Forum Aomori Branch*  
Rokkasho-mura 14 July 2007 (in Japanese)
- Radiation Education Forum Aomori Branch (ed)  
2007-2 "Radon Spa, its Components and Health  
Effects" *Proceedings of second seminar of  
Radiation Education Forum Aomori Branch*  
Rokkasho-mura 10 November 2007 (in Japanese)

# Proposal for active use of $^{68}\text{Ge}$ - $^{68}\text{Ga}$ milking generator in education of various categories

T. Nozaki

*Honorary Scientist of RIKEN, and Retired Professor of Kitasato University, Japan.*

*Home address: 4-2-3-105 Higashinaruse, Isehara, Kanagawa 259-1117, Japan*

Milking generator of  $^{68}\text{Ge}$ - $^{68}\text{Ga}$  can be regarded as highly useful for education of various categories, offering by actual experiments experiences of the handling of radiation and radioactivity as well as some knowledge about the nature itself. The measurement of decay curve over several half-lives, the most basic experiment in radiation education, is thought to be highly instructive for students of high schools and universities of all fields and adults of all occupations, arousing notable interest in the exponential decrease. This experiment can be meaningful enough for economists and politicians, to whom thorough understanding of exponential function is now indispensable. The cow and daughter of this generator both are of nuclear properties well suitable for the education use. The following experiments with related lectures and exercises are probably interesting and impressive for science-oriented students: (1) observation of approach to radiochemical equilibrium; (2) distribution measurement of positron emitters; (3) preparation of  $^{68}\text{Ga}$ -labeled compounds and their tracer use. For wide education use of the generator, organizations should be founded for producing and keeping large numbers of the generator and for supplying them to users preferably under rental system.

*Keywords:*  $^{68}\text{Ge}$ - $^{68}\text{Ga}$  milking generator; education; decay measurement; exponential function; distribution measurement; positron emitters

## 1. Introduction

Radionuclides have existed on the earth since its birth, and now their unique properties provide us with information valuable for the elucidation of the nature itself as well as various means widely useful in our modern life, as shown in Table 1. The author believes that radionuclides can be used effectively also for the education of students and adults of almost all situations to give vivid experiences of actual observation of natural phenomena, although *Radiation Education* now means usually the teaching on radiation and radioactivity themselves. Particularly important and effective would be the decay curve measurement for the teaching on the exponential change, which should have been thoroughly understood by politicians and economists before the present world-wide economical crisis.

Table 1. Main characteristics and use of radioisotopes

Characteristics	Use
1. Decay properties: Exponential decay independent of chemical state and environment	Age determination, dating Education of exponential function and reaction kinetics
2. Behavior identical with stable isotopes	Radiotracer studies of various kinds
3. Emission of radiations: Capability of high- sensitivity determination; localization; and non- destructive, continuous measurement	Radiation source for reactions of radiation chemistry and biology Elemental analysis Gauging source Diagnosis and therapy

Corresponding author: Tel: +81-463-92-3136;

fax: +81-463-92-3136; e-mail: nozatadism@nifty.com

Milking generators are regarded as the best source of radioactivity for these uses. Of them, the  $^{68}\text{Ge}$ - $^{68}\text{Ga}$  generator can be expected to be the most suitable. In the education of science-oriented students, this generator can offer a variety of uniquely interesting subjects of experiment.

Table 2. Nuclear properties of  $^{68}\text{Ge}$  and  $^{68}\text{Ga}$

Nuclide	$^{68}\text{Ge}$	$^{68}\text{Ga}$
Half-life	288 d	68.1 m
Decay mode	EC (100 %)	$\beta^+$ (90 %), 1.89 MeV EC (10 %)
Gamma-ray	none	1.08 MeV (1 %); etc.

## 2. Materials and Methods

Based on experiences of research on the production of radionuclides and labeled compounds in RIKEN, Japan, and of the education by lectures and experiments in radiochemistry and related fields in Kitasato University, Waseda University and Radioisotope School, JAERI, Japan, the author has looked for subjects of experiments well adoptable in university curricula to provide students with vivid impressions effective for understanding fundamental principles in natural and social phenomena. Lectures and exercises related to the experiments have also been considered.

Some candidate experiments were tested in the School of Hygienic Sciences, Kitasato University by the use of its facilities and instruments for undergraduate experiments. As the radiation detector, 2"x2" NaI scintillators were mostly used under suitable shielding or collimation with lead blocks, often with single-channel pulse-height selectors. Two scintillators operated in coincidence were used for the determination of  $^{68}\text{Ga}$  positron activity. Some other detectors were also used for comparison. All reagents were of reagent grade and used without purification.

Milking generators were selected under consideration of the half-life for the cow and daughter, usefulness, accessibility, and various other factors. An aged  $^{68}\text{Ge}$ - $^{68}\text{Ga}$  generator made as calibration source was offered from a hospital and

used. The  $^{68}\text{Ga}$  was eluted from this generator with dilute hydrochloric acid.

## 3. Results

### 3-1. Usefulness of the generator

The nuclear properties in Table 2 together with some experimental results proved the  $^{68}\text{Ge}$ - $^{68}\text{Ga}$  generator to be more suitable than the following generators often used for the education of undergraduate students:  $^{137}\text{Cs}$ (30.2 y) -  $^{137\text{m}}\text{Ba}$ (2.55 m),  $^{90}\text{Sr}$ (28.8 y) -  $^{90}\text{Y}$ (64.1 h),  $^{140}\text{Ba}$ (12.8 d) -  $^{140}\text{La}$ (40.2 h), and  $^{99}\text{Mo}$ (66.0 h) -  $^{99\text{m}}\text{Tc}$ (6.02 h). Half-lives of  $^{68}\text{Ge}$  and  $^{68}\text{Ga}$  are highly suitable for cow and daughter, respectively, and  $^{68}\text{Ga}$  can be measured easily and reliably by many kinds of common detectors in the presence of  $^{68}\text{Ge}$ . Also, some interesting radiotracer experiments are found by the use of  $^{68}\text{Ga}$ , as shown later in this article..

### 3-2. Milking and decay curve measurement

First of all, the milking property of the given generator should be known by receiving the milking eluate in small fractions and measuring  $^{68}\text{Ga}$  activity in each fraction to give the elution curve. For the measurement of decay, the following procedure is thought to be suitable: (1) Elute  $^{68}\text{Ga}$  at once from the generator, and divide the eluate in fractions each containing  $(1\sim 10) \times 10^4$  cpm of  $^{68}\text{Ga}$  in dishes or vials for counting; (2) Measure the radioactivity frequently for the first 1 hour and then with intervals conveniently selected, or continuously by the use of a recorder for 12 hours or more; (3) After the subtraction of background, draw the decay curve on semi-logarithmic papers; (4) Obtain the half-life and the decay constant of  $^{68}\text{Ga}$ , and, discuss on possible uncertainty in the result..

This experiment, coupled with suitable exercise problems, is thought to be highly effective for the understanding of exponential and logarithmic functions, particularly for those who are not directly related with science and technology. Before the advent of electronic calculators, many people unconsciously became acquainted with the exponential change by the use of slide rule and in the play of mahjong. The author guesses with great regret: "If scientist had taught the property of

exponential function to politicians and economists who continue to regard exponential economic expansion as profitable or even indispensable, the present world financial crisis would have been in much mitigated form." Some comments after the experiment, however, would be necessary on the fact that "Radionuclides are always decaying, but borrowed money is ever growing due to the interest, both exponentially".

The following are examples of exercise problems.

(1) How many hours does it take for  $^{68}\text{Ga}$  radioactivity to decrease to 1/10 and 1/1000? Obtain from your experimental result and by calculation from the half-life of 68.1 min..

(2) (a) How much is the decrease of radioactivity in 1/10 half-life ?, and (b) How many half-lives does it take for the radionuclide to decay to 1/1000 ? You had better to remember the two results in approximate values of 7 % and 10 half-lives, respectively, for mental arithmetic.

(4) Half-life of  $^{11}\text{C}$  is 20.4 min, and thus its radioactivity decreases about 3.5 % in every minute. The entire production and consumption in the world, on the other hand, were growing about 3.5 % per year just before the financial crisis. Calculate by mental arithmetic how many times the world economy would expand in 20, 40, 60 and 100 years, if the expansion rate would remain constant at this level. How many years, do you think, the nature could withstand such an expansion of economy?

(5) Who noticed as early as in 1798 that population would increase exponentially but food production only linearly, to result in starvation age? Similar notice is now imposed on the human society in modernized and more urgent form (Brown and Kane 1994).

(6) Aging is inevitable for all animals and plants, but radionuclide will decay away suddenly without aging. What is the reason of this difference? In measuring radioactivity, we can only observe the decay of individual atoms occurring independently with one another; but any life phenomenon takes place as the result of collective change of huge numbers of constituent atoms in various parts of body working in correlation with one another.)

### 3-3. Experiments and exercises for science-oriented students

(A) The obtained decay curve is a beautiful example to depict the first order reaction in the study of chemical kinetics.

(B) Growth of  $^{68}\text{Ga}$  radioactivity after milking can be observed easily by the measurement of annihilation radiation from the cow. It is highly instructive to examine the fitting of the observed growth curve with the curve obtained from the differential equations. It should be remembered in the curve fitting that  $^{68}\text{Ga}$  cannot be eluted quantitatively in each milking.

(C) Coincidence measurement of the location of point-source positron emitters is effective for understanding the principle of PET (positron emission tomography). For the preparation of positron source, the eluate containing 10-50 kBq  $^{68}\text{Ge}$  is evaporated close to dryness and absorbed in a micro ball of filter paper (less than 3 mm diameter), which is then covered with thick aluminum foils for the annihilation of positron. Two scintillators shielded by lead plates with beam entrance holes (1 cm diameter) are carefully placed face to face, with one straight line passing through the centers of both holes. The radiation source is placed at various positions on and near the straight line, and count rate of annihilation radiation from the source was measured by the two detectors operated both in coincidence and as individual detectors.

The result is then examined to indicate a dramatically sharp change of positional sensitivity in the coincidence counting of positron emitters. It is now the opportunity to give a lecture on PET, preferably showing real images for medical diagnosis. (D) In nuclear medicine  $^{67}\text{Ga}$  (78.3 h, EC) in various chemical forms has been used widely (Weiner and Thukur 2003), and  $^{68}\text{Ga}$  has recently been actively studied as PET radiopharmaceuticals, as can be consulted, e.g., in Google, Internet. In spite of the short life,  $^{68}\text{Ga}$  is useful in the study of coordination chemistry as well as plant physiology.

(E) By simultaneous use of two isotopic tracers, the resident time (turnover time) together with the distribution pattern can be measured for this element or its compounds in various parts of the sample (Nozaki and Saito 1955). For this use,  $^{67}\text{Ga}$ - $^{68}\text{Ga}$  is thought to be a suitable pair. Although somewhat high level knowledge, experiences and techniques

would be required for such uses of  $^{68}\text{Ga}$ , students and instructors are encouraged to try such a measurement.

#### 4. Discussion

Although many Japanese people are nervous in the use of radioactivity in our every-day life, as is often called 'radiation allergy', PET is exceptionally welcomed and prosperous in Japan as well as some other Oriental countries at present. This is another profitable reason for the education use of  $^{68}\text{Ge}$ - $^{68}\text{Ga}$  generator.

Many universities in Japan have withdrawn experiments using radionuclides from their education curricula, due principally to too complicated control by the law (Ministry 2007). The maximum radioactivity permitted to be used without the law control is 100 kBq for both  $^{68}\text{Ge}$  and  $^{68}\text{Ga}$  existing separately and also for  $^{68}\text{Ge}$  as the cow. These activity levels are enough or superfluous for the experiments given above. In the experiment of 'milking and decay measurement', for example, the decay of 4 kBq  $^{68}\text{Ga}$  can be followed for 12 hour under a suitable background shielding. Hence, from a generator giving 60 kBq  $^{68}\text{Ga}$  in the first milking, 15 samples of 4 kBq  $^{68}\text{Ga}$  are given in the first time and then every 7 samples are repeatedly given with 1 hour intervals.

For wide education use of the generator, it is necessary for us to propose to the government the addition of a new item to the law concerning the handling of radioactivity in education. It is also needed to set up an organization to produce, keep and supply the generator preferably under a rental system. The organization should be responsible to the check on the breakthrough of  $^{68}\text{Ge}$ . A cyclotron giving several tens MeV protons is needed for the production of  $^{68}\text{Ge}$ , a long-lived even-even nuclide, but the production efficiency is rather low for any nuclear reaction. The production of such kinds of useful but expensive nuclides under collaboration of Oriental countries can be expected to offer fruitful results.

#### 5. Conclusions

Radionuclides can be utilized as highly effective tools for the education of large varieties of people to give interest in undertaking experiments by themselves and some knowledge on properties, rules and laws in natural and social phenomena. As the source of radionuclides in this use, milking generators are almost always the most suitable, and the  $^{68}\text{Ge}$ - $^{68}\text{Ga}$  generator is now probably of the widest utility. Various kinds of experiments can be prepared by the use of this generator for individual categories of people. Decay-curve measurement with related exercises is guessed to be highly instructive to almost all categories of people, and to be particularly useful for teaching the exponential function to non-scientific specialists. These educations with experimental practice can be expected also to give some feeling of intimacy with radioactivity to many attendants. This will deepen people's understanding of science and technology in related fields, to result in the activation of these fields. For realizing wide education use, efforts should now be made also in some non-scientific works.

#### Acknowledgements

The author would like to express his sincere thanks to Dr. Koji Ogawa, School of Allied Health Sciences, Kitasato University, for his valuable and effective suggestions and aids.

#### References

- Brown LR and Kane H (Worldwatch Institute) 1994 Full House W.W. Norton & Company New York.
- Japan ministry of education, culture, sports, science, and technology 2007 Law concerning prevention from radiation hazards due to radioisotopes Tokyo.
- Nozaki T. and Saito J. 1995 Isotopic double tracers for the measurement of the biological half-life of an element or compound, exemplified by  $^{125}\text{I}$ - $^{131}\text{I}$  taken up in a seaweed Appl. radiat. isot. 46 1299-1305.
- Weiner R.E. and Thukur M.L. 2003 Chemistry of gallium and indium radiopharmaceuticals in Handbook of radiopharmaceuticals — Radiochemistry and application Ed. Welch M.J. and Redvanly C.S. John Wiley Sussex p.p. 363-40

**A new monitoring system of natural radionuclides  
on air-borne dust sample combined with  $\beta$ - $\alpha$  correlated events  
as a teaching material for public and student radiation-literacy**

○Tetsuo Hashimoto\*, Hisanobu Ishiyama\*\*, Shigeki Itou\*\*\*

\* *Emeritus Professor of Niigata University (NRI-Institute), 2-2-10 Teraomae-dori, Nishi-ku, Niigata 950-2053, Japan*

\*\* *Niigata Prefectural Institute of Environmental Radiation Monitoring, 314-1 Sowa, Nishi-ku, Niigata 950-2144, Japan*

\*\*\* *Z-COSMOS Ltd., 1962 Sone, Nishikan-ku, Niigata 959-0422, Japan*

In front of public or educational radiation-literacy places, an on-line demonstration of natural radioactivities on the air-borne dust samples should be efficient for easy understanding of radionuclides existing in nature.

For this purpose, a phosfich-type  $\alpha$ - and  $\beta$ -ray radiation counter, which is distinguishable into  $\alpha$ - and  $\beta$ -rays combined with a ZnS(Ag) and a plastic scintillation detector, respectively, was fixed just above the dust-collecting filter paper within a space in few mm. Both  $\alpha$ - and  $\beta$ -ray pulses from the counter were provided to a rapid pulse interval analyzing (TIA) system during continuous collection of air-borne dust. Both pulse input times were registered into the memory buffer in the TIA system, followed immediately to the data processing using a MTA (multiple TIA) technique. Resultant  $\beta$ - $\alpha$  TIA-spectrum (or decay-curve of  $\beta$ - $\alpha$  correlated events due to interpolating short-lived nuclide with  $\mu$ s life) and changing trends of  $\alpha$ - and  $\beta$ -counting rates, which can confirm preferably the naturally occurring radio-activities, were demonstrated on a PC-display with on-line controlling software, having time resolution in  $\mu$ s scale.

Thus, three practical values, including  $\beta$ - $\alpha$  correlated event rates ( $n_{\alpha\beta}$ ) according to the TIA-analysis between  $\beta$ - and  $\alpha$ -pulses,  $\alpha$ - ( $n_{\alpha}$ ), and  $\beta$ -ray counting rates ( $n_{\beta}$ ) were demonstrated on the PC-display as well as final acquisition of real data in excel-format, from the present TIA-measurement system.

A uranium deposited Al-plate (as mixture of  $\alpha$ - and  $\beta$ -ray emitters), a uranium mineral powder specimen fixed on an adhesive tape, and a  $^{226}\text{Ra}$ -source (as  $\beta$ -source) showed negligible contribution on  $\beta$ - $\alpha$  correlated events in TIA-spectrum, giving constant  $\alpha/\beta$  counting ratios. In the case of air-borne dust samples, the  $\beta$ - $\alpha$  correlated events in TIA-spectrum showed certainly a presence of 164  $\mu$ s decay-curve due to  $^{214}\text{Po}$ , based on successive decay process of  $^{222}\text{Rn}$  progenies such as  $^{214}\text{Bi}$  ( $\beta$ )  $\rightarrow$   $^{214}\text{Po}$  ( $\alpha$ :  $T_{1/2}=164 \mu$ s) $\rightarrow$  by passing through a short-life nuclide with  $\mu$ s orders.

By using three measuring values, new parameters,  $R_\alpha$  and  $R_\beta$  [equal to  $(n_\alpha \text{ or } n_\beta) * (n_\alpha + n_\beta) / n_{\alpha\beta}$ ], have been introduced for real-time indicators of naturally occurring radionuclides on the air-borne dust as seen in Fig. 1. Practically,  $R_\alpha$  and  $R_\beta$  -values usually give respective constant ones because of constant proportion of  $\alpha$ - and  $\beta$ -counting rates against  $\beta$ - $\alpha$  correlated event rate within the  $^{222}\text{Rn}$  progenies.

Otherwise, this new parameters can be utilized as a highly sensitive index for the existence of artificial nuclides, even under the inevitable existence of  $^{222}\text{Rn}$  progenies in the air-borne dust sample.

The present radiation measurement system, combined with  $\beta$ - $\alpha$  correlated events, has been proved to be useful for the detection of extremely small contamination with artificial  $\alpha$ -nuclides and  $\beta$ -nuclides as well as the preferable demonstration of existence of naturally occurring radionuclides in a radiation literacy room for general public and students. Additionally, this rapid TIA system serves as to a remote monitoring of artificial radionuclides from nuclear facilities and so on.

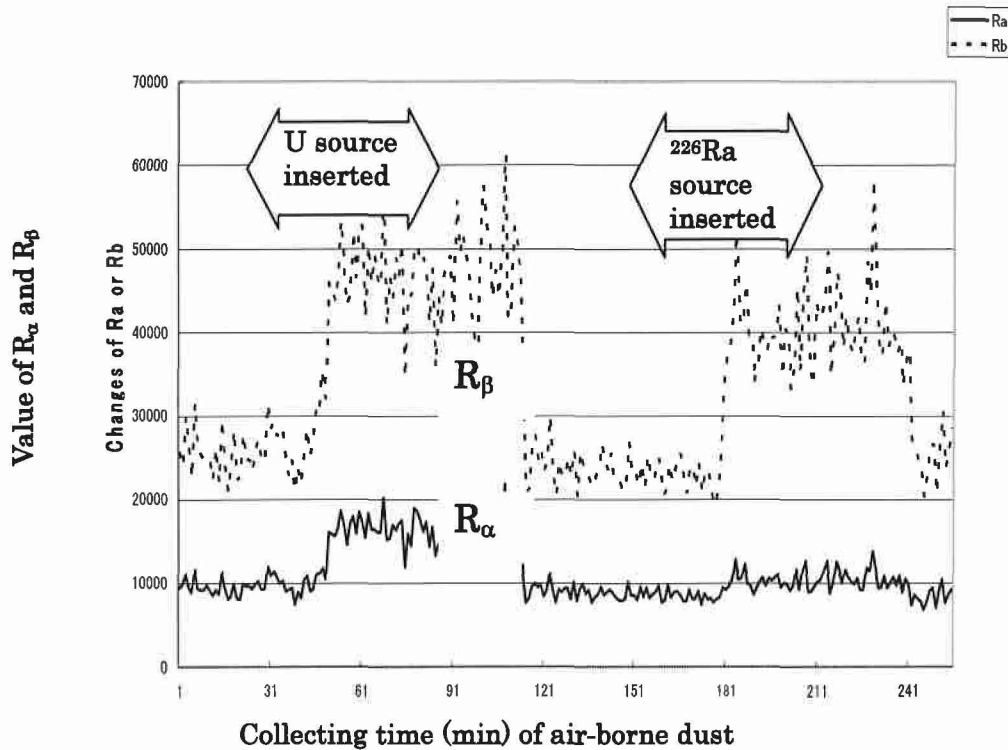


Fig. 1 Changes of parameter  $R_\alpha$  and  $R_\beta$  from air-borne dust sample without and with insertion of radioactive sources

## Revival of “Radiation” in the New Curriculum Guideline for Junior High Schools in Japan

Ryuichi Tanaka

*NPO Radiation Education Forum  
Daiichi Shirakawa-Building  
3-23-6 Nishishimbashi, Minato, 103-0013 Tokyo*

Learning of “the property and utilization of radiation” is required in science classes in junior high schools the first time in 30 years in Japan by recent curriculum guideline reform. This revival of radiation education in compulsory education is quite significant, because the education has been in difficult situation in senior high schools under restrictions due to current system of subject selection, college entrance exam and etc.

Considerable numbers of science and engineering college students are not aware of natural radiation and radioactivity, and most students and the community have a fear of radiation, even if the extremely small amount of it. This has a major impact on risk perception of nuclear energy.

It is expected that such situation will be improved on the basis of the revised guideline. The revival of radiation education will help students develop comprehensive understanding of energy and environment issues.

The paper describes historical background of radiation education in national curricula and essential educational contents for students to be acquired on “the property and utilization of radiation”.

1. Main points of the new curriculum guideline for science in junior high schools from the viewpoints of energy, nuclear power, and radiation

(1) Emphasis on education of energy and environments

- Emphasis on energy conversion (science) and requirement of relevant technology study (industrial arts and homemaking)
- Revival of “radiation” and “structure of atom” and addition of “global warming” in keywords to be studied

(2) A new viewpoint “sustainable society”

Science: Effective use of limited resources. Comprehensive judgment\_

Social studies: Qualities and ability for active participation in public matters

Industrial arts and homemaking: The relation of technology with society and environments

## 2. History of guidance on “radiation” in curriculum guidelines for junior high schools

- 1951 In a revised tentative guideline, a learning target was set for study of the properties and utilization of X-rays, based on the recognition that development of science has expanded visible world.
- 1958 The guideline was set as a minimum national standard. Radiation education was positioned in the study of atomic structure and followed by next revision in 1969. It was introduced on the basis of peaceful use of nuclear power.
- 1977 “Radiation” disappeared in the curriculum guideline.
- 2008 “Radiation” reappeared in the curriculum guideline.

## 3. A recommended curriculum for study of property and utilization of radiation

A property of radiation, transmission, is studied by radiation penetration through matter, in the same way as reflection and refraction are studied as basic properties of light. Another concept of radiation, action of radiation, is required to understand the fact that the detected number of penetrated radiation decreases with thickness of the matter.

It is important to understand that radiation loses its energy in the matter by repeated actions to the matter during transmission into the matter. Basic recognition of transmission and action leads students to understand the influence of radiation on human body and the utilization of radiation on matters.

## **A few special educational schemes for the course of radiation measurement laboratory in National Tsing Hua University**

Chih-Hao Lee, H.P.Chou and S.H.Jiang

*Department of Engineering and System Science, National Tsing Hua University, Hsinchu, Taiwan.*

*Institute of Nuclear Engineering and Science, National Tsing Hua University, Hsinchu, Taiwan.*

A few special designed schemes for the course of radiation measurement laboratory were introduced in past 35 years to educate the students major in nuclear engineering in setting up a wholesome concept on radiation measurement. During the past years of teaching history, the radiation measurement experimental schemes were modified many times to inspire the creativity of the students and to learn the correct concepts by making errors. A few good examples were elucidated in the following: (1) In the experiment of setup of basic nuclear electronic modules, to measure the output of a modules using a T-connector is found to be different from the voltage measured with open loop measurement. The students learn that the output voltage will be dropped due to the loading effect or impedance mismatch. (2) In the dead time measurement of a G-M counter using a two-source method, a weak radiation source was deliberately used resulting in a very bad statistical error in determining the dead time. Many groups of students found a negative dead time after the error propagation in data analysis. Those negative dead time measured were automatically deleted by students and never reported, resulting in a biased statistical distribution in the error determination. (3) To test the function of low level discriminator using the output of a pulser as an input source, the instructor asked students to adjust the gain of pulser to obtain half of the count. A difficulty was faced to adjust the gain to an exact half of the counting rate due to the high precision of electronics. Only the noisy electronics can easily achieve half count. By counting the data many times, the standard deviation reveals the noisy situation of the electronics system. (4) For the student to learn about the P-value in the counting statistics, a counting statistics on the output of pulser was use to show a large P value, and the effect of electronic noise to show a small P value. (5) To really measure the right pulse shape on the oscilloscope, the trigger level and slope should be set at right position. A pulse with shape of overshoot was prepared on purpose by detuning the P/Z cancellation for student to try. Many students can not get the right pulse shape shown on the oscilloscope. In order to perform this experiment, only analogy oscilloscope was used instead of using the very popular digital oscilloscope. (6) To teach students in understanding the right concept of counting

statistics, a group of 30 counts experiments with each measurement 10 s is conducted. The standard deviation obtained from the counting of 30 times is to compare the one measurement with 300 s. Students might not know which counting scheme can get a better counting statistics error. (7) For a neutron proportional counter measurement, a  $^{60}\text{Co}$  gamma source was put very close to the  $\text{BF}_3$  detector after calibrating by neutron nuclear reaction peaks but found no peak for  $^{60}\text{Co}$  at the position of 1.172 and 1.332 MeV on MCA. Can students really understand why these peaks are missed? (8) To measure the difference of the slopes of counting rate vs. applied bias on  $\text{BF}_3$  counter and boron lining neutron detector to understand the importance of the response function of a detector under applied bias related to the discrimination levels. (9) In the alpha spectroscopy measurement, two kinds of  $^{241}\text{Am}$  alpha sources were used. One of them is a thick  $^{241}\text{Am}$  source results in a peak shift to the lower energy and a poor energy resolution. Students to learn that some problems were not due to the detector system all the time. (10) For the gamma ray spectroscopy, usually 3000 V is needed on an HPGe detector. The instructor asked students to compare the response function of detector run at only 300 V to see the peak broaden, peak shift and decrease of Compton to peak ratio for them to really understand the function of HPGe detector. (11) In the HPGe measurement, the keV/channel was obtained using calibration sources  $^{22}\text{Na}$ ,  $^{60}\text{Co}$  and  $^{137}\text{Cs}$ . Then, using the calibrated keV/channel value to predict the peak position of  $^{241}\text{Am}$  source. Usually, the measured one is different from the prediction one due to the non-zero offset of MCA which was deliberately detuned by the instructor. (12) In the HPGe background measurement for 30 min, usually a few peaks can be found. The most pronounced peak is  $^{40}\text{K}$  and the intensity can be increased if many students getting together to share one detector. This is to illustrate that the major radiation background comes from a human being. A very important radiation concept on the nature background can be set quantitatively. Another peak,  $^{41}\text{Ar}$ , was frequently found when the THOR reactor was on. The intensity of  $^{41}\text{Ar}$  usually is smaller than  $^{40}\text{K}$  to show the radiation safety of the operation of THOR. (13) Finally, an X-ray fluorescence (XRF) measurement was carried out using an Amptek Si pin diode and digital processor system. The students learn that the traditional analogy amplifiers and ADC might be obsolete in the future. The USB connection to a PC might be the best data acquisition system for a great convenience. The XRF experiment is to identify the composition of a material. Usually, a currency coin was used as a standard sample together with a token coin (a fake coin) measurement for students to learn the forensic science. After this experiment, students are eagerly to put their golden rings or platinum necklaces to check their genuineness. It is an experiment of great interest for the students.

## The current basic nuclear education in Taiwan and suggestions

Yu-Tzu Huang

*Department of Bioenvironmental Engineering, Chung-Yuan Christian University*

The forth-nuclear power plant is going to be built in Taiwan, and there will be eight nuclear reactors for operation. The density of nuclear power plants in a small area with a lot of people like Taiwan will be close to the highest in the world. However, when we look at the basic education on the nuclear energy, there is nearly no nuclear-related knowledge in the textbooks in the primary and junior high schools and only some information about the nuclear reactions in the senior high schools. In Japan, on the contrary, the basic education of nuclear energy is wider than Taiwan, and they also have some experimental discipline for the detection of nuclear radiation in the emergency case. Therefore, we strongly suggest that we should actively increase our basic knowledge about the nuclear safety, nuclear utilization, and the advantages/disadvantages of nuclear power. In order to do so, we should encourage the primary, junior high and senior high school teachers to pursue further education, promote basic education on nuclear energy and safety training, and educate all citizens the correct knowledge and attitude of nuclear power.

### 台灣的基礎核能教育之現況與建議

黃郁慈

中原大學生物環境工程學系

台灣即將有四座核能發電廠，預計有八座機組可供運行，對地狹人稠的台灣而言，核能發電廠的密度將位居世界前幾位。檢視目前台灣的基礎核能教育，在義務教育的國小自然課和國中理化課課程中，鮮少提及核能相關知識，僅高中的物理課和化學課課程中，有教導核反應等基礎知識。反觀鄰近國家如日本除了基礎核能教育的授課內容比台灣廣泛之外，也有核能偵測等相關實驗的訓練，以因應危急時的處理。因此建議台灣也應該積極的對核能安全、核能使用、核能的優缺點等方面，加強國中小和高中相關課程教師的進修，以提升基礎的核能教育與安全訓練，進而建立全民對核能的正確觀念與態度。

## **The Communication and Personnel Training Programs of Taiwan's Regulatory Authority in the Field of Atomic Energy**

Chen, Wen-fang\*    Ang, Su-hui\*\*

*\*Senior Engineer & Section Chief, Department of Planning,  
Atomic Energy Council, Executive Yuan*

*\*\*Associate Technical Specialist, Department of Planning,  
Atomic Energy Council, Executive Yuan*

It is well known that the deep fostering of knowledge start to accumulate since elementary schools, and the knowledge related with radiation and nuclear safety is essential for each modern citizen. However, in our current educational system, basic radiation concepts has not been brought into the curriculum. The result is that we are unable to meet the requirements in this aspect. In order to let the general public understand the basic knowledge of nuclear and radiation safety, Taiwan's regulatory authority on ionizing radiation and nuclear safety, the Atomic Energy Council (AEC) of the Executive Yuan, is providing the general public information on atomic energy, nuclear power and radiation safety via the internet, various flyers, advertisements, publications, and by holding press conferences, exhibitions, and through the media to promote our citizens' cognition on nuclear and radiation safety.

Over the past few years, several colleges and universities in Taiwan have provided courses such as "Nuclear energy, Radiation, and Life" to their students and these courses become more popular by them. In addition, pro-active approaches were made by AEC's staffs through visiting different city and county high schools and their supervising institutes of education in Kaohsiung, Pingtung and Tainan with supports of nuclear energy and radiation related speeches, demonstration and exposition services regarding radiation measurement to help deliver proper knowledge to high school teachers. The AEC has also set up a free channel named "Radiation to you and me" to provide the general public information regarding radiation and nuclear energy safety for their daily life.

Talents of people are the foundation for knowledge-based economy era. Over the past few years, the AEC has done trainings including on-the-job training, collaboration and exchange training courses with universities, industrial group planning and science and technology academic cooperation with the National Science Council ( the AEC/NSC mutual fund) to strengthen the development of personnel skills-on nuclear and radiation safety.

## Effect of Hydrophilic and Hydrophobic Monomers Grafting on Biodegradable Poly (3-hydroxybutyrate) using Irradiation

Wen-Chuan Hsieh<sup>a\*</sup>, Chih-Pong Chang<sup>b</sup>, Yuki Wada<sup>c</sup>, Hiroshi Mitomo<sup>c</sup>, Noriaki Seko<sup>d</sup> and Masao Tamada<sup>d</sup>

<sup>a</sup>Department of Biological Science and Technology, I-Shou University

<sup>b</sup>Department of Textile Engineering, Chinese Culture University

<sup>c</sup>Department of Biological and Chemical Engineering, Gunma University, Japan

<sup>d</sup>Environment Industrial Materials Research Division, Japan Atomic Energy Agency, Japan

The radiation-induced graft polymerization of hydrophilic [sodium *p*-styrene sulfonate (SSS), acrylic acid (AAc)] and hydrophobic [styrene (St), methyl acrylate (MAAc)] monomers onto microbial poly (3-hydroxybutyrate) (PHB) powder was performed and the characteristics of the both grafting films obtained after remolding were compared. The grafting of various monomers onto the PHB powder increased with reaction time. The degree of grafting (Xg) onto the PHB by these various monomers followed the order St,SSS, MAAC and AAc. The PHB films onto which were grafted St, SSS, MAAC and AAc were characterized by measuring the contact angle, the adsorption of enzyme PHB depolymerase, and biodegradability, as well as by differential scanning calorimetry. Both hydrophobic and hydrophilic monomers affected the contact angle of grafted PHB film with St, SSS, MAAC and AAc monomers. However, the adsorption of enzyme on the grafted PHB film increased with the amount of hydrophilic monomer and degree of grafting. Consequently, the enzyme PHB depolymerase easily approached the PHB film when the hydrophilic groups were grafted onto its surface. The enzymatic degradation of grafted PHB films with hydrophilic monomer proceeded more quickly than that of hydrophobic monomers.

**Keywords:** Grafting; Biodegradable poly (3-hydroxybutyrate); Enzymatic degradation; Irradiation.

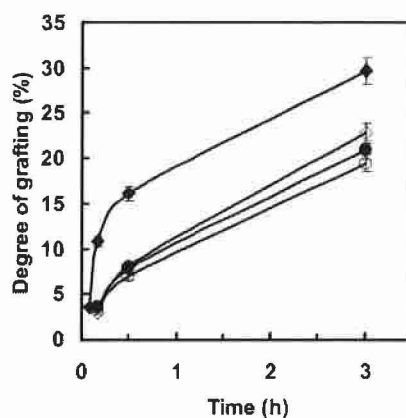


Fig. 1. Relationship between reaction time and degree of grafting (Xg). Monomer concentration: (◆): 100wt% St; (◇): 0.5 M SSS; (●): 10 wt% MAAC; and (○): 30 wt% AAc.

# Effect of Hydrophilic and Hydrophobic Monomers Grafting on Biodegradable Poly(3-hydroxybutyrate) using Irradiation

NSC 97-2221-E-214-014, 97-2815-C-214-001-E

Wen-Chuan Hsieh<sup>\*a</sup>, Chih-Pong Chang<sup>b</sup>, Yuki Wada<sup>c</sup>, Hiroshi Mitomo<sup>c</sup>,  
Noriaki Seko<sup>d</sup> and Masao Tamada<sup>d</sup>

<sup>a</sup>Department of Biological Science and Technology, I-Shou University; <sup>b</sup>Department of Textile Engineering, Chinese Culture University; <sup>c</sup>Department of Biological and Chemical Engineering, Gunma University, Japan; <sup>d</sup>Environment and Industrial Materials Research Division, Japan Atomic Energy Agency, Japan; \*Email: [wenchuan@isu.edu.tw](mailto:wenchuan@isu.edu.tw)

## Abstract

The radiation-induced graft polymerization of hydrophilic [sodium *p*-styrene sulfonate (SSS), acrylic acid (AAc)] and hydrophobic [styrene (St), methyl acrylate (MAAc)] monomers onto microbial poly(3-hydroxybutyrate) (PHB) powder was performed and the characteristics of the both grafting films obtained after remolding were compared. The grafting of various monomers onto the PHB powder increased with reaction time. The degree of grafting (Xg) onto the PHB by these various monomers followed the order St, SSS, MAAc and AAc. The PHB films onto which were grafted St, SSS, MAAc and AAc were characterized by measuring the contact angle, the adsorption of enzyme PHB depolymerase, and biodegradability, as well as by differential scanning calorimetry. Both hydrophobic and hydrophilic monomers affected the contact angle of grafted PHB film with St, SSS, MAAc and AAc monomers. However, the adsorption of enzyme on the grafted PHB film increased with the amount of hydrophilic monomer and degree of grafting. Consequently, the enzyme PHB depolymerase easily approached the PHB film when the hydrophilic groups were grafted onto its surface. The enzymatic degradation of grafted PHB films with hydrophilic monomer proceeded more quickly than that of hydrophobic monomers.

**Keywords:** Grafting; Biodegradable poly(3-hydroxybutyrate); Enzymatic

degradation; Irradiation.

## 1 Introduction

The microbial polyesters poly(3-hydroxybutyrate) P(3HB), is a biocompatible and biodegradable thermoplastic polymer that is produced by various bacteria in nature as an intracellular carbon and energy source [1,2]. The degradable P(3HB) had attracted considerable attention for its many agricultural, industrial, and medical applications [2]. However, the brittleness and stiffness of PHB limit its range of practical applications, and the enzymatic degradability of PHB must be controlled to enable utilization.

Three techniques have been applied to overcome this shortcoming of PHB. One of the approaches is to biosynthesize copolymers that contain Poly(hydroxyalkanoate) (PHA) units. The second is to prepare the blend polymers of PHB and other chemical synthesized polymers. The third is radiation grafting onto PHB. Another application of radiation graft polymerization is developmental research into the separation and refinement of proteins to separate functional materials [3]. For environmental reasons, materials are being developed as graft adsorbents to remove toxic metals from industrial waste waters and the harmful constituents of the atmosphere [4-6]. Research into the recovery of useful rare metals from sea water and hot springs is currently being undertaken [7]. The graft adsorbent has been used to recover rare metals such

as scandium (Sc), vanadium (V) and arsenic (As) from the hot springs of Kusatsu in the Gunma Prefecture. These graft adsorbents are improved by changing the functional groups on the graft chains to promote the recovery of required metals.

This authors' research group recently succeeded in controlling the enzymatic degradability of PHB using the radiation graft copolymerization method [8-12]. In an earlier work our group described grafted hydrophilic monomers (2-hydroxyethyl methacrylate (HEMA) [9], acrylic acid (AAc) [8] and the hydrophobic monomers, styrene (St) [10-12] and methyl methacrylate (MMA) onto PHB. These experiments indicated that while grafting PHB into the hydrophobic MMA sharply reduced its enzymatic degradability, introducing hydrophilic HEMA increased enzymatic degradability [9]. Accordingly, the effect of the hydrophilicity of the grafting chains on the enzymatic degradation of the PHB was approximately determined.

In this work, onto microbial PHB was grafted various hydrophilic monomers, including sodium *p*-styrene sulfonate (SSS) and acrylic acid (AAc), and hydrophobic monomers, such as styrene (St) and methyl acrylate (MAAc), using  $\gamma$ -rays. The thermal properties of grafted PHB were determined. Furthermore, the enzymatic degradability, contact angle and enzymatic adsorption of the grafted samples were discussed.

## 2 Experimental

### 2.1 Materials

PHB was purchased from Aldrich Chemical Co., Ltd. (USA). PHB was purified as follows: PHB (20 g) was dissolved in chloroform (1000 mL) and then poured into a solvent that consisted of *n*-hexane and methanol (2000 mL, 1:1 vol%). The precipitated PHB powder was then isolated by filtration and dried under vacuum. The mean particle size of the obtained PHB powder was about 20  $\mu$ m. The St monomer, purchased from Kanto Chemical Co., Inc., was used after the inhibitor was removed at graft proceeding. The monomers of SSS, AAc (purchased from Tokyo Kasei Kogyo Co., Ltd.) and MAAc (purchased from Kanto Chemical Co., Inc.) were used without further

purification

### 2.2 Radiation-induced graft polymerization onto PHB powder

The PHB-g-SSS, PHB-g-St, PHB-g-AAc, and PHB-g-MAAc powders were prepared by the pre-irradiation before radiation-induced graft polymerization. The PHB powder (2.0 g) was placed on one side of an H-shaped glass ampoule that was sealed at reduced pressure ( $10^{-3}$  torr). The PHB was then pre-irradiated with  $^{60}\text{Co}$   $\gamma$ -rays (dose rate = 10 kGy/h) at 10 kGy in the glass ampoule at  $-70$  °C. Following irradiation, the monomer (10 ml) was poured into the opposite side of the ampoule, and it was resealed and evacuated ( $10^{-3}$  torr). The degree of grafting ( $X_g$ ) given by the following equation [13]:

$$X_g(\%) = (W_g - W_0) \times 100 / W_0 \quad \text{-----(1)}$$

where  $W_0$  and  $W_g$  are the weights of the PHB powder before and after the graft polymerization, respectively.

The grafting reactions of the St, SSS, AAc and MAAc monomers proceeded in a temperature-controlled water bath at 60 °C for 10 min, 30 min and 3 h before the grafted powders were immersed in a solvent to terminate the grafting reaction and to remove the homopolymers. The concentration of monomer in the St was denoted 100 wt% solution in this study. The monomer concentration of the SSS solution was adjusted to 0.5 M using water as the solvent and the monomer concentrations of the AAc and MAAc solutions were adjusted to 30 and 10 wt%, respectively, using methanol as the solvent.

### 2.3 Thermal analysis

The thermal properties of the PHB powder and film were investigated using a Shimadzu DSC-50 (Japan). About 2 mg of the sample was packed in an aluminum pan and heated from 25 °C to 190 °C at a rate of 10 °C/min in a 30 ml/min nitrogen flow. The enthalpy of melting ( $\Delta H_m$ ) was determined by DSC from the area under the endothermic peak. The temperature was calibrated using highly pure benzoic acid standards.

The  $\Delta H_m$  value was corrected using the weight fraction of PHB in the grafted

samples and the following equation [8,9] (Corrected enthalpy of melting ( $\Delta H_m$ )corr.).

$$\Delta H_m / (\Delta H_m)_{\text{corr.}} = (100 - X_g) / 100 \quad (2)$$

## 2.4 Measurement of contact angle (PHB film)

The contact angles of various monomers on the grafted PHB films were measured using a contact-angle meter (Kyowa Scientific Co., Ltd.). The contact angles were determined using a drop of 0.05 M NaOH solution at room temperature.

## 2.5 Enzymatic degradation

The grafted PHB powder was formed into a film by hot-pressing at 190 °C. The obtained films were 150  $\mu\text{m}$  thick and were isothermally crystallized at 90 °C for one week before use. The enzymatic degradation of the irradiated PHB films was evaluated at 37 °C in 0.1 M phosphate buffer (pH 7.4). PHB depolymerase purified from *Ralstonia pickettii* T1 [14] was used. The irradiated PHB films (150- $\mu\text{m}$  thick) were cut into squares of 10 mm  $\times$  10 mm and then placed in small test tubes that contained 1.0 ml of buffer solution. The reactions were initiated by adding 4  $\mu\text{g}$  of PHB depolymerase. The weight loss of the film was periodically measured after it was removed and washed using methanol and distilled water. In this work, the weight loss ( $\text{mg}/\text{cm}^2 \cdot \text{h}$ ) was calculated from the weight after 48 h of enzymatic degradation.

## 3 Results and discussion

### 3.1 Grafting PHB powder with acrylic acid

Acrylic acid (AAc) was grafted onto the PHB powder with 20 wt% ( $\blacktriangle$ ), 30 wt% ( $\circ$ ), and 50 wt% ( $\bullet$ ) monomer solutions at 10 KGy. Figure 1 plots the relationship between the reaction time and degree of grafting ( $X_g$ ). The  $X_g$  of PHB increased with the reaction time on the grafted PHB powder for each concentrations of monomer solution. Moreover, the monomer concentration affected the degree of grafting. The  $X_g$  of PHB increased with the monomer concentration ( $\bullet$ : 50 wt% AAc >  $\circ$ : 30 wt% AAc >  $\blacktriangle$ : 20 wt% AAc) over a

reaction time of three hours.

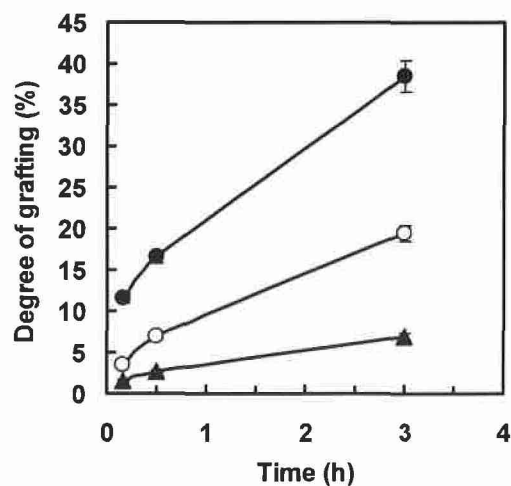


**Figure 1:** Relationship between reaction time and degree of grafting ( $X_g$ ). monomer concentration: ( $\blacktriangle$ ): 20 wt% AAc solution, ( $\circ$ ): 30 wt% AAc solution, ( $\bullet$ ): 50 wt% AAc solution.

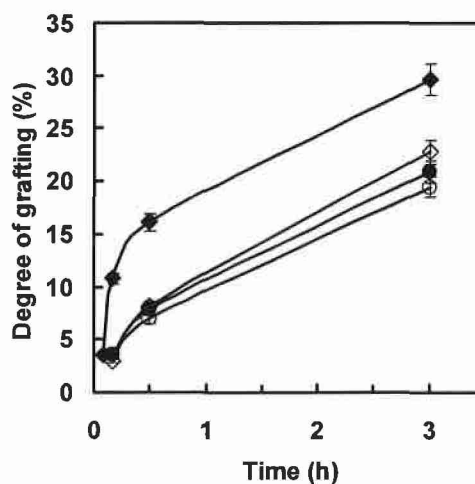


**Figure 2:** Relationship between reaction time and degree of grafting ( $X_g$ ). monomer concentration: ( $\blacklozenge$ ): 100wt% St; ( $\diamond$ ): 0.5 M SSS; ( $\bullet$ ): 10 wt% MAAc; and ( $\circ$ ): 30 wt% AAc.

### 3.2 Grafting PHB powder with hydrophobic / hydrophilic monomers

To evaluate the effect of the grafting of hydrophobic/hydrophilic monomers onto the PHB powder, St (100 wt%;  $\blacklozenge$ ), SSS (0.5 M;  $\diamond$ ), AAc (30 wt%;  $\circ$ ), and MAAc (10 wt%;  $\bullet$ ) were grafted onto the PHB powder using various

concentrations of the monomer solutions. Figure 2 plots the relationship between the reaction time and the degree of grafting (Xg). The grafting ratios of grafted PHB powder to various monomers increased with the reaction time to 3h. The degree of grafting (Xg) onto the PHB by these various monomers decreased in the order St, SSS, MAAc, and AAc. Grafted PHB powders, such powders were made by hot pressing to evaluate their contact angle, adsorption of enzyme and biodegradability.

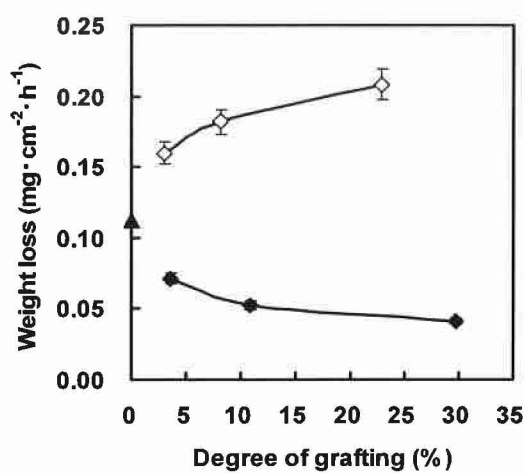


**Figure 3:** Enzymatic degradation of PHB and grafted PHB films against degree of grafting (%). ( $\diamond$ ): PHB-g-SSS film; ( $\blacktriangle$ ): PHB film; ( $\blacklozenge$ ): PHB-g-St film.

### 3.3 Enzymatic degradation of PHB film grafting various monomers

The hot-pressed PHB and various grafted monomer (St, SSS, MAAc, AAc) films were degraded using the enzyme PHB depolymerase. Figure 3 plots the relationship between Xg [PHB-g-St ( $\blacklozenge$ ) & PHB-g-SSS ( $\diamond$ )] and weight loss after 48 h of enzymatic degradation. The weight loss of PHB-g-St significantly declined and that of PHB-g-SSS substantially increased as Xg increased. This difference between the weight loss characteristics of the two grafted films was related to the presence or absence of the hydrophilic side chains on the graft chains, indicating that the grafting of St (PHB-g-St) and SSS (PHB-g-SSS) onto PHB powders affected their enzymatic degradability, although St and SSS have

similar chemical structures, they have different hydrophilic properties.

Figure 4 plots the relationship between Xg [PHB-g-AAc ( $\circ$ ) & PHB-g-MAAc ( $\bullet$ )] and weight loss after 48 h of enzymatic degradation. The difference between the enzymatic degradability of the PHB powder to which was grafted AAc (PHB-g-AAc) and that to which was grafted MAAc (PHB-g-MAAc) was examined. These results demonstrate that the weight loss of PHB-g-MAAc was lower than that of the PHB film, while that of PHB-g-AAc was higher, in each case to an extent that increased with the Xg of the samples: the degradation of grafted PHB-g-AAc polymer increased with the amount of hydrophilic monomer (AAc) after grafting, while that of grafted PHB-g-MAAc polymer declined as the amount of hydrophobic monomer (MAAc) increased after grafting. Similar results were obtained, as indicated above, for the grafting of St and SSS monomers onto PHB powder.

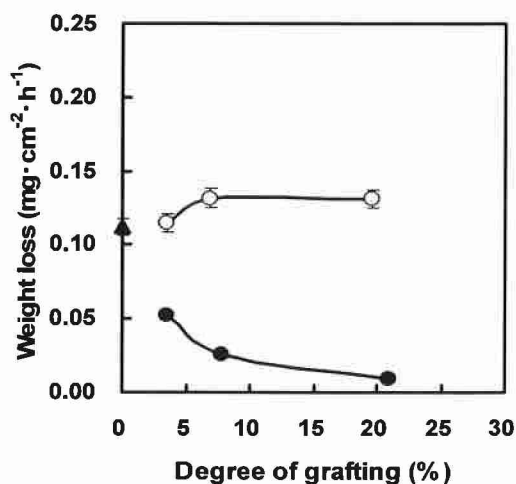


**Figure 4:** Enzymatic degradation of PHB and grafted PHB films against degree of grafting (%). ( $\circ$ ): PHB-g-AAc film; ( $\blacktriangle$ ): PHB film; ( $\bullet$ ): PHB-g-MAAc film.

## 4 Conclusions

The grafting of various monomers to the PHB powder increased with the monomer concentration and reaction time. The degree of grafting (Xg) onto the PHB by these various monomers decreased in the order St, SSS, MAAc, and AAc.

The thermal properties of the

PHB-g-St, PHB-g-SSS, PHB-g-MAAc and PHB-g-AAc films were very similar. A comparison of the enzymatic degradability of the pair of PHB-g-St and PHB-g-SSS films with the pair of PHB-g-MAAc and PHB-g-AAc films demonstrated that the presence of hydrophilic groups in the grafting chains affected the enzymatic degradability of the grafted PHB films.

The grafted PHB film was hydrophilic because of the grafting of hydrophilic monomers. Therefore, the enzyme PHB depolymerase easily approached the surface of the PHB film. Accordingly, the enzymatic degradability of these grafted PHB films exceeded that of films to which were grafted with hydrophobic monomers.

#### References

1. Anderson, A.J., and E.A. Dawes, *Microbiol. Mol. Biol. Rev.*, **54**, 450-457, 1990.
2. Doi, Y., *Microbial polyesters*. New York, NY: VCH publishers (1990).
3. Miyoshi K., Saito K., Shiraishi T., and Sugo T., *J. Membrane Sci.*, **264**, 97-103, 2005.
4. Seko N., Katakai A., Hasegawa S., Tamada M., Kasai N., Takeda H., Sugo T. and Saito K., *Nucl. Technol.*, **144**(2), 274-278, 2003.
5. Shiraishi T., Tamada M., K. Saito and Sugo T., *Radiat. Phys. Chem.*, **66**, 43-47, 2003.
6. Seko N., Katakai A., Tamada M., Sugo T., and Yoshii F., *Sep. Sci. Technol.*, **39**(16), 3753-3767, 2004.
7. Seko N., Tamada M., Yoshii F., *Nucl. Instr. And Meth. in Phys. Res. B*, **236**, 21-29, 2005.
8. Mitomo H, Sasaoka T, Yoshii F, Saito T, *Sen'i Gakkaishi (Japan)*, **52**, 623-627, 1996.
9. Mitomo H, Enjoji T, Watanabe Y, Yoshii F, Saito T, *J. Macromol. Sci.A*, **32**, 429-442, 1995.
10. Bahari K, Mitomo H, Enjoji T, Yoshii F, *Polym Degrad Stab.*, **61**, 245-252, 1998.
11. Bahari K., Mitomo H., Enjoji T., Hasegawa S., Yoshii F., *Die Angew. Makromol. Chem.*, **250**, 31-44, 1997.
12. Cakmakli B, Hazer B, Borcakli M, *Macromol. Biosci.*, **1**, 348-354, 2001.
13. Basuki, F., Tamada, M., Seko, N., Sugo, T., Kume, T., *J. Ion Exchange*, **14**, 209-212, 2003.
14. Yamada K, Mukai Y, Doi Y, *Int J Biol Macromol.*, **15**, 215- 1993.

## **Rapid Deployment of Monte Carlo simulation system by Diskless Remote Boot in Linux**

Yan-Lin Liu, Jay Wu

*Department of Radiological technology, Central Taiwan University of Science and Technology.*

Monte Carlo simulation is a usually used as a golden standard for analyzing radiation doses in medical physics. This technique solves complex problems by a stochastic way to improve the accuracy of results, but it requires longer processing time. Through the use of high-performance computing clusters, we can improve the operation efficiency. However, clusters cannot be applied for other purposes. In this study, we installed the Diskless Remote Boot in Linux (DRBL) and Linux OS on the experiment environment containing one server and 50 non-hard disk computing nodes. Without affecting the internal system, DRBL can provide the services of the Dynamic Host Configuration Protocol Server (DHCP), Trivial File Transfer Protocol server (TFTP), Network File System (NFS), and Network Information Service (NIS). Through the Internet, the simplified Linux OS was transferred to each computing node as well as the MCNP 4C (Monte Carlo N-Particle Transport Code Version 4C) simulation program. Through the Parallel Virtual Machine (PVM), the efficiency of the Monte Carlo simulation can be raised and the clusters can be extensive uses. We conclude that The DRBL allows Monte Carlo simulations to be used broadly on the research and on the radiology education.



# FEYNMAN

費曼科技股份有限公司

E-mail: service@feynman.com.tw

地址: 106台北市敦化南路二段5號7樓之2

行政院原子能委員會認可輻射防護訓練業執照字第000-四號

電話: (886)2-2706-6088

傳真: (886)2-2700-4197

行政院原子能委員會認可輻射防護偵測業執照字第000三二號

## RADIATION

## PROTECTION

- ✦ X光機屏蔽計算/輻射量測
- ✦ 設施規劃/施工諮詢
- ✦ 操作人員十八小時取代輻安證書訓練
- ✦ 企業或醫療院所內部定期輻防教育訓練服務
- ✦ 直線加速器輻射安全評估/光子及中子滲漏輻射量測
- ✦ 放射性物質生產設施規劃/評估/輻射量測
- ✦ 放射性物質作業場所輻射安全評估/輻射防護偵測
- ✦ 放射性物質運送有關之輻射防護及偵測
- ✦ 輻射防護設備/輻射偵檢儀器採購諮詢服務/校正代送服務

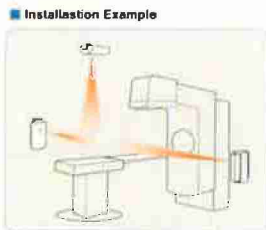


## THERAPY

TAKEX Optics-Laser Alignment Marking Devices



LSP-1300

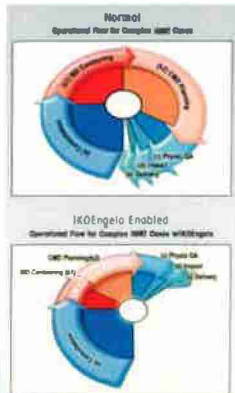


Installation Example  
Wall mounted Medical Laser Alignment system

IKOE-Auto contouring System



THE IKOEengelo™ SYSTEM



## RADIATION MONITORING SYSTEM

ALOKA CO.,LTD.(JP)

-Radiation Monitoring System



Survey Meter



Personal Dosimeter



中央監視装置

## SHIELDING

Wardray Premise Ltd.(UK)

-Radiation shielding for medical and industrial applications



Mobile Screen



X-Ray Protective Apron



MR Trolley